Title
Learning and Control Systems for the Integration of Renewable Energy into Grids of the Future

Author
Hidalgo-Gonzalez, Patricia

Publication Date
2020

Peer reviewed|Thesis/dissertation

Learning and Control Systems for the Integration of Renewable Energy into Grids of the Future

by

Patricia Hidalgo-Gonzalez

A dissertation submitted in partial satisfaction of the

requirements for the degree of

Doctor of Philosophy

in

Energy and Resources

in the

Graduate Division

of the

University of California, Berkeley

Committee in charge:

Professor Claire J. Tomlin, Co-chair
Professor Daniel M. Kammen, Co-chair
Professor Duncan S. Callaway
Professor Shmuel S. Oren

Spring 2020

Learning and Control Systems for the Integration of Renewable Energy into Grids of the Future

Abstract

Learning and Control Systems for the Integration of Renewable Energy into Grids of the Future

by

Patricia Hidalgo-Gonzalez

Doctor of Philosophy in Energy and Resources

University of California, Berkeley

Professor Claire J. Tomlin, Co-chair

Professor Daniel M. Kammen, Co-chair

For over 30 years we have been negotiating agreements that try to reduce greenhouse gas emissions. The aim is to stabilize their concentration in the atmosphere at a level that would prevent dangerous anthropogenic interference with the climate system. In 2018, the Intergovernmental Panel on Climate Change stated that the 1.5°C goal could be achieved if the electricity sector would become net zero emissions by 2050. Different countries have been pushing the frontier to reduce their emissions by deploying renewable energy sources (RES). Despite these efforts, we still have a long way to go. Research on how and when to install and how to operate more RES in power systems needs to continue advancing as we aim to reach higher levels of penetration. In addition, academics need to translate and communicate these findings to policy makers.

The contributions of this dissertation in this field have been to:

1. propose a new time-varying representation for power dynamics that reflects the presence of RES,

2. design through machine learning a stable time-invariant frequency controller for the new time-varying power dynamics,

3. explore the trade-off between information availability to the frequency control agents and their performance and stability,

4. show the cost effectiveness of stronger RES targets in the U.S. by 2030 given the carbon reductions goals of 2050, and

5. model climate change uncertainty through a stochastic formulation of the capacity expansion of power systems in the U.S. with high penetration of RES.

As more non-synchronous RES participate in power systems, the system's inertia decreases and becomes time dependent, challenging the ability of existing control schemes to maintain frequency stability. System operators, research laboratories, and academic institutes have expressed the importance to adapt to this new power system paradigm. However, power dynamics have been modeled as time-invariant, by not modeling the variability in the system's inertia. To address this, we propose a new modeling framework for power system dynamics to simulate a time-varying evolution of rotational inertia coefficients in a network. Power dynamics are modeled as a hybrid system with discrete modes representing different rotational inertia regimes of the network.

Using this new hybrid model for power dynamics, we present a framework to design a fixed learned controller based on datasets of optimal time-varying LQR controllers. We test the performance of the controller in a twelve-bus system. By adding virtual inertia we can guarantee stability of high-renewable (low-inertia) modes. The novelty of our work is to propose a design framework for a stable controller with fixed gains for time-varying power dynamics. This is relevant because it would be simpler to implement a proportional controller with fixed gains compared to a time-varying control. To expand this work, we introduce a framework to learn sparse time-invariant frequency controllers in a power system network with a time-varying evolution of rotational inertia. We design a controller that uses as features the system's states. In other words, we design a control proportional to the angles and frequencies. Virtual inertia is included in the controllers to ensure stability. One of the findings is that it is possible to restrict communication between the nodes by reducing the number of features in the controller (from 22 to 10 in our case study) without disrupting performance and stability. Furthermore, once communication between nodes has reached a threshold, increasing it beyond this threshold does not improve performance or stability. There is a correlation between optimal feature selection in sparse controllers and the topology of the network.

In the second part of this dissertation we study the cost and lock in of carbon intensive technologies due to weak medium-term policies. We use SWITCH WECC– a power system capacity expansion optimization model with high temporal and geographical resolution. We test three carbon cap scenarios. For each scenario, we optimize the power system for a medium timeframe (2030) and a long timeframe (2050). In the medium timeframe optimizations, by 2030 coal replaces gas power. This occurs because the long optimization foresees the stronger carbon cap in 2050. Therefore, it is optimal to transition towards cleaner technologies as early as 2030. The medium-term optimization has higher costs in 2040 and 2050 compared to the long optimization. Therefore, to minimize total costs to reduce emissions by 80% in 2050, we should optimize until 2050 or have stronger carbon cap policies by 2030 (such as a 26% of emissions reductions from 1990 levels by across the WECC).

Typical electricity-grid capacity expansion models make investment decisions with fixed inputs (e.g., fixed electricity demands and hydro-power availability). The resultant electricity supply system may not be robust to future climate change-driven uncertainties in energy demand and supply. We present the first climate change stochastic long-term (2050) capacity expansion and operation electricity grid model for the Western North America electricity

region, with high temporal and spatial resolution. The Stochastic SWITCH WECC model generates a least cost portfolio of power plants that is robust to varying future climate conditions using a multi-stage optimization approach with varying electricity-demand and hydropower-availability inputs under three climate change scenarios. Results show that an optimal robust electricity supply portfolio in the WECC for 2050 has about 4% higher overall installed capacity than the average mix of the three scenarios modeled separately, and about 5.6% higher installed gas capacity, due to the greater need for operational flexibility under the wider range of possible conditions.

To the hope for a better world, and to my mom.

Contents

Contents **ii**

List of Figures **iv**

List of Tables **vii**

1 Introduction **1**
1.1 Background and Motivation 1
1.2 Research Questions 3
1.3 Contributions and Dissertation Outline 4

I Frequency Regulation in Low and Variable Inertia Grids **6**

2 Power System Dynamics as a Hybrid System **7**
2.1 Preface 7
2.2 Introduction 7
2.3 Problem Formulation 9
2.4 Case Study: Twelve-Bus Three-Region Network 12
2.5 Conclusions 17

3 Frequency Regulation using Learned Controllers **18**
3.1 Preface 18
3.2 Frequency Regulation using Data-Driven Control 18
3.3 Frequency Regulation using Sparse Learned Controllers 26

II Long-term Capacity Expansion Planning **39**

4 Cost and Impact of Weak Medium Term Policies in the Electricity System in Western North America **40**
4.1 Preface 40
4.2 Introduction 40

4.3 Problem Formulation 41
4.4 Scenarios 44
4.5 Results and Analysis 45
4.6 Conclusions and Policy Implications 53

5 Power System Planning in Western North America: Deterministic and Stochastic Scenarios under Climate Change 54
5.1 Preface 54
5.2 Introduction 54
5.3 Long-term Power System Planning in Western North America: Deterministic Scenarios 56
5.4 Stochastic Optimization Under Climate Change Uncertainty 72

6 Conclusions and Future Directions 81
6.1 Summary of Findings 81
6.2 Future Directions 84

A SWITCH 86
A.1 Objective Function 87
A.2 Operational Constraints 87
A.3 Investment Constraints 89
A.4 SWITCH Modules 89

Bibliography 103

List of Figures

2.1 Case study: Twelve-bus three-region network from [59], [82], and [15]. 13
2.2 Inertia Placement: Histogram of optimal controller u^* at all nodes, all time steps, and all scenarios. 15
2.3 Dynamic Inertia Placement: Histogram of optimal controller u^* at all nodes, all time steps, and all scenarios. 15
2.4 Inertia Placement: Histogram of optimal cost J^* at all time steps and all scenarios. 16
2.5 Dynamic Inertia Placement: Histogram of optimal cost J^* at all time steps and all scenarios. 16

3.1 Eigenvalue placement for the closed loop system in mode q_1 using the learned controller K_{L} (crosses) and adding virtual inertia control $K_{\mathrm{L}} + \mathrm{VI}$ (circles). . . . 23
3.2 Frequency deviations for node 1 for 5 different controllers from a hybrid system simulation. 25
3.3 Mean Squared Error (MSE) from training and cross-validating controllers with different numbers of features. 32
3.4 Frequency deviation evolution using learned controllers with an initial deviation of -0.15Hz and a system's inertia of 0.2 seconds. 33
3.5 Eigenvalues of all controllers j for the closed loop system with inertia of 9 seconds. 34
3.6 Maximum eigenvalue real part for all controllers j under 0.2s (green square), 2s (red cross), 5s (blue dot) and 9s of inertia (black asterisk). 34
3.7 Heat map of learned controller for $\lambda = 0$, meaning each node uses up to 22 features. 36
3.8 Heat map of learned controller with λ-values tuned such that each node uses up to 5 features. 37

4.1 WECC carbon cap scenarios. In green is the 80% emissions reductions from 1990 levels by 2050 scenario (labeled as "80% by 2050"), in blue the Clean Power Plan scenario (labeled as "CPP"), and in red 40% emissions reductions by 2030 (labeled as "40% by 2030"). 44
4.2 Energy generation share (as a fraction) per fuel per period for the long optimization for the scenarios studied. On the left side is the "80% by 2050" scenario, in the middle the "CPP", and on the right side the "40% by 2030". 46

4.3 Change in capacity installed in gigawatts per fuel by 2030 for the scenarios studied. The difference corresponds to capacity per fuel installed by 2030 in the medium optimization minus the capacity installed in 2030 in the long optimization. On the left is the "80% by 2050" scenario, in the middle the "CPP" scenario (where more coal and less gas are installed in the medium optimization), and on the right side the "40% by 2030" scenario. 48
4.4 Change in energy generated in terawatt hour per fuel during the period 2030 for the scenarios studied. The difference corresponds to the generation per fuel by 2030 in the medium optimization minus the generation in 2030 in the long optimization. On the left is the "80% by 2050" scenario, in the middle the "CPP" scenario (where more coal and less gas are deployed in the medium optimization), and on the right side the "40% by 2030" scenario. 48
4.5 CO_2 emissions in the year 2030 for the medium (yellow) and long optimization (blue). The red dashed line represents the carbon cap for the year 2030 for each scenario. On the left side is the "80% by 2050" scenario, in the middle the "CPP" scenario, and on the right side the "40% by 2030" scenario. 49
4.6 Change in gas (top) and coal (bottom) power plants' capacity in gigawatts by 2030 for "CPP" scenario. The difference corresponds to capacity installed by 2030 in the medium optimization minus the capacity installed by 2030 in the long optimization. 51
4.7 Increase in cost per period from using the medium optimization instead of the long optimization. The red solid line represents cost increases from "40% by 2030" scenario, the short dashed green line corresponds to "80% by 2050," and the long dashed blue line represents "CPP" scenario. 52

5.1 List of Modules in SWITCH 2.0. 55
5.2 WECC Divided in 50 SWITCH Load Zones 57
5.3 In light blue are non-existing lines, but that can be installed in the optimization. Each black dot represents the largest substation in the load zone. 58
5.4 Electricity Demand Scenarios for the WECC. 60
5.5 Electricity Demand Scenarios for California. 60
5.6 Example Constraints on Charging Profiles on Different PEVs. 62
5.7 Average Bounds on Cumulative Charging Trajectories. 63
5.8 Installed Capacity in the WECC by 2050 for All Scenarios. 64
5.9 Installed Capacity in California by 2050 for All Scenarios. 65
5.10 Existing and New Transmission Lines Capacity for All Periods and All Scenarios Between California and the Rest of the WECC. 66
5.11 Existing and New Transmission Lines Capacity for All Periods in the WECC for All Scenarios. 67
5.12 Existing and New Transmission Lines Capacity for All Periods and All Scenarios Between Load Zones in California. 68
5.13 Yearly Generation in the WECC by 2050 For All Scenarios. 69

5.14 Yearly Generation in California by 2050 for All Scenarios. 70
5.15 Installed Capacity in the WECC Without and With Flexibility from EV and DR. 70
5.16 Fraction of Generation in the WECC and California Systems Without/With Flexibility of EV and DR. 71
5.17 Decision Variables for Stochastic SWITCH WECC Python. 75
5.18 Installed Capacity in the WECC by 2050 for Deterministic and Stochastic Climate Change Scenarios. 77
5.19 Installed Capacity in California by 2050 for Deterministic and Stochastic Climate Change Scenarios. 78
5.20 Existing and New Transmission Lines Capacity for All Periods in the WECC for Deterministic and Stochastic Climate Change Scenarios. 79
5.21 Existing and New Transmission Lines Capacity Between California and the WECC for All Periods, for the Deterministic and Stochastic Climate Change Scenario. . 80

List of Tables

2.1 Parameters for the twelve-bus three-region case study [59], [15]. 13
2.2 Summary: mean and standard deviation of objective function J^*, optimal control u^*, and frequency ω. 14

3.1 Comparison of learned controller (K_{L}) and learned controller with virtual inertia ($K_{\mathrm{L}}+\mathrm{VI}$) against optimal control from LQR under different inertia modes. Units are in percentages (%). 24
3.2 Performance metrics for learned controller under different inertia systems. . . . 32

4.1 Capacity installed in gigawatts in the WECC per fuel by 2030 for the scenarios studied. The columns show installed capacity from the medium and long optimization for each scenario in 2030. 47

5.1 Electricity demand scenarios modeled. 59
5.2 Expected Device Stocks in Millions and Energy Required for Charging per Zone and Year. 61
5.3 Fraction of Shifted Demand by Period and Zone. 63

A.1 Model components defined in the `timescales` module. 90
A.2 Model components defined in the `financials` module. 90
A.3 Model components defined in the `balancing.load_zones` module. 91
A.4 Model components defined in the `energy_sources.properties` module. 91
A.5 Model components defined in the `generators.core.build` module. 92
A.6 Model components defined in the `generators.core.dispatch` module. 93
A.7 Model components defined in the `generators.core.no_commit` module. 93
A.8 Model components defined in the `generators.core.commit.operate` module. . 94
A.9 Model components defined in the `energy_sources.fuel_costs.simple` module. 95
A.10 Model components defined in the `energy_sources.fuel_costs.markets` module. 95
A.11 Model components defined in the `generators.core.commit.fuel_use` module. Components marked with * are local to the module (some read from input tables), and are not added to the main model. 96
A.12 Model components defined in the `transmission.transport.build` module. . . 97
A.13 Model components defined in the `transmission.transport.dispatch` module. 98

A.14 Model components defined in the `balancing.demand_response.simple` module. 99
A.15 Model components defined in the `generators.extensions.hydro_simple` module. 99
A.16 Model components defined in the `generators.extensions.storage` module. . . 100
A.17 Model components defined in the `policies.rps_unbundled` module. 101
A.18 Model components defined in the `policies.carbon_policies` module. 102

Acknowledgments

I would like to thank my advisor Claire J. Tomlin for her unconditional support and trust. Claire, I profoundly enjoyed working with you and learning from you. Your advice and critical thinking always allowed me to develop sound research questions and tackle them with the best suited tools from control theory and machine learning. Thanks to you, not only did I deepen my technical expertise, but I was also able to witness how you navigate life with compassion and assertiveness, an art in itself. I will treasure this lesson forever and will do my best to try to foster it. Although I am graduating, I would be honored to continue working together through my career. I not only think of you as a role model and academic mother (and now colleague?!), but also as my good friend. Thank you for making my experience at UC Berkeley so rich in different realms.

I would like to show my appreciation to Daniel M. Kammen, the first faculty at UC Berkeley who believed in me as an undergraduate and accepted me in his research group. Thank you, Dan, for your strong support, academically and personally, through all these years. It has been a pleasure to work with you at the frontier of renewable energy integration and policy. Thank you for the opportunity to work with you and your talented group of graduate students. I will be forever grateful for all the lessons learnt. Thanks, Josiah Johnston, for teaching me some of your computer scientist tricks. These skills have helped me develop and share my research more efficiently. Juan Pablo Carvallo, I enjoyed our time working together, and I hope we join forces again in the near future.

I would also like to thank Duncan S. Callaway. Thanks, Duncan, for advising me along my journey towards the Electrical Engineering and Computer Sciences department. I treasure all the engaging conversations about power systems we had. You always made sure to keep me on my toes. This enabled me to work on a solid line of research to integrate renewable energy into our grids. I also admire how humble you are and I hope to develop that quality through my career. And thank you for originally suggesting to work with Claire.

Shmuel Oren, Max Wei, Laurent El Ghaoui and Alexandre Bayen, thank you for working with me during my Ph.D. I had a wonderful time teaching convex optimization with you, collaborating and learning from you. Laurent and Alex, thank you for supporting my academic job search. You helped me succeed in a very competitive endeavour. I would also like to thank the faculty, staff, departments and institutions that hosted me as a faculty candidate and made the end of my Ph.D. even more exciting: Mechanical and Aerospace Engineering at the University of California, San Diego, Electrical and Computer Engineering at Purdue University, Electrical Engineering and Computer Science at the Massachusetts Institute of Technology, and Mechanical Engineering at the University of Wisconsin-Madison.

Special thanks to my funding agencies: the NSF Graduate Research Fellowships Program (GRFP), The Siebel Scholars Foundation and the California Energy Commission. My work was also supported by NSF PIRE: Science of Design for Societal-Scale Cyber-Physical Systems. Thank you, as well, to the institutions I have collaborated with: California Energy Commission (Sonya Ziaja, Guido Franco), Lawrence Berkeley National Laboratory, National Renewable Energy Laboratory, Energy and Environmental Economics, Natural

Resources Defense Council, Industrial Economics, State Grid Corporation of China, Chinese National Development and Reform Commission, AI Now Institute, ETH Zurich (Stavros Karagiannopoulos, Gabriela Hug), Tufts University (Deborah Sunter), UC Irvine, Tsinghua University, Chongqing University and Renmin University of China.

This section could not end without thanking my partner in crime, Rodrigo Henriquez-Auba. Thank you, Rodrigo, for all the fun times working together and attending conferences. All this work was also possible thanks to you. I look forward to continuing our collaborations in the years to come. Roel Dobbe, thank you for helping me to transition into the field of power dynamics. I treasure our research discussions –developing ideas with you was intellectually engaging and entertaining. I look forward to continuing to work with you through our careers. Julia Szinai, it has been a gift to be able to work with you at the end of my journey as a graduate student. Thank you for your support in the last few projects. I am excited to continue working together in the immediate term and also in the long-term. Thank you for the camaraderie, feedback on my work and support to the Hybrid Systems lab, SWITCHers, RAEL, EMAC, ERG and EECS. Special thanks to Julia Szinai, Margaret Chapman, Marine Boudot, Michel Brun, Sylvia Herbert, Somil Bansal, David Fridovich-Keil, Elsa Lemaître-xavier, Nikky Avila, Cecilia Springer, Grace Wu, Ranjit Deshmukh, Chris Hyun, Anne-Perrine Avrin, Jess Goddard, Jess Reilly, Anna Brockway, Jonny Lee, Sergio Castellanos, Kripa Akila, Laura Moreno, Niklas Lollo, Emma Tome, Diego Ponce de Leon Barido, Juan Pablo Carvallo, Josiah Johnston, Ana Mileva, Jimmy Nelson, Michaelangelo Tabone, Sascha von Meier, Isha Ray, Kay Burns, Jessica Gamble, and Shirley Salanio. Thank you to my soccer team! It was so helpful to release some adrenaline and have some fun during our games throughout graduate school. Thank you, Qualcomm Café (2014 - 2017) and Brewed Awakening, for providing caffeine when I needed it the most. Thanks to Bongo Burger for becoming my traditional place to celebrate small academic victories.

My deepest gratitude goes to Vipassana meditation as taught by S.N. Goenka in the tradition of Sayagyi U Ba Khin[1]. Thank you for providing free access to any person to this wonderful meditation technique. At your meditation centers I was able to reconnect and ground myself during challenging and mundane times. I feel so much gratitude for the gift I have found in this meditation technique. Being a graduate student at UC Berkeley allowed me to attend periodically your 10-day, 3-day and 1-day courses and that was an integral part of my growth during these years. Thank you for the work you do, it has been a joy to participate. I also feel so much gratitude for the beautiful community and friendships this meditation has led me to.

Last but not least, I would also like to thank my mom for her unconditional support, prayers, and love. Thanks to all your efforts I was able to have access to quality education, and now I can call myself a Doctor. Eliacim, Dani and Carmen, thank you for supporting me through my toughest times. Your friendship means the world to me, and I am so lucky to be part of your lives. Thank you to all my friends and family in Chile and Louisiana (Mandi et al.); you made every visit incredibly fun and very recharging for my soul. Alex Keller,

[1] www.dhamma.org

thank you, too, for your love and support, specially through hard times. I am so fortunate to have you in my life. Anna Matsokina, I feel so much gratitude for the spiritual growth I have been able to attain thanks to our friendship. I look forward to continue growing. And last but not least, I would like to thank Laurel Selvig. Thank you for joining the ride in the last part of my stay in graduate school. Your love and support during my faculty candidate interviews, paper submissions, and final push for my dissertation has meant the world to me. I feel so much gratitude and I am so excited to go to UC San Diego with you!

Chapter 1

Introduction

1.1 Background and Motivation

Scientists have been warning us for decades about the impacts from climate change. These impacts include glaciers melting [32], [65], [64], [99], ocean acidification and marine biodiversity loss [53], [38], [57], [81], [52], biodiversity loss [27], [10], [9], [46] agriculture and food availability [105], [75], [84], [28], weather changes [97], [28], hydrology and water resource availability [39], [18], [41], [2], wildfire risk [1], [90], [68], [73], among other impacts. In 2007, the Intergovernmental Panel on Climate Change (IPCC) released a report that confirmed that climate change was already taking place and that it was mostly a result of human activity [93]. The report illustrates some of the impacts from climate change and shed light on what impacts could be expected in the future. It also describes adaptation and mitigation options to reduce societal vulnerability, as well as policies and technologies that could help limit the magnitude of future climate change impacts. More specifically, it recommends limiting global warming to 2°C. This 2°C goal could be achieved if different economic sectors in industrialized countries would reduce their emissions to specific targets. The electricity sector in particular would have to reduce its emissions to 80% below 1990 levels by 2050. This is a challenging task considering current emissions are 9% below 1990 levels [6]. In 2015, the 21st Session of the Conference of the Parties to the United Nations Framework Convention on Climate Change (COP 21) took place in Paris, France. Its main outcome was the reaffirmation to limit global temperature increase below 2°C compared to pre-industrial levels, while urging efforts to limit the increase to 1.5°C [54].

In 2018, the IPCC published a Special Report on Global Warming of 1.5°C approved by governments [74]. The aim of this report is to highlight some of the climate change impacts that could be avoided if we limit global warming to 1.5°C instead of limiting it to 2°C. For example, the probability of an Arctic Ocean free of sea ice in summer would be once per century compared to at least once every ten years with 2°C of global warming. The importance of limiting global warming to 1.5°C is not only important due to the milder impacts we would face but also because some of the impacts from 2°C of warming would be

irreversible. The report also addresses ways for the economy to stay below 1.5°C of warming, what it would entail, and what impacts we could face. According to the report, world-wide carbon dioxide emissions would need to decrease by 45% from 2010 levels by 2030, and net zero emissions would be required by 2050. If global warming goes above 1.5°C we would need to rely on carbon capture technologies– for which it has not been possible to prove their effectiveness at large scale.

Therefore, if we plan to keep global warming below 1.5°C with the available technologies, this would entail worldwide electricity systems supplied exclusively with generation from renewable energy sources (RES) by 2050. Power systems supplied solely by RES bring a set of technical challenges that researchers and power systems engineers have been working on and more advances need to take place. These challenges can be classified by time scope as follows:

- **Years to decades:** The challenge of RES integration in the time span of years to decades corresponds to the power system capacity expansion [22], [23], [37]. We need to optimize how the grid should expand its capacity and operate because power plants and transmission lines have long lifetimes and high capital costs making this task non-trivial to solve. In addition, the problem becomes more challenging due to the seasonal and hourly variability and geographic resource specificity of RES.

- **Hours to minutes:** The challenge of RES integration in the hourly and sub-hourly time resolution corresponds to how to optimally dispatch the generators in a grid to optimally supply demand at all times. In the presence of RES, generators are not controllable and the power injections they can provide to the system are time-varying and are probabilistic. These characteristics and the non-convexity of power flow equations call for advances in the mathematical formulation (e.g. [86]), and also the need to adjust the more sophisticated frameworks to ease their implementation. In addition, power systems use heuristics to determine operating reserves levels (e.g., operating reserves in Western North America [24]). A scheme to determine operational reserves that would take advantage, for example, of probabilistic approaches would improve the efficiency of integrating of RES.

- **Seconds:** The challenges associated to this time scope correspond to the new physics of electric power dynamics due to RES. As more non-synchronous RES participate in power systems, the system's inertia decreases and becomes time dependent, challenging the ability of existing control schemes to maintain frequency stability [95]. Additionally, as more Photovoltaics distributed generation gets deployed, voltage regulation issues arise, as well as reverse power flow impacts [61]. Lastly, some classical power systems stability issues are synchronization of phase angles [31] and waveform stability [100].

These challenges show specific variations depending on the subsystem of the power system:

- Transmission system
- Distribution system
- Microgrids and islanded networks

At the same time as challenges arise, there are opportunities that can be taken advantage of to aid the integration of RES:

- **Flexibility:** Electrical Vehicles (EV) charging and discharging to provide grid services, deployment and management of storage technologies, demand response (DR) and controllable loads.
- **Distributed Energy Resources (DER):** The deployment of DER and microgrids can alleviate the need to rely on the transmission system by supplying local electricity demand with local electricity production.
- **Market redesign:** Create new market products to aid the integration of renewable energy such as capacity markets, probabilistic supply curves for operational reserves, peer-to-peer economies for DER, rate design for microgrids, incentives design for EV/DR, etc.
- **Methods:** Controller design via machine learning coupled with control theory, stochastic optimization for capacity expansion and optimal power flow, distributed control, etc.

As it has been discussed, in a non-exhaustive manner, the research space for the integration of RES is ample. We require the engineering and scientific community to join efforts and advance its frontier to achieve 100% renewable energy power systems worldwide by 2050 to maintain global warming below 1.5°C. The work presented in this dissertation addresses some of these questions and sets the stage for more contributions to come.

1.2 Research Questions

The body of work in this dissertation is motivated by the challenge of RES integration. As it was described in the previous section, there are different time scopes and systems where there is a need to advance knowledge. Driven by intellectual curiosity, societal and environmental needs, and the lack medium and long-term electricity policy design, the work started with studying how the electricity system in Western North American (i.e. WECC– Western Electricity Coordinating Council) can optimally expand its electricity grid under different scenarios, as well as under uncertain impacts from climate change. Results from this study show that by 2050 the power system needs to be mostly composed by RES. As more non-synchronous RES participate in power systems, the system's inertia decreases and becomes time dependent, challenging the ability of existing control schemes to maintain

frequency stability. This result inspired the next portion of this dissertation: how to operate in real-time a power system dominated by RES, in particular with respect to electric power dynamics and frequency regulation. Thus, the research questions this dissertation addresses are:

- *How can we better represent mathematically the new system dynamics introduced by non-synchronous RES?*
- *How to design via learning a fixed and stable frequency controller in a network with these new time-varying power dynamics? What is the trade-off between full access to information and reducing communication between the control agents in the network?*
- *What are the costs and impacts of weak medium-term electricity policies in the WECC? What policies should be in place in the medium-term to aid a long-term least cost transition?*
- *How should we expand and operate the WECC under different scenarios? How should we optimally expand the electricity infrastructure to guarantee a robust system to different climate change impacts?*

1.3 Contributions and Dissertation Outline

The contributions of this dissertation are organized as follows:

- **Chapter 2:** The work in this chapter is motivated by the need to better represent power system dynamics in the presence of RES connected to the grid by inverters. To address this need, we introduce a new framework to model frequency dynamics as a time-varying system due to the variability of the inertia coefficients in a network. More specifically, we propose to model power dynamics in a network as a Switched Affine Hybrid system where the time-varying components are the inertia coefficients of the nodes in a grid.
- **Chapter 3:** The natural question that stems from facing new frequency dynamics due to the presence of RES is how to design a controller that is easy to implement in power systems and that has stability guarantees. This chapter addresses this question by presenting a framework to learn a fixed and stable frequency controller that is able to return the frequency to its nominal value for any mode of the hybrid system. Additionally, we explore the trade-off in performance and stability of reducing communication between the control agents in the network.
- **Chapter 4:** In this chapter we study the cost and lock in of carbon intensive technologies due to weak medium-term policies. To address this question we use the (AMPL) SWITCH WECC model– a power system capacity expansion optimization model with

high temporal and geographical resolution. Through this study we are able to draw policy recommendations for the electricity system in Western North America.

- **Chapter 5:** We implemented the SWITCH WECC Python model for the study shown in this chapter. The work explores least cost electricity systems under different levels of electricity demand growth, electrification of end uses, energy efficiency, electrical vehicles penetration and climate change impacts in Western North America. Furthermore, we also developed and implemented the first climate change stochastic long-term (2050) capacity expansion and operation electricity grid model for the Western North America electricity region, with high temporal and spatial resolution. The Stochastic SWITCH WECC model generates a least cost portfolio of power plants that is robust to varying future climate conditions using a multi-stage optimization approach with varying electricity-demand and hydropower-availability inputs under three climate change scenarios.

- **Chapter 6:** In this chapter we conclude with a summary of our main findings. We also discuss future promising directions of research: wildfire risk mitigation through technical and market design of microgrids and DER in the distribution network, design of new ancillary services for the new power dynamics and power flow paradigms with high penetration of RES, graph theory and information theory approach to frequency regulation controller design, and machine learning and safety for power systems.

Part I

Frequency Regulation in Low and Variable Inertia Grids

Chapter 2

Power System Dynamics as a Hybrid System

2.1 Preface

The work discussed in this chapter corresponds to the publication titled "Frequency Regulation in Hybrid Power Dynamics with Variable and Low Inertia due to Renewable Energy" by Patricia Hidalgo-Gonzalez, Roel Dobbe, Rodrigo Henriquez-Auba, Duncan S. Callaway and Claire J. Tomlin [48]. We presented this publication at the 57th IEEE Conference on Decision and Control in Miami, Florida, United States.

2.2 Introduction

In power systems, frequency will deviate from its nominal value when there is a mismatch between electricity generation and consumption [59]. There exists a set of mechanisms to prevent frequency excursions. The first automatic response when frequency starts to deviate is the inertial response. This inertial response is originated from the kinetic energy supplied to the grid by the synchronous generators. This inertia (present in rotating masses of generators and turbines) determines the instantaneous frequency change when imbalances of active power occur. Therefore, more inertia in the system will translate into a slower rate of change of the frequency. As the frequency starts deviating, some generators will respond automatically through governor response [34]. Governor response or droop control is an automatic control proportional to the frequency deviation. After droop control starts actuating, slower mechanisms (e.g. spinning reserves) participate to restore frequency to its nominal value [34].

It is a crucial aspect for the operation and stability of electrical systems to maintain the grid frequency within acceptable ranges. Nowadays, large shares of renewable energy sources (RES) are being integrated into power systems. Several countries have set ambitious goals for the future to provide more electricity using renewable energy [80] and/or reducing their

CO_2 emissions. This global drive will steer the power system to a grid dominated by RES [102]. In this scenario, renewable sources, such as wind and solar, are usually connected to the grid through inverters, which decouple their rotational inertia (if existing) from the grid.

Usually, depending on the configuration of the inverters, no inertial response is delivered to the grid. With this increasing penetration of RES, the global system inertia of the power systems is decreasing and time-varying. This can provoke an increment in the variation of frequency under abrupt changes in generation and demand. If no actions are taken, this can lead to cases in which standard frequency control schemes are too slow to mitigate arising contingencies [95].

A possible solution for this issue is to use RES inverters or large scale storage to provide inertia. This can be done by operating the RES or storage's inverters as virtual inertia (control proportional to the derivative of the frequency), that could allow large penetration of RES without jeopardizing the system's stability [13]. Previous work studying virtual inertia can be found in the literature. In [92], a detailed survey of different virtual inertia techniques, topologies and future directions are presented. [107] introduces the concept of inverters that emulate the response of a synchronous machine. [72] proposes a new controller to address low inertia. This work argues that virtual inertia could amplify noise in an unbounded manner. The work from [96] discusses virtual inertia (or inertia mimicking) by enabling inverter-connected generation units to quickly modify their power output via Model Predictive Control (MPC), mimicking the dynamic response of conventional units. In a similar line of work, [15] studies the effect that changes in inertia have on power system stability, and how to best place devices providing virtual inertia. Most recently [82] studied optimal placement of virtual inertia in different nodes of a network.

The body of work around virtual inertia has mostly focused on the effects on the grid and on its optimal allocation. The frequency dynamics have been modeled as a time-invariant system. However, when we take into account the nature of the changes of rotational inertia in the grid, it requires a new modeling framework that represents this time dependence and variability of the system's inertia. Thus, the contributions of this work are the following:

- We propose a new modeling framework for power system dynamics to simulate a time-varying evolution of rotational inertia coefficients in the network. To do this, we model power dynamics as a hybrid system [14] where each mode corresponds to a rotational inertia regime. At each time step of the simulation the dynamical system mode can switch to a different rotational inertia mode in an exogenous fashion.

- We test the performance of two classical controllers from the literature (optimal closed-loop controller from MPC and virtual inertia placement) in this new hybrid modeling framework.

- We propose a new controller (Dynamic Inertia Placement) to more efficiently address low and variable inertia in the grid.

We conclude that the new modeling framework we develop is necessary to design controllers that address frequency regulation in power systems with high RES penetration. We

also find that the optimal linear closed-loop controller (referred as Linear MPC in this work) performs best in terms of cost and energy injected/absorbed to control frequency. Lastly, we find that our proposed controller for Dynamic Inertia Placement (when modeling dynamics with variable inertia) is more efficient in terms of cost and energy usage than the classical Inertia Placement from the literature.

The rest of the chapter is organized as follows: Section 2.3 presents the problem formulation, Section 2.4 shows simulations from a study case, and finally Section 2.5 concludes with our main findings.

2.3 Problem Formulation

Power system dynamics as a hybrid system

We consider an electric power network modeled as a graph with N nodes and $N(N-1)/2$ possible edges connecting them. The swing equation model used for this network is based on [59], where dynamics are given by

$$m_i\ddot{\theta}_i + d_i\dot{\theta}_i = p_{\text{in},i} - \sum_j b_{ij}(\theta_i - \theta_j), \quad i \in \{1, ..., N\} \tag{2.1}$$

m_i corresponds to the equivalent rotational inertia in node i, d_i is the droop control, $p_{\text{in},i}$ represents the power input at node i, b_{ij} is the susceptance of the transmission line between nodes i and j, and θ_i is the voltage phase angle at node i. The state space representation of the model is given by

$$\begin{bmatrix} \dot{\theta} \\ \dot{\omega} \end{bmatrix} = \begin{bmatrix} 0 & I \\ -M^{-1}L & -M^{-1}D \end{bmatrix} \begin{bmatrix} \theta \\ \omega \end{bmatrix} + \begin{bmatrix} 0 \\ M^{-1} \end{bmatrix} p_{\text{in}} \tag{2.2}$$

where the states correspond to the stacked vector of angles and frequencies at each node $(\theta, \omega) \in \mathbb{R}^{2n}$, $M = \text{diag}(m_i)$ is a diagonal matrix with rotational inertia coefficients, $D = \text{diag}(d_i)$ is a diagonal matrix with droop control coefficients, p_{in} corresponds to the power input, and $L \in \mathbb{R}^{n,n}$ is the Laplacian of the network. The network Laplacian is defined as $\ell_{ij} = -b_{ij}$ when $i \neq j$, and $\ell_{ii} = \sum_{i \neq j} b_{ij} + y_{i,s}$, where $y_{i,s}$ are all shunt admittances connected at node i.

In the traditional paradigm of power systems, where generation has been dominated by thermal generation, the inertia at each node m_i has been considered constant. However, in recent years, it has been observed that due to the increase in generation from RES, the rotational inertia in the network has become lower and time-varying [95], [35]. In order to model power dynamics taking into account the variability of inertia at each node, our work proposes a new framework for modeling frequency dynamics. Instead of assuming equation (2.2) as a time-invariant dynamical system, we propose to model it as a Switched Affine hybrid system [14], where each mode will be given by a predetermined set of values of m_i at each node. The switching between the different m modes depends on the current online

generators. In this work, the mix of online generators at each time step t is modeled as an exogenous input. Therefore, power dynamics will be given by

$$\begin{bmatrix} \dot{\theta} \\ \dot{\omega} \end{bmatrix} = \begin{bmatrix} 0 & I \\ -M_{q(t)}^{-1}L & -M_{q(t)}^{-1}D \end{bmatrix} \begin{bmatrix} \theta \\ \omega \end{bmatrix} + \begin{bmatrix} 0 \\ M_{q(t)}^{-1} \end{bmatrix} p_{\text{in}} \tag{2.3}$$

where $M_{q(t)}$ represents the inertia matrix M in the current mode $q(t) \in \{1, ..., m\}$. The switching between modes q_i to q_j is probabilistic and can occur from any time step t to $t+1$. The probability $\mathbb{P}(q(t+1) = q_j | q(t) = q_i)$ comes from a uniform distribution with possible outcomes:

- No change of inertia
- Increase of inertia from q_i to q_{i+1}
- Decrease of inertia from q_i to q_{i-1}

Thus, the evolution over time of the matrix $M_{q(t)}$ is modeled as a Markov Chain. For simplicity, for a given mode $q(t)$ we assume the same inertia coefficients for all nodes. Section 2.4, describes in more detail the assumption on inertia coefficients at the nodes of the network.

Power input at node i, can be expressed as

$$p_{in} = \big(\delta + u\big), \quad \delta_i \sim N(0, 0.1) \quad i = 1...N \tag{2.4}$$

where δ is a time-varying vector whose components, δ_i, are disturbances at each node i (modeled as white noise), and the vector u is the controller (power injection). Thus, equation (2.3) can be written as

$$\begin{aligned} \begin{bmatrix} \dot{\theta} \\ \dot{\omega} \end{bmatrix} = \begin{bmatrix} 0 & I \\ -M_{q(t)}^{-1}L & -M_{q(t)}^{-1}D \end{bmatrix} \begin{bmatrix} \theta \\ \omega \end{bmatrix} \\ + \begin{bmatrix} 0 \\ M_{q(t)}^{-1} \end{bmatrix} \big(\delta + u\big) \end{aligned} \tag{2.5}$$

$$\begin{bmatrix} \dot{\theta} \\ \dot{\omega} \end{bmatrix} := \; A_{q(t)} \; \begin{bmatrix} \theta \\ \omega \end{bmatrix} + \; B_{q(t)} \; \big(\delta + u\big) \tag{2.6}$$

In this hybrid formulation, the design of the optimal controller u is more complex than in the traditional linear time-invariant (LTI) case. Recent work has shown the relevance of the optimal placement of virtual inertia in the grid [82], which expanded on previous work that studied the effects of rotational inertia in a network [15]. In this study we build on this work by including the evolution over time of the rotational inertia at each node. Using receding horizon Model Predictive Control we study three different designs for the controller u in equation (2.5).

Optimal frequency control for low and time-varying rotational inertia coefficients

In order to minimize an objective function with the states and controller as variables, we consider three possible controllers u. In addition, we take into account a constraint to maintain the frequency ω at all time t in a predefined safe interval. The receding horizon MPC formulation can be summarized by the following optimization problem:

$$\min_{x(t),u(t)} \quad \int_{t=t_0}^{T} x(t)^\top Q x(t) + u(t)^\top R u(t) dt \tag{2.7}$$

$$\text{s.t. } x(t_0) = x_0 \tag{2.8}$$

$$\dot{x}(t) = A_{q(t)} x(t) + B_{q(t)}\big(\delta(t) + u(t)\big), \quad t \in (t_0, T) \tag{2.9}$$

$$\underline{b} \leq x(t) \leq \bar{b}, \quad t \in (t_0, T) \tag{2.10}$$

$$\delta_i(t) \sim N(0, 0.1), \quad i \in \{1, ..., N\}, \quad t \in (t_0, T) \tag{2.11}$$

where x is the vector of the states (θ, ω), u the controller, Q and R are symmetric positive definite matrices, t_0 the initial time, T the final time, $\underline{b}$ and $\bar{b}$, lower and upper bounds for the frequency, and x_0 the initial state. As it was mentioned earlier, the hybrid modes $q(t)$ transition at each time step t using a Markov Chain. We consider three designs for optimal controllers u obtained using receding horizon MPC:

1. Linear MPC:

$$u_i(t) \text{ unconstrained}, \quad i \in \{1, ..., N\}, \quad t \in (t_0, T) \tag{2.12}$$

2. Inertia Placement [82]:

$$u_i(t) = -M_i \dot{\omega}_i, \quad i \in \{1, ..., N\}, \quad t \in (t_0, T) \tag{2.13}$$

3. Dynamic Inertia Placement:

$$u_i(t) = -M_i(t) \dot{\omega}_i, \quad i \in \{1, ..., N\}, \quad t \in (t_0, T) \tag{2.14}$$

The receding horizon MPC formulation (2.7) - (2.12) is classified as a quadratic problem with linear constraints, thus a convex problem. The receding horizon MPC formulation for inertia placement, (2.7) - (2.11), (2.13) and (2.7) - (2.11), (2.14), are non convex problems. To model the first formulation we use CVX [44], [45]. To model the non convex formulations we use the parser YALMIP [69], and solved the optimization problem using an interior point method.

In the case of the Linear MPC formulation, the controller $u_i(t)$ does not have any constraints imposed. Implying that the feasible set of the Linear MPC formulation and the

feasible set of the problem given by (2.7) - (2.11) are equivalent. The Dynamic Inertia Placement formulation introduces a new variable $M_i(t)$. This new variable needs to be optimized for all nodes i at all time steps t. The controller $u_i(t)$ is constrained to be equal to $-M_i(t)\dot{\omega}_i$, serving as virtual inertia. The fact that the Dynamic Inertia Placement formulation has an extra set of constraints on $u_i(t)$ implies that the feasible set of this problem is contained in the feasible set of the Linear MPC formulation. Finally, the Inertia Placement formulation, in addition to having the constraint on the structure of $u_i(t)$ as the Dynamic Inertia Placement had, it has an additional set of constraints. This extra set of constraints forces $M_i(t)$ to be equal to M_i for all t. In other words, the design of the virtual inertia controller cannot be specific to a node and time, but a fixed design over time for each node. Thus, the Inertia Placement formulation has its feasible set contained in the feasible set of the Dynamic Inertia Placement formulation. In summary, the Linear MPC formulation has the largest feasible set, followed by the Dynamic Inertia Placement which has more constraints. Finally the Inertia Placement formulation comes in third place with the most restrictive feasible set. Due to this, we expect solutions u^* from the Linear MPC formulation to be best, attaining the lowest value in its objective function. We expect the Dynamic Inertia Placement case to come in second place with a higher optimal value for its objective function compared to the Linear MPC formulation. The formulation with the highest optimal value of its objective function would be the Inertia Placement formulation.

One of the contributions of this work is to assess the grid's performance when virtual inertia is optimized over time and location (Dynamic Inertia Placement). We also compare inertia placement with the Linear MPC formulation. The latter sheds light on how the performance of frequency dynamics could improve with a more flexible controller (not constrained to be a derivative control law as inertia placement is).

In Section 2.4 we compare these three formulations. We utilize the study case (originally from [59]) used in some recent virtual inertia placement work [15] and [82].

2.4 Case Study: Twelve-Bus Three-Region Network

Data description

Errata: The values we use for the elements, m, in the diagonal matrix M in this work are inertia values, however $m = \frac{2hS}{w}$*, where h is the inertia coefficient, S the rated power, and w the angular frequency. Therefore, we test the system under lower values of inertia than intended. We expect results to hold given that this change would imply re-scaling our matrices A and B with a diagonal and nonsingular matrix. For such transformation, stability properties of the hybrid system hold.*

The twelve-bus three-region network used in this study has also been used in [59], [15], and [82]. The full network was modeled, without using any simplifications (e.g. no Kron reduction of the graph). Therefore, twelve nodes were modeled with two states each (angle and frequency). Table 2.1 shows the parameters of the network.

Table 2.1: Parameters for the twelve-bus three-region case study [59], [15].

Parameter	Value
Transformer reactance	0.15 p.u.
Line impedance	(0.0001 + 0.001j) p.u./km
Base voltage	230 kV
Base power	100 MVA
Droop control	1.5 %/%

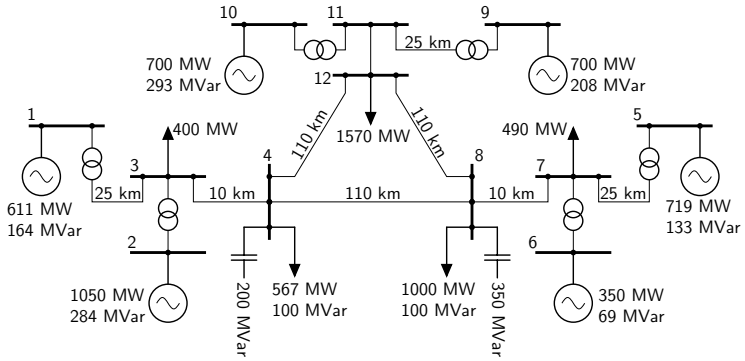

Figure 2.1: Case study: Twelve-bus three-region network from [59], [82], and [15].

The positive definite matrices Q and R from the objective function in problem (2.7) that we use in the case study are the identities. With this selection we are equally penalizing frequency deviations from zero and energy injection/absorption from the controller. This assumption can be changed to, for example, represent the real economic cost to the grid that frequency deviations and energy injection/absorption from the controller represent. This in itself is an open research question.

As it was discussed in Section 2.3, the inertia matrix M is modeled as a diagonal matrix $\text{diag}(m_i)$, whose elements m_i reflect the rotational inertia at the bus i. We assume the same rotational inertia in all buses for a given time step t ($m_i(t) = m(t)$ for all i). This implies a similar fraction of renewable energy generation for all nodes, which is common in large networks. However, this assumption can be easily extended. In this work, we model the variability of the rotational inertia in the system as a hybrid system switching modes as the inertia changes. Each mode of the hybrid system is given by one value of inertia. For the study case we predefined possible inertia values for the system: $\{0.1, 0.5, 1, 1.5, 2, 2.5, 3, 3.5, 5, 9\}$. The average of this set of possible inertia values is 2.8 seconds, which is equivalent to having 28 percent of thermal generation (10 s of inertia) and 72 percent of RES with zero inertia. Each simulation starts with 2 seconds of inertia, and from there- based on a uniform distribution draw- the inertia (hybrid mode) of the system at time $t + 1$ will remain the same, increase, or decrease (Markov Chain with 1/3 probability for each possible mode transition). This process is repeated until each time step t in the time horizon T has assigned a rotational

Table 2.2: Summary: mean and standard deviation of objective function J^*, optimal control u^*, and frequency ω.

Moments	Linear MPC	Inertia Placement	Dynamic Inertia Placement
$\mu(J^*)$	0.17	0.92	0.24
$\sigma(J^*)$	0.07	1.66	0.30
$\mu(u^*)$ p.u.	-0.004	-0.018	-0.005
$\sigma(u^*)$ p.u.	0.13	0.29	0.15
$\mu(\omega)$ mHz	-0.34	0.93	8.10
$\sigma(\omega)$ Hz	0.07	0.04	0.05

inertia mode.

The safety bounds for frequency are ± 0.1 Hz ($\underline{b}$ and $\bar{b}$ in equation (2.10)).

Results

Each receding horizon MPC formulation is run for eight time steps (T) and 100 possible realizations (or scenarios) from the Markov Chain of the rotational inertia matrix $M_{q(t)}$. Thus, for each formulation we obtain an optimal value of the objective function at each time step and each scenario (i.e. 800 values). The number of nodes, N, is 11 because node 11 and 12 are the same (refer to Fig. 2.1). We also obtain N control actions (one per node) for each time step and for each scenario (i.e. 8800 values), and N frequency measurements for each time step and for each scenario (i.e. 8800 values). Using these sets of results we calculate moments and show histograms for the three formulations in order to compare them.

Table 2.2 shows the mean and standard deviation of the set of optimal values of the objective function (J^*) at all times t and all scenarios for the three formulations. The same moments are shown for optimal control (u^*) and frequency (ω) for the three optimization problems. As discussed in Section 2.3, the Linear MPC formulation shows the lowest average and standard deviation values in its objective function compared to the other two formulations. The average of the objective function for the Linear MPC is 0.17 cost units, and its standard deviation 0.07. In the case of the average, it corresponds to 18 percent of the average in the Inertia Placement formulation and 71 percent of the average in the Dynamic Inertia Placement case. This result can be interpreted as the Inertia Placement formulation resulting in non zero frequency deviations and non zero control actions 82 percent more of the time compared to the Linear MPC formulation (on average). This result sheds light on the suboptimality of the virtual (dynamic and static) inertia controllers compared to the closed-loop formulation (Linear MPC). Thus, there is an incentive to continue designing controllers that try to address low and variable inertia coefficients in the grid.

Another relevant result is the fact that our proposed Dynamic Inertia Placement formula-

tion provides better performance than the Inertia Placement formulation in terms of average cost and energy usage in the controller u^*. This is expected as well because we provide more flexibility for the controller to inject/absorb energy depending on not only the node, but also on the time step. The average objective value in the Dynamic Inertia Placement formulation is 39 percent of the average optimal value of the objective function in the Inertia Placement case.

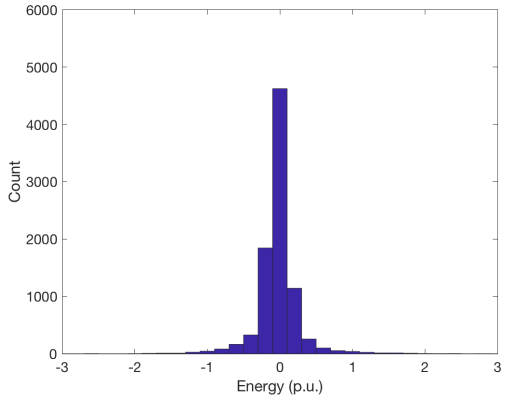

Figure 2.2: Inertia Placement: Histogram of optimal controller u^* at all nodes, all time steps, and all scenarios.

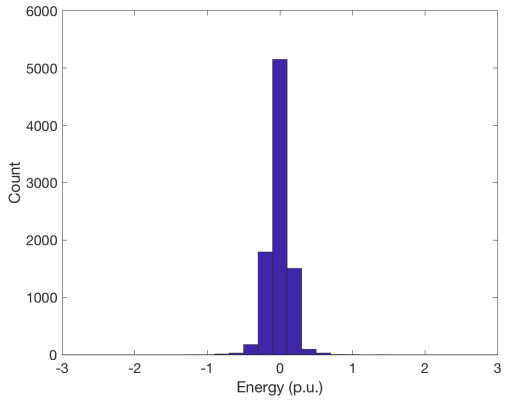

Figure 2.3: Dynamic Inertia Placement: Histogram of optimal controller u^* at all nodes, all time steps, and all scenarios.

Fig. 2.2 and 2.3 show histograms of the optimal controllers u^* for the Inertia Placement formulations. Statistics in Table 2.2 show that the optimal controller for the Linear MPC formulation case uses less energy on average to maintain the frequency within the allowed bounds. Its maximum injection/absorption is between ± 0.3 p.u. (not shown in Table 2.2).

The optimal injection from the Inertia Placement formulation ranges between -2.6 and 2.8 p.u. to maintain the same safety bounds for the frequency. The control range from the Dynamic Inertia Placement is smaller (-1.2 and 1.4 p.u.) compared to the spread observed in the energy absorbed/injected by the Inertia Placement controller. Therefore, it shows a more efficient frequency control design.

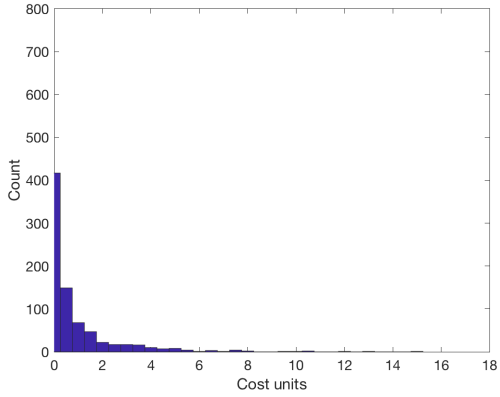

Figure 2.4: Inertia Placement: Histogram of optimal cost J^* at all time steps and all scenarios.

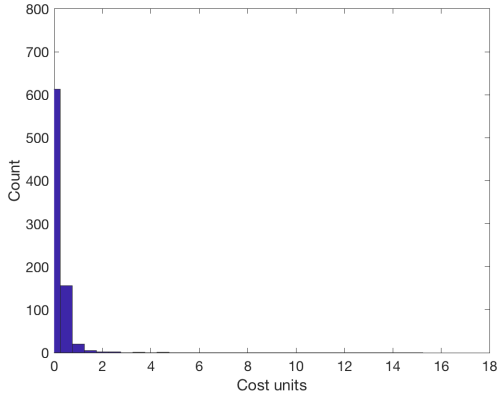

Figure 2.5: Dynamic Inertia Placement: Histogram of optimal cost J^* at all time steps and all scenarios.

Fig. 2.4 and 2.5 show histograms of optimal costs for the Inertia Placement formulations. The moments in Table 2.2 show that the optimal values for the Linear MPC formulation are concentrated around zero. However, the Inertia Placement formulations show more spread, reaching extreme costs of 15 units (Inertia Placement) and 4.3 units (Dynamic Inertia Placement). The distribution of the costs for the Dynamic Inertia Placement controller is

more skewed and its tail does not reach as high of values (Fig. 2.5) compared to the tale of the cost distribution in the Inertia Placement design (Fig. 2.4).

2.5 Conclusions

We propose a new modeling framework for power systems dynamics that captures the variability of rotational inertia over time. Our proposed model is a Switched Affine hybrid system, whose modes change based on the change of inertia in the nodes. The transition from one mode to another is determined by a Markov Chain at each time step of the simulation. With this new framework, we test two standard frequency control designs and propose a third design: Linear MPC, Inertia Placement, and Dynamic Inertia Placement. As expected, the Linear MPC formulation is better in terms of cost and energy injection/absorption to control frequency. This finding encourages researchers to continue designing controllers in order to attain such optimality without having to optimize in real time (closed-loop MPC).

Another relevant finding is the fact that the Dynamic Inertia Placement proves to be more efficient in terms of cost and energy usage of the controller compared to the classical Inertia Placement case. This finding sheds light on the importance of modeling dynamics over time assuming temporal variability in the system's inertia. Additionally, it highlights the importance of designing a more flexible controller that would adapt over time. For future work we plan to study stability of the hybrid system and design a controller that is more efficient in terms of energy usage than the current virtual inertia schemes. We also plan to characterize the disturbances at each node of the network and to model the switching of modes of the hybrid system with data-driven approaches.

Chapter 3

Frequency Regulation using Learned Controllers

3.1 Preface

The work in this Chapter corresponds to the publication titled "Frequency Regulation using Data-Driven Controllers in Power Grids with Variable Inertia due to Renewable Energy" by Patricia Hidalgo-Gonzalez, Rodrigo Henriquez-Auba, Duncan S. Callaway and Claire J. Tomlin [49] and "Frequency Regulation using Sparse Learned Controllers in Power Grids with Variable Inertia due to Renewable Energy" by Patricia Hidalgo-Gonzalez, Rodrigo Henriquez-Auba, Duncan S. Callaway and Claire J. Tomlin [50]. We presented this work at the 2019 IEEE Power & Energy Society General Meeting in Atlanta, Georgia, United States and at IEEE 58th Annual Conference on Decision and Control in Nice, France.

3.2 Frequency Regulation using Data-Driven Control

Introduction

Our earlier work [48], introduces a new modeling framework for power system dynamics to simulate a time-varying evolution of rotational inertia coefficients in the network. To do this, power dynamics are modeled as a hybrid system in which each mode corresponds to a rotational inertia regime. The novelty of this work is the design of a fixed and stable frequency controller under a paradigm of time-varying inertia. We choose a fixed controller because it is simpler to implement (compared to a time dependent controller) given the existing droop control in the grid. In addition, the controller we propose does not require information about the current hybrid mode of the system or its uncertainty. Thus, our contributions are the following:

- In the time-varying framework for power dynamics, we design a controller with fixed gains, proportional to the system's states (angles and frequencies). We design the

controller by learning its parameters from the optimal control solution of a hybrid systems linear-quadratic regulator (LQR) formulation of power dynamics.

- For each mode of the hybrid system, we test the performance of the learned controller against the optimal time-varying controller from the LQR formulation.
- We add virtual inertia control (linear on the derivative of the frequency) to guarantee stability for all modes of the hybrid system when using the learned controller.

We conclude that for the hybrid power dynamics formulation it is possible to design, through learning, a static frequency controller proportional to the system's states that performs similarly to the optimal time-varying controller from LQR. It is possible to guarantee stability for the hybrid system when we add virtual inertia to the learned control.

The rest of the Section is organized as follows: problem formulation, stability analysis of the hybrid system and analysis of the performance of the controller in different settings, and finally, we conclude with our main findings.

Problem Formulation

Power grid dynamics as a hybrid system

We consider an electric power grid modeled as a graph with n nodes and $n(n-1)/2$ possible edges connecting them. The swing equation model, based on the direct current approximation [82], used for the network is given by

$$m_i\ddot{\theta}_i + d_i\dot{\theta}_i = p_{\text{in},i} - \sum_{j\in\mathcal{N}_i} b_{ij}(\theta_i - \theta_j), \quad i \in \{1,\dots,N\} \tag{3.1}$$

where m_i corresponds to the equivalent rotational inertia in node i, d_i is the droop control, $p_{\text{in},i}$ represents power mismatch at node i, $\mathcal{N}_i$ is set of nodes connected by an edge to node i, b_{ij} is the susceptance of the transmission line between nodes i and j, and θ_i is the voltage phase angle at node i. The state space representation of the model can be written as

$$\begin{bmatrix}\dot{\theta}\\ \dot{\omega}\end{bmatrix} = \begin{bmatrix}0 & I\\ -M^{-1}L & -M^{-1}D\end{bmatrix}\begin{bmatrix}\theta\\ \omega\end{bmatrix} + \begin{bmatrix}0\\ M^{-1}\end{bmatrix} p_{\text{in}} \tag{3.2}$$

where the states correspond to the stacked vector of angles and frequencies at each node $(\theta^\top, \omega^\top)^\top \in \mathbb{R}^{2n}$, $M = \text{diag}(m_i)$ is a diagonal matrix with rotational inertia coefficients, $D = \text{diag}(d_i)$ is a diagonal matrix with droop control coefficients, I is the $n \times n$ identity matrix, p_{in} corresponds to the power input, and $L \in \mathbb{R}^{n,n}$ is the Laplacian of the network. The network Laplacian is defined as $\ell_{ij} = -b_{ij}$ when $i \neq j$, and $\ell_{ii} = \sum_{j\in\mathcal{N}_i} b_{ij}$.

To capture the variability of the inertia coefficients, we model power dynamics with the formulation introduced in Section 2.3. Frequency dynamics are modeled as a Switched-Affine

hybrid system [14], where each mode has a predetermined set of values of equivalent inertia m_i at each node [48]. Thus, the power dynamics are given by

$$\begin{bmatrix}\dot{\theta}\\ \dot{\omega}\end{bmatrix} = \underbrace{\begin{bmatrix}0 & I\\ -M_{q(t)}^{-1}L & -M_{q(t)}^{-1}D\end{bmatrix}}_{\hat{A}_{q(t)}}\begin{bmatrix}\theta\\ \omega\end{bmatrix} + \underbrace{\begin{bmatrix}0\\ M_{q(t)}^{-1}\end{bmatrix}}_{\hat{B}_{q(t)}} p_{\text{in}} \tag{3.3}$$

where $M_{q(t)}$ represents the inertia matrix in the mode $q(t) \in \{1, \dots, m\}$. Using a zero-order hold discretization with time step T_s, we obtain the discretized time-varying dynamics

$$x_{t+1} = A_{q(t)}x_t + B_{q(t)}u_t \tag{3.4}$$

where x_t is the stacked vector of discretized angles and frequencies, $(\theta_t^\top, \omega_t^\top)^\top$, u_t is the control action by generators and converters, $A_{q(t)} = \exp(\hat{A}_{q(t)}T_s)$ and $B_{q(t)} = \int_0^{T_s} \exp(\hat{A}_{q(t)}\tau)\hat{B}_{q(t)}d\tau$.

In this work, as it was described in Section 2.3, the switching between modes occurs between each time step, and it is given by a uniform distribution with the following possible outcomes: no change of inertia, increase of inertia, or decrease of inertia. For simplicity, for a given mode $q(t)$ we assume the same inertia coefficient for all nodes $M_q = m_q I_{n\times n}$. We assume that power electronics converters exist at every node to provide/absorb power, i.e. $p_{\text{in},t} = u_t \in \mathbb{R}^n$.

Using an LQR formulation we study the problem of returning to a steady-state configuration x_{ss}, assuming a perturbed initial condition $x_0 \neq x_{\text{ss}}$ due to a contingency.

Optimal frequency control for low and time-varying rotational inertia coefficients

To minimize an objective function where the states and controllers are decision variables we consider the LQR formulation

$$\begin{aligned}\min_{\boldsymbol{x},\boldsymbol{u}} \ & \sum_{t=0}^{T} x_t^\top Q x_t + u_t^\top R u_t\\ \text{s.t.} \ & x_0 = x^{(0)}\\ & x_{t+1} = A_{q(t)}x_t + B_{q(t)}u_t, \ t \in \{0, T-1\}\end{aligned} \tag{3.5}$$

where Q is a positive semidefinite matrix, R is a positive definite matrix, and $x^{(0)}$ is the initial state. Depending on the modeling goal, matrices Q and R can be modified to promote a specific behavior. The optimal solution of (3.5) for a fixed mode q in the entire time horizon (i.e. a linear time-invariant system) and with $T \to \infty$, can be found via the discrete time algebraic Ricatti equation [14]:

$$\begin{aligned}P_q &= A_q^\top P_q A_q - A_q^\top P_q B_q (R + B_q^\top P_q B_q)^{-1} B^\top P_q A_q + Q\\ K_q &= (R + B_q^\top P_q B_q)^{-1} B_q^\top P_q A_q\\ u_t &= -K_q x_t\end{aligned} \tag{3.6}$$

For a hybrid system with time-varying inertia, (3.5) is a Quadratic Programming problem that can be solved directly, using for example CVX [44]. We use the solution of (3.5) as a benchmark of an optimal controller for our problem.

Data-driven based controller

In the presented framework of variable inertia we are interested in learning a time-invariant controller of the form $u_t = -K_{\mathrm{L}} x_t$ where K_{L} is a constant matrix. The training dataset $(\boldsymbol{x}^{(k)}, \boldsymbol{u}^{(k)})$ we use comes from the optimal solution to (3.5) under different scenarios $k = \{1, \dots, K\}$. The learning algorithm we use is least-squares:

$$\min_{K_{\mathrm{L}}} \sum_{k=1}^{K} \sum_{t=1}^{T} \left|\left| u_t^{(k)} - K_{\mathrm{L}} x_t^{(k)} \right|\right|_2^2 \tag{3.7}$$

It is interesting to notice that when we solve (3.5) for a single mode q (in the entire time horizon) and a sufficiently long time horizon T, least-squares returns the analytical solution K_q from the LQR problem (3.6). This is because the optimal controller from (3.5) is linear on the states, and with sufficient training data $(\boldsymbol{x}^{(k)}, \boldsymbol{u}^{(k)})$, (3.7) is a convex optimization program that achieves K_q, and hence the optimal value is equal to zero.

We assume a stressed case in which the equivalent inertia can change rapidly over time. Thus, inertia is allowed to change over time steps in each scenario. However, an equivalent training set can be generated by fixing the mode q at each scenario k, and only changing the mode between different scenarios. Each scenario in this training set would represent, for instance, a different hour of the year. During an hour, inertia could be considered fixed, and a different optimal controller would be obtained for each scenario.

Incorporating virtual inertia in the system

Depending on how we generate the training set $(\boldsymbol{x}^{(k)}, \boldsymbol{u}^{(k)})$, the controller we propose may not be stable in modes where the inertia is too low. The learned controller may not be fast enough to compensate the rate of change of the frequency. As an alternative, a controller that depends on the derivative of the frequency, $K_{\mathrm{V}}\dot{\omega}$, can be used as a virtual inertia resource for the system. Indeed, consider the fixed inertia continuous time system and assume a controller of the form

$$u = -K_{\mathrm{L}}(\theta^\top, \omega^\top)^\top - K_{\mathrm{V}}\dot{\omega} = -K_{\mathrm{L}} x - \tilde{K}_{\mathrm{V}} \dot{x} \tag{3.8}$$

where $\tilde{K}_{\mathrm{V}} = [0 \;\; K_{\mathrm{V}}]$, then:

$$\dot{x} = \begin{bmatrix} 0 & I \\ -M^{-1}L & -M^{-1}D \end{bmatrix} x - \begin{bmatrix} 0 \\ M^{-1} \end{bmatrix} (K_{\mathrm{L}} x + \tilde{K}_{\mathrm{V}} \dot{x})$$

Rearranging terms the system can be written

$$(I + \hat{B}\tilde{K}_V)\dot{x} = (\hat{A} - \hat{B}K_{\mathrm{L}})x$$

and hence

$$\begin{aligned}\dot{x} &= (I + \hat{B}\tilde{K}_V)^{-1}(\hat{A} - \hat{B}K_{\mathrm{L}})x \\ &= \begin{bmatrix} I & 0 \\ 0 & I + M^{-1}K_{\mathrm{V}} \end{bmatrix}^{-1} \\ &\quad \times \begin{bmatrix} 0 & I \\ -M^{-1}(L + K_{\mathrm{L},\theta}) & -M^{-1}(D + K_{\mathrm{L},\omega}) \end{bmatrix} x \\ &= \begin{bmatrix} 0 & I \\ -\tilde{M}^{-1}(L + K_{\mathrm{L},\theta}) & -\tilde{M}^{-1}(D + K_{\mathrm{L},\omega}) \end{bmatrix} x\end{aligned}$$

where $\tilde{M} = M(I + M^{-1}K_{\mathrm{V}}) = M + K_{\mathrm{V}}$ provides a new system wide equivalent inertia due to the virtual inertia controller K_{V}. To determine a proper K_{V} we develop a heuristic using a bisection method. We assume K_{V} of the form $K_{\mathrm{V}} = k_{\mathrm{v}} I_{n\times n}$. Iterating over k_{v}, and assuming that $\dot{x}$ in the right hand side of the discretized system can be approximated by $[x_t - x_{t-1}]T_s^{-1}$, we modify k_{v} until the discretized closed loop system for the low inertia modes has all its eigenvalues inside the unit circle, making it stable.

Simulations and Results

Data description

Errata: The values we use for the elements, m, in the diagonal matrix M in this work are inertia values, however $m = \frac{2hS}{w}$, where h is the inertia coefficient, S the rated power, and w the angular frequency. Therefore, we test the system under lower values of inertia than intended. We expect results to hold given that this change would imply re-scaling our matrices A and B with a diagonal and nonsingular matrix. For such transformation, stability properties of the hybrid system hold.

Using MATLAB® we model the twelve-bus three-region network (Fig. 2.1) that was described in Section 2.4, which has also been used in [15], [82], [48] and [59]. Each node has two states (angle and frequency). Table 2.1 shows the parameters of the network.

We assume the same rotational inertia in all buses for a given time step t ($m_i(t) = m(t)$ for all i). This implies a similar fraction of renewable energy generation for all nodes, but this assumption can be easily extended. Each mode of the hybrid system is given by one value of inertia. For the study case we predefined possible inertia values for the system: $m_q \in \{0.2, 0.5, 1, 1.5, 2, 2.5, 3, 3.5, 5, 9\}$. The average of this set of possible inertia values is 2.8 seconds, which is equivalent to having 28 percent of thermal generation (10 s of inertia) and 72 percent of RES with zero inertia. Each simulation starts with 2 seconds of inertia (mode q_5), and from there– based on a uniform distribution draw– the inertia (hybrid mode) of the system at time $t+1$ will remain the same, increase, or decrease. In our simulations we only allow the possibility to change modes every 1, 4 or 10 time steps. For all the simulations we use a time step of $T_s = 0.01$s. We generate $K = 400$ scenarios of 7 seconds each ($T = 700$). The initial conditions we use in (3.5) are randomly drawn from a normal distribution with

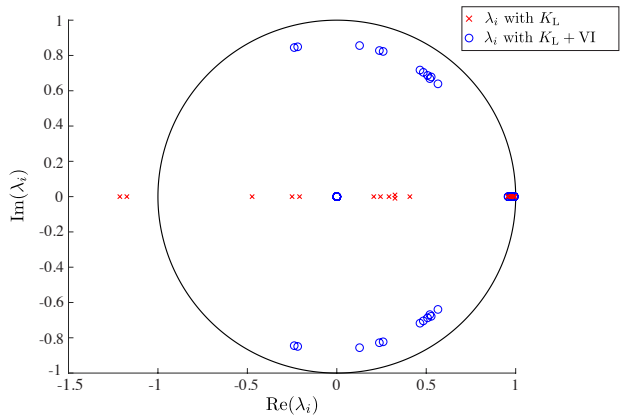

Figure 3.1: Eigenvalue placement for the closed loop system in mode q_1 using the learned controller K_L (crosses) and adding virtual inertia control $K_\mathrm{L} + \mathrm{VI}$ (circles).

zero mean and unitary variance. The training set we use to learn the controller K_L using (3.7) are the optimal solutions $(\boldsymbol{x}^{(k)}, \boldsymbol{u}^{(k)})$ from (3.5).

Stability analysis

The design of the controller K_L through learning provides a stable closed loop system $A_q - B_q K_\mathrm{L}$ for every mode except for q_1. To correct this issue we use an approximated virtual inertia controller $\tilde{K}_\mathrm{V}(x_t - x_{t-1})T_s^{-1}$ with $\tilde{K}_\mathrm{V} = [0 \quad K_\mathrm{V}]$. The new dynamics can be written as:

$$\begin{aligned} x_{t+1} &= A_q x_t + B_q[-K_\mathrm{L} x + T_s^{-1}\tilde{K}_\mathrm{V}(x_t - x_{t-1})] \\ &= [A_q - B_q(K_\mathrm{L} - T_s^{-1}\tilde{K}_\mathrm{V})]x_t - T_s^{-1}B_q\tilde{K}_\mathrm{V}x_{t-1} \end{aligned}$$

Augmenting the states as $z_{t+1} = (x_t^\top, x_{t+1}^\top)^\top$, our new system can be written as:

$$z_{t+1} = \begin{bmatrix} 0_{2n\times 2n} & I_{2n\times 2n} \\ -T_s^{-1}B_q\tilde{K}_\mathrm{V} & A_q - B_q(K_\mathrm{L} - T_s^{-1}\tilde{K}_V) \end{bmatrix} z_t \tag{3.9}$$

For the learned controller, adding a virtual controller of the form $K_\mathrm{V} = 0.15 I_{n\times n}$ results in eigenvalues of the augmented system for mode q_1 inside the unitary circle. This is depicted in Figure 3.1, where it can be observed that there are two modes that are unstable for the closed loop system only using the learned controller (in red). When we incorporate the virtual inertia controller all modes are stable (in blue).

Controllers' comparison for fixed inertia

For each mode q, we compare the performance of the learned controller K_L and the learned controller with virtual inertia, $K_\mathrm{L} + \mathrm{VI}$, against the optimal controller from the LQR

Table 3.1: Comparison of learned controller (K_{L}) and learned controller with virtual inertia (K_{L} + VI) against optimal control from LQR under different inertia modes. Units are in percentages (%).

Metric	q_1	q_2	q_3	q_4	q_5	q_6	q_7	q_8	q_9	q_{10}
$\|\|f_{K_{\mathrm{L}}}\|\|_\infty$	Unstable	−21.1	−10.4	−5.4	−1.1	2.6	5.9	8.8	11.9	14.4
$\|\|f_{K_{\mathrm{L}}+\mathrm{VI}}\|\|_\infty$	106.7	−16.1	−8.8	−4.3	−0.2	3.5	6.5	9.5	12.4	14.4
$\|\|f_{K_{\mathrm{L}}}\|\|_2$	Unstable	−9.0	−7.1	−5.5	−3.9	−2.5	−1.1	0.2	3.7	11.2
$\|\|f_{K_{\mathrm{L}}+\mathrm{VI}}\|\|_2$	−7.2	−8.9	−7.4	−5.8	−4.3	−2.9	−1.5	−0.3	3.2	10.9
$\|\|u_{K_{\mathrm{L}}}\|\|_\infty$	Unstable	3.2	−2.7	−5.9	−8.2	−10.2	−11.9	−13.3	−17.1	−15.2
$\|\|u_{K_{\mathrm{L}}+\mathrm{VI}}\|\|_\infty$	87.9	3.2	−2.7	−5.9	−8.2	−10.2	−11.9	−13.3	−17.1	−15.2
$\|\|u_{K_{\mathrm{L}}}\|\|_1$	Unstable	13.3	6.2	2.5	−0.3	−2.7	−4.7	−6.5	−11.0	−19.7
$\|\|u_{K_{\mathrm{L}}+\mathrm{VI}}\|\|_1$	78.1	19.0	8.6	4.2	1.1	−1.4	−3.6	−5.5	−10.2	−19.1
$\|\|u_{K_{\mathrm{L}}}\|\|_2$	Unstable	12.2	6.0	4.6	4.4	4.6	4.9	5.3	6.5	9.2
$\|\|u_{K_{\mathrm{L}}+\mathrm{VI}}\|\|_2$	45.2	16.4	8.7	6.6	5.9	5.8	5.9	6.1	7.1	9.4
$J_{K_{\mathrm{L}}}$	Unstable	29.8	39.9	49.2	57.8	65.7	73.2	80.2	98.9	138.1
$J_{K_{\mathrm{L}}+\mathrm{VI}}$	39.1	31.6	40.2	49.0	57.4	65.3	72.6	79.5	98.1	137.3

formulation. Table 3.1 shows peaks (ℓ_∞ norm), ℓ_2 and ℓ_1 norms for frequency deviations f and control inputs u, and objective function values J for the different controllers under different inertia modes (columns). The values in table 3.1 represent increases in percentage with respect to the metrics for the LQR controller. The learned controller is unstable in the critical inertia regime (q_1, lowest inertia). When adding virtual inertia, the controller becomes stable. The objective values for the data-driven controllers are greater than for the LQR. This is intuitive because the learned controllers have fixed parameters over time while the LQR changes its parameters for each mode. The ℓ_2 norm for the frequency is in general smaller for the learned controllers than for the LQR controllers. On the other hand, the ℓ_2 norm of the control action is higher than in the LQR case.

Controllers' comparison for time-varying inertia

We evaluate the performance of different controllers in a simulation of the hybrid system switching among different inertia modes. We assume that the system starts in mode q_2 = 0.5s, and possible transitions of inertia can occur every 4 time steps. Figure 3.2 depicts the evolution of frequency deviation in node 1, under 5 different controllers for an initial condition $f_0 = -0.15$ Hz at every node. The controllers we use are the following: In blue, the frequency is controlled using the learned controller K_{L}. In red, we show the learned and virtual inertia controller $K_{\mathrm{L}} + \mathrm{VI}$ (ensure stability). Similarly, cyan depicts a controller that uses K_{L} and virtual inertia only when the system is in the unstable mode q_1. In black and green we use the optimal controllers K_q obtained from (3.6) for modes q_3 = 1s and

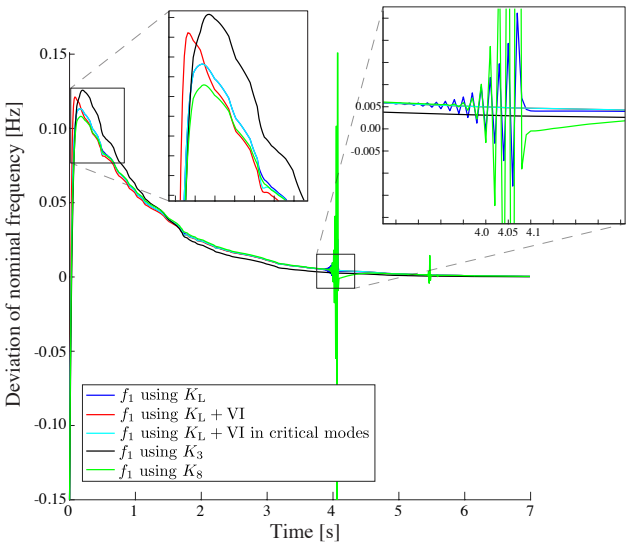

Figure 3.2: Frequency deviations for node 1 for 5 different controllers from a hybrid system simulation.

$q_8 = 5$s, respectively. Around 4 seconds of the simulation, the system enters mode q_1 for around 0.4 seconds. This provokes an instability for controllers K_8 and K_L. After leaving the unstable mode the frequency is stabilized again. The other controllers are able to maintain stability in all the modes. In addition, key differences can be observed at the beginning of the simulation. Controller K_3 shows the highest overshoot of the simulation, while controller $K_L + \text{VI}$ (in red) is the fastest to peak due to the usage of the derivative of the frequency. Finally, the frequency for the first and third case (in blue and cyan) are almost identical except when the system is in the mode q_1. This shows that if we can detect when the system is in critical modes, we can apply virtual inertia control only when it is necessary to obtain a better performance.

Conclusions

In this work we propose a new framework for obtaining a constant data-driven controller for uncertain and time-varying power system dynamics. This is relevant because it can be intractable to solve frequency dynamics in real time (time-varying LQR) in large power networks. In addition, time-varying controllers, as the one from LQR, rely in the ability to predict or identify the current mode of the hybrid system. Finally, given the existing infrastructure and droop control, it would be simpler to implement a proportional controller with fixed gains compared to a time-varying control.

We use a switched affine hybrid system, where its modes change based on the changes of inertia in the system [48], we find optimal controllers using an LQR formulation. We use the solution (x, u) from the LQR as a dataset to train a fixed controller. We test our learned

controller in different modes against optimal controllers. Results show that our learned controller can be used to obtain a similar performance as the optimal LQR controllers in the different modes. Finally, we show that adding a virtual inertia controller can stabilize the system for low inertia modes. This highlights the importance of using more flexible controllers when considering temporal variability in the system dynamics. For future work we plan to explore the performance of our controller with AC power flow, voltage dynamics, machine dynamics and power electronics (inverters) approximate dynamics. We will also compare our proposed controller with a robust controller. We also plan to study different learning algorithms with new features to test the efficiency of the learned controller, in particular promoting sparsity and information requirements using Lasso or Block Sparse Regression.

3.3 Frequency Regulation using Sparse Learned Controllers

Introduction

Our publication [48], proposes for the first time a new modeling framework for power system dynamics to simulate a time-varying evolution of inertia in the network due to the time dependent participation of RES. We model power dynamics using a Switched-Affine hybrid system to consider different modes corresponding to different inertia coefficients. Time-varying power system dynamics pose a new set of challenges for frequency control. Now control design must take into account the time dependence of the dynamical model.

In recent years, techniques from machine learning have become popular in the field of control design [67], [78]. Interesting applications have been developed for distributed control of power flow in power systems [89], [11]. In [49] we design a fixed and stable frequency controller under the paradigm of time-varying inertia. We use angles, frequencies and derivatives of the frequencies as features or input for the controllers. An interesting question that stems from this work is the potential trade-off of restricting communication between controllers. Information availability between nodes entails a cost (sensing and broadcasting), thus designing communication restricted control schemes, i.e. sparse controllers, is of particular interest in power systems. In a similar line of thought, [29] studies from an information theoretic approach, the trade-off between performance and communication between control agents.

In this Section we study how sparsity can be induced in a time-invariant learned controller for a time-varying dynamical system. This application is of particular interest because of its potential for aiding safe RES integration. Additionally, power system dynamics are a relevant application for this control research question thanks to the added complexity of operating on a graph (transmission network). Finally, information availability between nodes entails a cost (sensing and broadcasting), thus designing communication-restricted control schemes is of particular interest in power systems.

The contribution of this work is the design of a sparse and guaranteed stable time-invariant frequency controller for time-varying power dynamics. We also test the improvement in performance metrics and stability of introducing more features to the controller than the minimum identified. Our work can be summarized as follows:

- In the time-varying framework for power dynamics, we design a controller with fixed gains, proportional to the system's states (angles and frequencies). We design the controller by learning its parameters from a training set generated by optimally solving a Model Predictive Control (MPC) problem for different scenarios of frequency regulation. We add virtual inertia to the controller to guarantee stability in all inertia modes [49].
- To test how sparse our learned controller can be and to investigate the trade-off between communication requirements and performance/stability we use a Lasso regression [94] for the controller at each node. We vary widely the sensitivity parameter associated to the regularization term in the learning problem.
- We shed light on the relevance of graph topology and optimal feature selection for the learned controller at each node.
- We show for some cases that it is not possible for the learned controller to steer frequency deviation back to zero when facing inertia coefficients that are not included in the training set. This validates the importance of controller design taking into account time-varying power dynamics.

We conclude that it is possible to design via learning a sparse, time-invariant and stable controller for the hybrid power dynamics formulation. Furthermore, we show that it is possible to reduce the number of features in the controller (from 22 to 10 in our case study) without disrupting performance and stability. Additionally, we depict how enabling more communication beyond a threshold does not improve performance or stability.

The rest of the Section is organized as follows: problem formulation, simulations, performance and stability analyses, and conclusions, our main findings and future work.

Problem Formulation

Power system dynamics as a hybrid system

Similarly as in Section 2.3 and 3.2, we model an electric power system network as a graph with n nodes and $n(n-1)/2$ possible edges. Using the direct current approximation for power flow, we can write the swing equation [82] as

$$m_i\ddot{\theta}_i + d_i\dot{\theta}_i = p_i - \sum_{j\in\mathcal{N}_i} b_{ij}(\theta_i - \theta_j), \quad i \in \{1,\dots,N\} \tag{3.10}$$

where m_i corresponds to the equivalent rotational inertia in node i, d_i is the droop control or frequency damping coefficient, p_i represents net power injection at node i, $\mathcal{N}_i$ is set of nodes connected by an edge to node i, b_{ij} is the susceptance of the transmission line between nodes i and j, and θ_i is the voltage phase angle at node i. The state space representation of the model can be written as

$$\begin{bmatrix}\dot{\theta}\\ \dot{\omega}\end{bmatrix} = \begin{bmatrix}0 & I\\ -M^{-1}L & -M^{-1}D\end{bmatrix}\begin{bmatrix}\theta\\ \omega\end{bmatrix} + \begin{bmatrix}0\\ M^{-1}\end{bmatrix} p_{\text{in}} \tag{3.11}$$

where the states correspond to the stacked vector of angles and frequencies at each node $(\theta^\top, \omega^\top)^\top \in \mathbb{R}^{2n}$, the frequency, ω, is the derivative of the angle, i.e. $\omega = \dot{\theta}$, $M = \text{diag}(m_i)$ is a diagonal matrix with rotational inertia coefficients, $D = \text{diag}(d_i)$ is a diagonal matrix with droop control coefficients, I is the $n \times n$ identity matrix, p_{in} corresponds to the power input, and $L \in \mathbb{R}^{n\times n}$ is the Laplacian of the network. The network Laplacian is defined as $\ell_{ij} = -b_{ij}$ when $i \neq j$, and $\ell_{ii} = \sum_{j\in\mathcal{N}_i} b_{ij}$.

To capture the variability of the inertia coefficients, we model power dynamics with the formulation introduced in Section 2.3. Frequency dynamics are modeled as a Switched-Affine hybrid system, where each mode has a predetermined set of values of equivalent inertia m_i at each node. The evolution of the inertia on the system depends on the current online generators and the connected power electronics converters. In this work, as it was described in Section 2.3, the inertia at each time step t evolves as an exogenous input. Thus, power dynamics are given by

$$\begin{bmatrix}\dot{\theta}\\ \dot{\omega}\end{bmatrix} = \underbrace{\begin{bmatrix}0 & I\\ -M_{q(t)}^{-1}L & -M_{q(t)}^{-1}D\end{bmatrix}}_{\hat{A}_{q(t)}}\begin{bmatrix}\theta\\ \omega\end{bmatrix} + \underbrace{\begin{bmatrix}0\\ M_{q(t)}^{-1}\end{bmatrix}}_{\hat{B}_{q(t)}} p_{\text{in}} \tag{3.12}$$

where $M_{q(t)}$ represents the inertia matrix in the mode $q(t) \in \{1, \ldots, m\}$. Using a zero-order hold discretization with time step T_s, we obtain the discretized time-varying dynamics

$$x_{t+1} = A_{q(t)}x_t + B_{q(t)}u_t \tag{3.13}$$

where x_t is the stacked vector of discretized angles and frequencies, $(\theta_t^\top, \omega_t^\top)^\top$, u_t is the discretized control action by generators and converters, $A_{q(t)} = \exp(\hat{A}_{q(t)}T_s)$ and $B_{q(t)} = \int_0^{T_s} \exp(\hat{A}_{q(t)}\tau)\hat{B}_{q(t)}d\tau$.

Generation of training set from optimal frequency control

In order to learn a time-invariant controller, we generate a training set from solving an MPC formulation. We minimize an objective function where the states and controllers are

decision variables

$$\begin{aligned} \min_{\boldsymbol{x},\boldsymbol{u}} \ & \sum_{t=0}^{T} x_t^\top Q x_t + u_t^\top R u_t \\ \text{s.t.} \ & x_0 = x^{(0)} \\ & x_{t+1} = A_{q(t)} x_t + B_{q(t)} u_t, \ t \in \{0, T-1\} \end{aligned} \tag{3.14}$$

$Q \in \mathbb{R}^{2n \times 2n}$ is a positive semidefinite matrix, $R \in \mathbb{R}^{n \times n}$ is a positive definite matrix, $x^{(0)}$ is the initial state, and T is the time horizon. Depending on the modeling goal, matrices Q and R can be modified to promote a specific behavior. This is a Quadratic Programming problem that can be solved directly, using for example CVX [44]. We describe the specifications for the simulations of this work in the Section "Data and simulation description".

Learned controller enhancing sparsity

In the setting of hybrid power dynamics with variable inertia, our control design via learning has two objectives:

- Learn a time-invariant frequency controller of the form $u_t = K_{\mathrm{L}} x_t$, where K_{L} is a constant matrix.
- Explore to what extent communication between nodes can be restricted to design a stable frequency controller. Communication between nodes i and j has to occur when the (i, j) entry of K_{L} is nonzero.

To accomplish these objectives we use a Lasso regression [94], [87] to learn optimal controllers at each node. The training set $(\boldsymbol{x}^{(s)}, \boldsymbol{u}^{(s)})$ we utilize comes from the optimal solution to (3.14) under different initial states. Each trajectory or optimal solution $(\boldsymbol{x}^{(s)}, \boldsymbol{u}^{(s)})$ for a given initial state defines a scenario s, with $s = \{1, \ldots, S\}$. We solve a Lasso regression for each node i as an independent controller $u_{i,t} = \beta_i^\top x_t$, where $\beta_i^\top \in \mathbb{R}^{1 \times 2n}$ is a row vector that has as components the gains of the controller at node i (i.e. $K_{\mathrm{L}} = \left[\beta_1 \ldots \beta_n\right]^\top$):

$$\min_{\beta_i} \ \sum_{s=1}^{S} \sum_{t=1}^{T} \left|\left| u_{i,t}^{(s)} - \beta_i^\top x_t^{(s)} \right|\right|_2^2 + \lambda ||\beta_i||_1 \tag{3.15}$$

The states that multiply the resulting nonzero components of the vector $\beta_i^\top$ correspond to the features that node i uses for its controller $u_{i,t}$. We solve (3.15) for each node for a range of the regularization sensitivity parameter λ using cross-validation. We vary the sensitivity parameter λ from zero (Least-Squares, i.e. using all possible $2n$ states as features) up to a value that would result in only one nonzero coefficient in the vector β_i.

Incorporating virtual inertia in the control

As we show in [49], to guarantee stability of a learned controller for hybrid power dynamics with variable inertia we include virtual inertia: a controller proportional to the derivative of the frequency, $K_{\mathrm{V}}\dot{\omega}$. To provide some intuition, consider a fixed inertia continuous time system and assume a controller of the form

$$u = K_{\mathrm{L}}(\theta^{\top}, \omega^{\top})^{\top} + K_{\mathrm{V}}\dot{\omega} = K_{\mathrm{L}}x + \tilde{K}_{\mathrm{V}}\dot{x} \tag{3.16}$$

where $\tilde{K}_{\mathrm{V}} = [0 \;\; K_{\mathrm{V}}]$, then:

$$\dot{x} = \begin{bmatrix} 0 & I \\ -M^{-1}L & -M^{-1}D \end{bmatrix} x + \begin{bmatrix} 0 \\ M^{-1} \end{bmatrix} (K_{\mathrm{L}}x + \tilde{K}_{\mathrm{V}}\dot{x}) \tag{3.17}$$

Rearranging terms the system can be written as

$$\begin{aligned} \dot{x} &= (I - \hat{B}_{q(t)}\tilde{K}_V)^{-1}(\hat{A}_{q(t)} + \hat{B}_{q(t)}K_{\mathrm{L}})x \\ &= \begin{bmatrix} I & 0 \\ 0 & I - M_{q(t)}^{-1}K_{\mathrm{V}} \end{bmatrix}^{-1} \\ &\quad \times \begin{bmatrix} 0 & I \\ -M_{q(t)}^{-1}(L - K_{\mathrm{L},\theta}) & -M_{q(t)}^{-1}(D - K_{\mathrm{L},\omega}) \end{bmatrix} x \\ &= \begin{bmatrix} 0 & I \\ -\tilde{M}_{q(t)}^{-1}(L - K_{\mathrm{L},\theta}) & -\tilde{M}_{q(t)}^{-1}(D - K_{\mathrm{L},\omega}) \end{bmatrix} x \end{aligned}$$

where $\tilde{M}_{q(t)} = M_{q(t)}(I - M_{q(t)}^{-1}K_{\mathrm{V}}) = M_{q(t)} - K_{\mathrm{V}}$ provides a new system wide equivalent inertia due to the virtual inertia controller K_{V}. To determine a proper K_{V} we utilize a heuristic using a bisection method. We assume K_{V} of the form $K_{\mathrm{V}} = k_{\mathrm{v}}I_{n\times n}$. We iterate over k_{v} until the closed loop system for each inertia mode has all its eigenvalues with negative real part, stabilizing the system's dynamics.

Simulations and Analysis

Data and simulation description

Errata: The values we use for the elements, m, in the diagonal matrix M in this work are inertia values, however $m = \frac{2hS}{w}$*, where h is the inertia coefficient, S the rated power, and w the angular frequency. Therefore, we test the system under lower values of inertia than intended. We expect results to hold given that this change would imply re-scaling our matrices A and B with a diagonal and nonsingular matrix. For such transformation, stability properties of the hybrid system hold.*

We use MATLAB® to model the twelve-bus three-region network (Fig. 2.1) that was described in Section 2.4, which has also been used in [15], [82], [48], and [49] and [59]. Each node has two states (angle and frequency). Table 2.1 shows the parameters of the network.

Notice bus 11 is directly connected to 12, thus we are effectively simulating an $n = 11$ node network.

We assume the same rotational inertia in all buses for a given time step t ($m_i(t) = m(t)$ for all i). This implies a similar fraction of renewable energy generation for all nodes, but this assumption can be easily extended. Each mode of the hybrid system is given by one value of inertia. For the study case we predefined possible inertia values for the system: $m_q \in \{0.2, 0.5, 1, 1.5, 2, 2.5, 3, 3.5, 5, 9\}$. The average of this set of possible inertia values is 2.8 seconds, which is equivalent to having 28 percent of thermal generation (10 s of inertia) and 72 percent of RES with zero inertia.

To generate the training set from (3.14), each scenario s starts with 2 seconds of inertia, and from there– based on a uniform distribution draw– the inertia (hybrid mode) of the system at time $t + 1$ will remain the same, increase, or decrease. We assume that power electronics converters and batteries exist at every node as control agents to provide/absorb power. The time interval T_s we use is 0.01 seconds and the time horizon T is 400, equivalent to 4 seconds. For each scenario s, the initial states are drawn randomly from a normal distribution with zero mean and 1.3Hz of variance to represent different perturbations in the system. We simulate $S = 400$ scenarios.

To learn the controllers, we optimize (3.15) for each node using 100 possible values for the regularization parameter λ and a 10-fold cross-validation. This allows us to obtain 100 different controllers for each node. These controllers show decreasing number of features as λ increases, ranging from all 22 ($2n$) states down to zero. In order to analyze results we choose to study the performance, stability and feature selection of a subset of controllers. We group controllers by the number of features used, i.e. number of nonzero elements in β_i. Specifically, we choose a control design where all nodes use at most the following number of features: 4, 5, 6, 10, 14, 17, and all 22 states. To all the learned controllers we add virtual inertia as we describe in 3.3. For the rest of the manuscript, each time we mention the learned controllers they also include virtual inertia.

Performance

In this section we explore the performance of the proposed learned controllers under different inertia modes for the hybrid system. Fig. 3.3 shows the box plot of the mean squared error (MSE) from training those controllers using cross-validation. As expected, the usage of more features allows to obtain a controller with reduced MSE in the training exercise. Nevertheless, the MSE does not significantly decrease beyond using 10 features. This sheds light on the possibility to substantially reduce the usage of features without losing significant performance. To show this we explore two performance metrics. One metric is the total absolute value of the control input and the other metric is the total absolute value of frequency deviation:

$$\langle u \rangle = \int_0^T \sum_{i=1}^{n} |u_i(t)| dt, \qquad \langle \omega \rangle = \int_0^T \sum_{i=1}^{n} |\omega_i(t)| dt$$

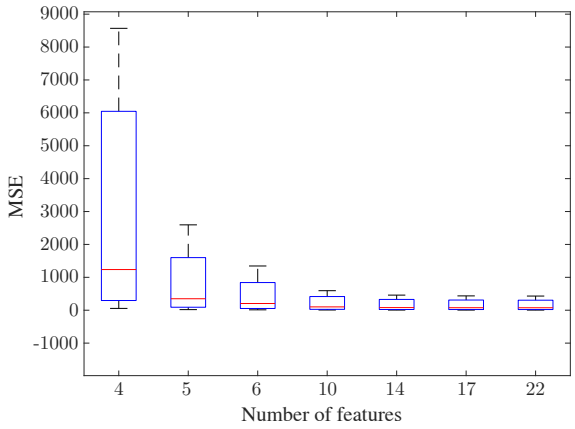

Figure 3.3: Mean Squared Error (MSE) from training and cross-validating controllers with different numbers of features.

Table 3.2: Performance metrics for learned controller under different inertia systems.

	$\langle u \rangle = \int_0^T \sum_{i=1}^n \lvert u_i(t) \rvert dt$		$\langle \omega \rangle = \int_0^T \sum_{i=1}^n \lvert \omega_i(t) \rvert dt$	
Number of features	$m = 0.2$s	$m = 9$ s	$m = 0.2$s	$m = 9$s
22	47.75	227.67	10.51	16.9
17	48.77	222.13	10.50	16.39
14	49.88	215.45	10.49	15.79
10	51.15	213.57	10.48	15.32
6	61.50	246.90	10.50	15.24
5	463.46	951.28	16.94	22.78
4	unstable	unstable	unstable	unstable

Table 3.2 shows the performance of the learned controllers with different numbers of features. We simulate the controllers on systems, different than the training set, with fixed low inertia ($m = 0.2$s) and fixed high inertia ($m = 9$s). In all simulations we consider an initial condition of -0.15Hz of frequency deviation at each node. Results in Table 3.2 show similar performance for the controllers with 10 or more features. The controllers with 6 and 5 features still perform well to steer the frequency deviation to zero, but they require more energy usage to achieve this. Fig. 3.4 depicts the frequency deviation evolution using the learned controllers for a system with inertia $m = 0.2$s. In the next section 3.3 we explore stability of the closed loop system with the proposed controllers, since, as observed in Table 3.2, the learned controller with only 4 features is not stable.

Stability analysis

We study stability in continuous time for the selected controllers. To do this, we calculate the eigenvalues of the closed loop system, derived from (3.14). We obtain

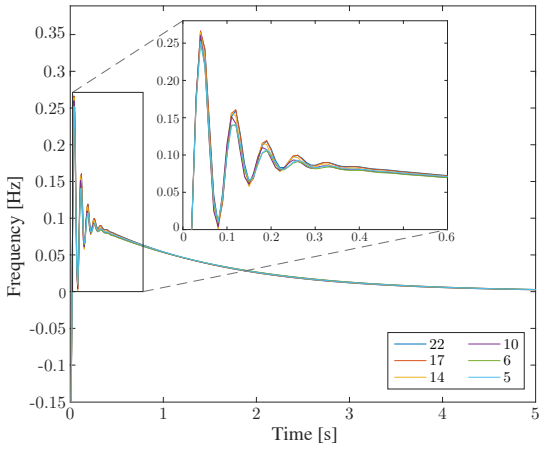

Figure 3.4: Frequency deviation evolution using learned controllers with an initial deviation of -0.15Hz and a system's inertia of 0.2 seconds.

$$\dot{x} = (I - \hat{B}_{q(t)}\tilde{K}_V)^{-1}(\hat{A}_{q(t)} + \hat{B}_{q(t)}K_{\mathrm{L}})x = A_{\mathrm{CL}(q(t))}x \tag{3.18}$$

Our dynamical system is a hybrid system, thus we calculate eigenvalues for all possible inertia modes q. We find that all controllers in all inertia modes are stable except for the controller with 4 features. The controller with 4 features is unstable for all inertia modes. The case of 9 seconds of inertia is the closest case to being stable for the controller with four features. Fig. 3.5 shows all eigenvalues for the seven controllers in the 9 seconds inertia mode. We can observe how all controllers show eigenvalues with negative real parts, except the controller with 4 features which shows in black triangles four eigenvalues close to zero but positive and one eigenvalue equal to 0.93.

Fig. 3.6 plots the maximum among the real parts of the eigenvalues for each controller under different inertia modes. We choose the maximum real part of the eigenvalues as a metric of stability. In Fig. 3.6, as we also observe in Fig. 3.5, the controller with 4 features is unstable. The 9 seconds of inertia mode is the closest it gets to attaining a non positive real part. As the system's inertia decreases, the maximum eigenvalue for this controller increases, potentially enhancing faster frequency deviations (more abrupt instability due to a faster exponential growth from the maximum positive real part). The observation where an increase of inertia results in a smaller maximum real part for the controller with 4 features cannot be observed for the other controllers. For these, their maximum eigenvalue real part occurs when the system shows it highest inertia ($m = 9$s). It is also relevant to notice that allowing the controller to have 6 or more features does not seem to impact the system's stability because the maximum real parts are similar.

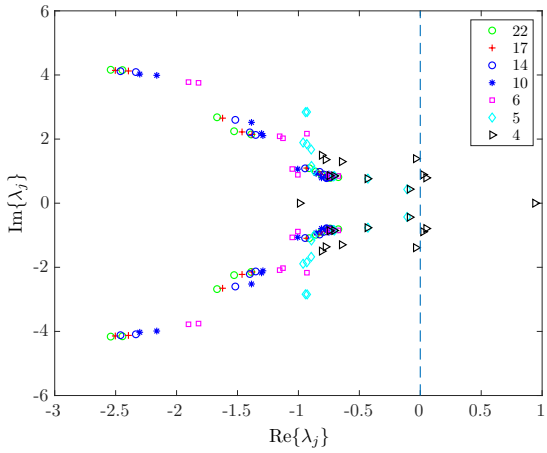

Figure 3.5: Eigenvalues of all controllers j for the closed loop system with inertia of 9 seconds.

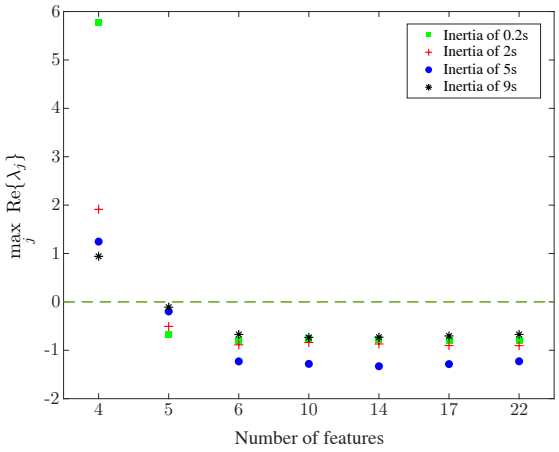

Figure 3.6: Maximum eigenvalue real part for all controllers j under 0.2s (green square), 2s (red cross), 5s (blue dot) and 9s of inertia (black asterisk).

Stability as a Switched-Affine hybrid system

In this section we study the stability of the hybrid system under *unconstrained switching* between modes. In other words, we are interested in studying the stability of the system if we allow any *adversarial* switching strategy (and possibly not realistic) for inertia modes. For example, it would be possible to switch from $m = 9$s to $m = 0.2$s at any moment. It is a well known result that for a Switched-Affine hybrid system, even if all modes are stable independently, a switching sequence could potentially be found to make the hybrid system unstable [16].

A strategy to study stability of a hybrid system is to find a common Lyapunov function that ensures global asymptotic stability (in the sense of Lyapunov) over the set of all

switching signals (Th. 1, p. 564 in [8]). The stability of a Switched-Affine hybrid system can be assessed by using a Lyapunov function of the form $V(x) = x^\top Px$, and by posing the following convex SDP problem:

$$\begin{aligned} \max_{P\in\mathbb{S}^{2n},r\in\mathbb{R},t\in\mathbb{R}} \quad & r+t \\ \text{s.t.} \quad & P \succeq rI_{2n\times 2n} \\ & A_{\mathrm{CL}(q)}^\top P + PA_{\mathrm{CL}(q)} \preceq -tI_{2n\times 2n},\ \forall q\in\{1,\dots,10\} \\ & \mathrm{Trace}(P) = 1 \end{aligned}$$

where $\mathbb{S}^{2n}$ denotes the vector space of symmetric matrices of size $2n \times 2n$. If the optimal solution yields $r > 0$ and $t > 0$, then $P \succ 0$ and $\dot{V}(x) < 0$. This implies global asymptotically stability of the system. We solve the previous problem using CVX for all the proposed controllers. Results show that controllers with only 10 or more features achieve a global asymptotic stability for the hybrid system. This illustrates that despite the fact our sparse controllers with 6 or 5 features achieve stability on every inertia mode, under stressed cases of fast varying inertia the system may be unstable. Future work will explore realistic conditions for mode switching that would preserve stability of the hybrid system using our proposed controllers with 5 or 6 features. In particular, we will explore the required dwelling time τ_d that would guarantee stability (minimum time the system would have to maintain the same inertia).

Optimal feature selection

In this section we explore which features are selected when we enhance sparsity in the learned controllers. Each controller (at each node) is allowed to use information of frequency and angles of any node in the system. This would require phasor measurement units (PMU) and instantaneous communication.

Fig. 3.7 depicts the heat map of the absolute value of the coefficients of the learned controller from the least-squares regression (i.e. $\lambda = 0$). The controllers prefer to use higher coefficients or gains in the angles than in frequency. It is important to notice that knowing the angles over time can be used to estimate changes of frequency as we show in equation (3.11). This explains the importance of angle states in feedback controllers. Nevertheless, a droop coefficient, related to their own local frequency, plays an important role in the stability of the closed loop system and is still considered critical in the regression. Feature selection in the learned controller with 4 features lacks coefficients on the frequencies (not pictured). This results in instability as we discuss in 3.3 and 3.3.

In comparison, Fig. 3.8, depicts the heat map of the absolute value of the coefficients of the learned controller from the Lasso regression, with at most 5 features per node. In this case we can observe that a node's own angle and frequency tends to be critical to ensure stability of the system (except for node 11). However, information from other nodes is also required. In particular, voltage angles of connected nodes have an important role. For

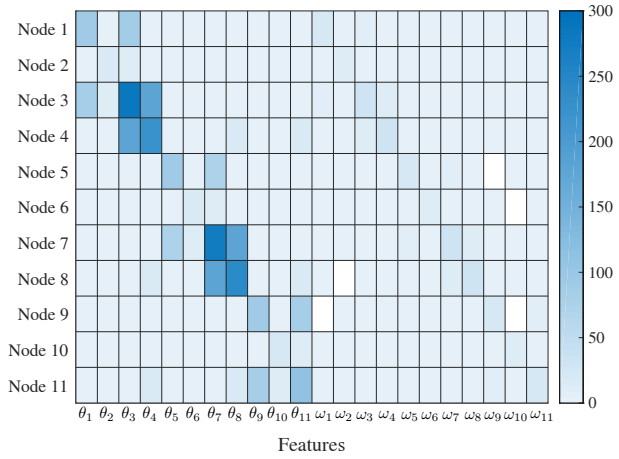

Figure 3.7: Heat map of learned controller for $\lambda = 0$, meaning each node uses up to 22 features.

example, node 1 has an important coefficient in θ_3, that is the node connected to node 1 via a transformer. Similarly, node 3 uses information from θ_1, θ_2 and θ_4, which are connected via lines or transformers to that node (see Fig. 2.1). This shows the importance of the network connectivity to understand which features have crucial roles in the stability of the system. For future work, we are interested to study how topology and size of different networks can affect the selection of features.

Learning controllers from training sets with fixed inertia

To illustrate the importance of creating training sets from time-varying dynamics, we generate a separate training set using fixed inertia of $m = 0.2$s. We then train the controllers with this set and test the performance of the controllers with 22 features in a system with inertia $m = 0.2$s and $m = 9$s, and an initial frequency deviation. The controllers are able to stabilize frequency deviation around zero for both inertia regimes. However, when $m = 9$s they do not perform as well as the controllers learned from the time-varying inertia coefficients that we show in 3.3.

We generate another separate training set using fixed inertia of $m = 9$s. We then train the controllers with this set and test the performance of the controllers with 22 features in a system with inertia $m = 0.2$s and $m = 9$. In this case, the controllers are able to stabilize frequency deviation around zero in the setting with $m = 9$s, but they are not able to steer it back to zero in the low inertia case ($m = 0.2$s).

From this exercise, we validate the importance of generating a training set with time-varying inertia. Training with these scenarios allows the learned controllers to be able to perform under different inertia regimes.

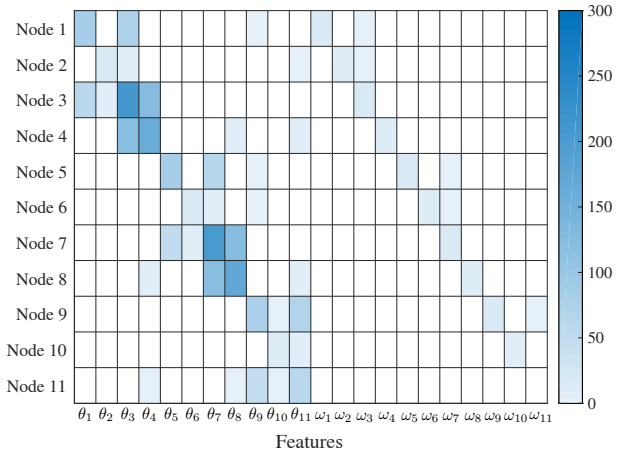

Figure 3.8: Heat map of learned controller with λ-values tuned such that each node uses up to 5 features.

Conclusions

In this work we study how restricting communication between nodes affects the performance and stability of a time-invariant controller designed for time-varying power system dynamics due to RES. To do this, we generate a training set by solving an MPC formulation for different scenarios of frequency control. We design controllers with different numbers of features (states) via Lasso regressions. We add virtual inertia to these controllers to guarantee stability. For the 11-bus test system we study, we are able to show that it is possible to reduce the number of features in the controller (to 5 in our case study) without negatively impacting performance and stability for any fixed inertia of the system. We also show how increasing information availability beyond a threshold (10 features) does not enhance performance or stability metrics. We are able to show global asymptotic stability for the hybrid system using controllers with 10 features or more. Finally, by analyzing optimal feature selection for sparse controllers, we find a positive correlation between feature selection and connectivity of the nodes. For future work, we are interested to study how our results hold for different topologies and sizes of different networks.

Our work lies at the intersection of three control theory topics: time-invariant controllers for time-varying dynamics, information availability between control agents, and control design via learning. In this work we are able to test performance and safety (stability) of a controller using this intersection of areas. However, safety is approached as a posterior analysis after the controller is designed. More inte-resting would be to design a controller

with safety guarantees already built-in. This motivates our future work where we aim to develop a mathematical framework to design sparse time-invariant controllers via learning while at the same time guaranteeing stability of the closed loop system.

Part II

Long-term Capacity Expansion Planning

Chapter 4

Cost and Impact of Weak Medium Term Policies in the Electricity System in Western North America

4.1 Preface

The work in this chapter is part of the work presented to the California Energy Commission through the technical report titled "Building a Healthier and More Robust Future: 2050 Low Carbon Energy Scenarios for California" by Max Wei, Shuba Raghavan and Patricia Hidalgo-Gonzalez (primary authors) [101].

4.2 Introduction

For over 20 years we have been negotiating agreements that try to reduce greenhouse gas emissions to stabilize their concentration [19]. A recent iconic international meeting was the 21st Session of the Conference of the Parties to the United Nations Framework Convention on Climate Change in 2015. Its main outcome was the reaffirmation of the goal of limiting global temperature increase below 2°C, while urging efforts to limit the increase to 1.5°C [54]. In 2007, the IPCC had stated that the 2°C goal could be achieved if different sectors of the economy in industrialized countries would reduce their emissions to specific targets. The electricity sector would have to reduce its emissions to 80% below 1990 levels by 2050 [93]. In an attempt to achieve this long-term goal, the U.S. proposed the Clean Power Plan (CPP) –which was repealed by the U.S. Environmental Protection

Agency in 2019 [7]. The target stated that the power system would need to reduce its emissions to 32% below 2005 levels by 2030 [4]. Additionally, California set its state-wide carbon cap target to reduce emissions 40% below 1990 levels by 2030 [43]. More recently, the IPCC stated that if global warming would be limited to 1.5°C, the avoided climate change impacts on sustainable development, eradication of poverty and reducing inequality would be greater compared to the impacts from 2°C [74]. These different emissions reductions goals with different timeframes present a challenge for power system regulators. What is the most economically efficient way to plan and operate the power system? Should we optimize investments on new power plants to reach 2030 emissions targets (e.g. CPP's intent) and from there optimize until 2050 to achieve the long-term emission targets (e.g. IPCC)? Or should we plan and optimize the power system capacity expansion from today until 2050? This question has been studied for the entire economic sector using different global integrated assessment models. It has been shown [70], [85], [58], [12], [88], [104] that weak climate near-term targets delay the transition towards a cleaner economy, which will require aggressive subsequent action to achieve climate stabilization goals. These studies also show that, due to the lack of foresight, unproductive near-term investments take place, which results in fossil fuels lock-ins and higher long-term mitigation costs. Therefore, it is relevant to study the impacts of short or medium-term policy for the electric power system. Additionally, the electricity and heat sector is particularly important because it is the greatest emitter in the world, accounting for 30.4% of total greenhouse gas emissions as of 2016 [55]. To the best of our knowledge, this type of analysis has not been applied to the electric power sector, and this study fills that gap. This chapter expands the work done for the California Energy Commission [101]. The main contribution of this work is to show the cost effectiveness of having stronger medium term (2030) policies that would promote an earlier transition towards lower carbon intensive technologies in the power system.

4.3 Problem Formulation

Description of the Optimization Problem

To study the consequences of weak short-sighted electricity policy we use the SWITCH model (AMPL version). SWITCH is a long-term power system capacity expansion model with high temporal and geographical resolution. So far, the SWITCH model has been developed for different regions and used for several studies [36], [103], [76], [77], [79], [101], [47], [17], [66]. This study uses SWITCH WECC (Western Electricity Coordinating Council) because the electricity system is the second highest-emitting economic sector in the U.S. with

a 32% share as of 2018 [5].

As an optimization problem, it is classified as a deterministic linear or mixed integer program. The objective function minimizes the total power system cost: investment and operation costs of generation and transmission. The decision variables of the optimization problem can be summarized in the following sets: capacity investment decisions for each potential new project in each period, capacity investment decisions for each potential new transmission line between any load areas in each period, hourly dispatch decisions for each existing and new generator installed in each period, decisions on hourly transmitted energy through the existing and new transmission lines. The main constraints in the optimization problem are: hourly demand in each load area has to be met by the generation and transmitted energy, capacity limits must be respected for generators and transmission lines, wind and solar generators are limited by their hourly geolocated capacity factors, generation from each hydropower plant is limited by historical monthly availability (minimum, average and maximum generation), biomass and geothermal deployment is limited by the resource availability in the WECC, hourly ramping restrictions for generators depending on their technology, respect yearly maintenance time for each generation technology, lifetime of different technologies must be respected, policy constraints as carbon cap, carbon tax, Renewable Portfolio Standards, among others. For a complete list and description refer to the Appendix A.

For this study, the optimization horizon is divided in four investment periods of ten years each: 2016 – 2025 (which we call "2020"), 2026 – 2035 ("2030"), 2036 – 2045 ("2040"), and 2046 – 2055 ("2050"). Each period simulates 72 hours of dispatch. For one year per period we sample every two months, two days per month (median and peak load days) and every four hours per day (6 months $\times$ 2 days/month $\times$ 6 hour/day = 72 hours). The peak days have the weight of one and the median days of n–1 where n is the number of days of that month, and this represents a full month.

Summary of Data Sources

Geographically, the SWITCH WECC model divides the WECC in 50 zones or load areas. The transmission system was obtained from Ventyx geolocated transmission line data [26] also using data on the thermal limits from the Federal Energy Regulatory Commission (FERC) [21]. In total, there are 105 existing transmission lines connecting load zones in SWITCH. SWITCH can decide to build more transmission lines if it is optimal. De-rating of lines and transmission losses are taken into account.

Electricity demand profiles come from historical hourly loads from 2006 [20], [25] (and ITRON). These profiles are projected for future years. Hourly existing and potential new

wind farm power output is derived from the 3TIER Western Wind and Solar Integration Study wind speed dataset [60], [63] using idealized turbine power output curves on interpolated wind speed values. For existing and potential new solar power plants, hourly capacity factors of each project over the course of the year 2006 were simulated using the System Advisor Model from the National Renewable Energy Laboratory. The optimization can choose from over 7,000 potential new geolocated generators in the WECC. Fuel prices projections for each load area were obtained from the U.S. Energy Information Administration (2017) [3]. Capital costs and operation and maintenance costs were obtained from Black and Veatch 2012 [98]. The historical pool of exiting power plants in the WECC was obtained from the U.S. Energy Information Administration (EIA-860, EIA-923, 2007 data).

Description of Medium and Long Optimization

In order to study the impact of insufficient planning horizons with weak near-term policies we use two optimization methods: "long optimization" and "medium optimization". The control case or long optimization is the traditional deterministic optimization from 2016 to 2055, taking into account carbon cap constraints for all the years.

The medium optimization was developed for this study to analyze the impacts of short term policy goals on the power system operations and capacity expansion. The basic idea behind the medium optimization is to break investment planning into two stages: present day until 2030, and 2030 – 2050. In the long optimization, the timeframe optimized is from 2016 until 2050. The medium optimization optimizes in a shortsighted manner by solving the problem in two consecutive stages: 1) optimizing the grid in 2016 – 2030 (without any information after 2030), 2) using the optimal buildout in 2030 from stage 1 optimizes from 2031 until 2050. In other words, the first step minimizes the cost of the operation and investment of the power system from 2016 to 2030 taking into account all policy constraints (e.g. yearly carbon cap). The second step consists of optimizing investments and operations from 2031 to 2055 with stronger emission policies for 2050 (i.e. 80% reductions). This medium optimization recreates the challenge of optimizing the expansion and operation of the power system in phases. First, only taking into account policies until 2030. Investment decisions made until 2030 become the initial state for the second step of the optimization. The second step optimizes decisions from 2031 to 2055 to comply with more stringent policies, specially by 2050. Therefore, the hypothesis is that the first step will expand and operate the system in a shortsighted way; having as a consequence carbon locks-in or a delayed transition towards technologies with lower CO_2 emissions. Thus, the second step will have to change the energy mix more aggressively to transition towards a cleaner electric grid by 2050 compared to the long optimization (which optimizes in only one step: 2016 – 2055, taking into account

the more stringent 2050 carbon cap constraints). The long and medium optimization use the same periods and hours sampled for consistency and to isolate the impact and carbon locks-in produced by weak medium-term electricity policies. The medium and long optimization are run for each of the three scenarios modeled (i.e. solutions from six optimization problems are studied in this work).

4.4 Scenarios

The scenarios that are used in this study are three different carbon cap scenarios shown in Fig. 4.1.

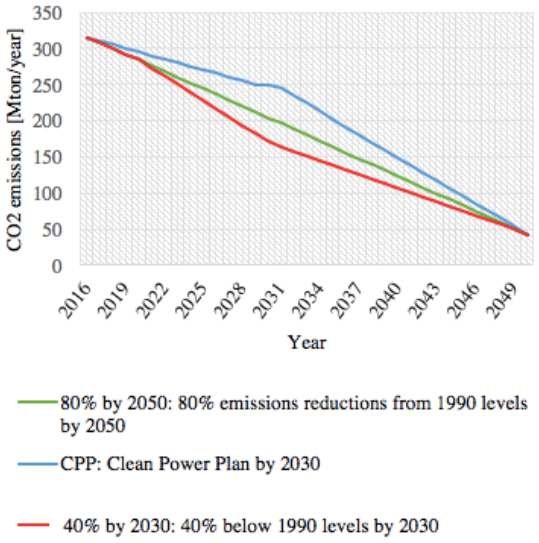

Figure 4.1: WECC carbon cap scenarios. In green is the 80% emissions reductions from 1990 levels by 2050 scenario (labeled as "80% by 2050"), in blue the Clean Power Plan scenario (labeled as "CPP"), and in red 40% emissions reductions by 2030 (labeled as "40% by 2030").

In Fig. 4.1, the scenario with the green line ("80% by 2050") corresponds to a linear decrease in emissions from 2016 until 2020 where emissions are restricted to 1990 levels [42]. Then a linear decrease from 2021 until 2050 where 80% reductions from 1990 levels are enforced [93]. The blue line ("CPP") corresponds to a linear decrease in emissions from 2016 until 2020 where emissions are restricted to 1990 levels and then a linear decrease in

emissions until 2030 where the CPP target is enforced (32% reductions from 2005 levels, or analogously, 11% reductions from 1990 levels). From 2031 until 2050 the cap has a linear decrease until 80% reductions from 1990 levels are achieved by 2050. Finally, the red line ("40% by 2030") corresponds to the same linear decrease in emissions from 2016 until 2020 where emissions are restricted to 1990 levels. Then a linear decrease until 2030 where 40% of reductions are enforced, simulating the case if the Californian executive order B-30-15 [43] were to be expanded to the WECC. And from 2030 until 2050 a linear decrease until 2050 when 80% reductions are mandated. Throughout this manuscript the three scenarios will be addressed as "80% by 2050", "CPP", and "40% by 2030" respectively.

The intuition behind the first step of the medium optimization is that it provides decisions that would be made until 2030 without considering the more stringent policy that will be enforced in 2050. Therefore, they reflect the signals that are currently given to the investors of the power system and to the grid's operators. On the other hand, the second step of the medium optimization faces the challenge of achieving the more stringent carbon caps from 2031 until 2050 having a grid already built by 2030 (from the first step) that did not take into account in its expansion carbon caps beyond 2030. Therefore, the medium optimization seeks to mimic the way we would expand the power system in the WECC if we keep imposing only near-term policies as we have done so far. The caveat of this study is that we assume we will have stringent carbon cap policies by 2050, whether they affect our 2030 decisions (long optimization) or not (medium optimization). Consequently, the research question we study is: How to plan and implement policy in the power system efficiently? From today until 2030 and then until 2050? Or plan from today until 2050?

4.5 Results and Analysis

Optimal energy mix for the three scenarios in the long optimization case

To understand the impacts of medium term planning, we must first examine results from the long-run optimizations (Fig. 4.2).

We can observe how in all the scenarios coal power plants are decommissioned progressively over the four periods. Each scenario presents a different transition rate for decommissioning and electricity generation reduction from coal power plants. By period 2030, the scenario that reduces coal power generation the most is "40% by 2030" with a 1.6% of participation of coal. The scenario "80% by 2050" follows it with 4.0% and finally the "CPP" scenario with 4.4% of energy generated by coal. From the 2020 period to the 2030

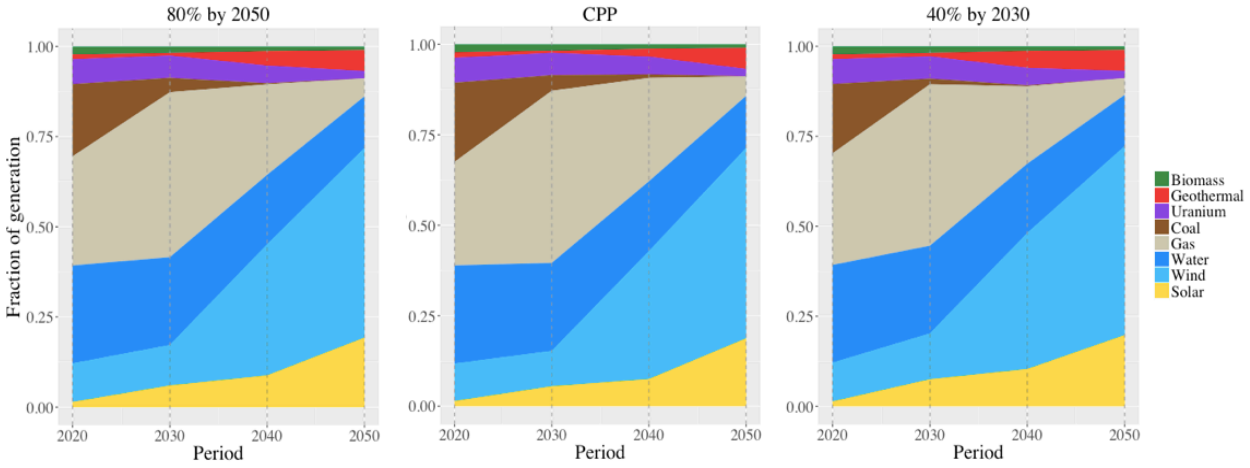

Figure 4.2: Energy generation share (as a fraction) per fuel per period for the long optimization for the scenarios studied. On the left side is the "80% by 2050" scenario, in the middle the "CPP", and on the right side the "40% by 2030".

period all scenarios present an increase in energy generated by gas power plants. This gas generation increase ranges from 45% by 2030 ("40% by 2030") to 48% ("CPP"). Another trend of interest is the consistent increase in wind and solar power generation from period 2020 until period 2050. Nonetheless, solar and wind generation reach a more significant share only by 2050. By 2050, solar power generates roughly 20% of the electricity, and wind power around 53%.

Comparison of optimal capacity installed in 2030 between medium and long optimization

Table 4.1 shows total capacity installed per fuel by 2030 for each of the scenarios under the medium and long-term optimizations.

Fig. 4.3 aids to identify key differences among the medium and long optimization by showing the difference in installed capacity per fuel in 2030.

By 2030, all scenarios in the medium optimization deploy coal, a technology more carbon emissions intensive (i.e. ton CO_2/MWh), at the expense of less deployment of a cleaner one, gas, compared to the long optimization. In the medium optimization cases, due to their lack of foresight of the stringent carbon cap by 2050, coal power plants are decommissioned at a slower rate than in the long optimization. This results in more installed capacity of

Table 4.1: Capacity installed in gigawatts in the WECC per fuel by 2030 for the scenarios studied. The columns show installed capacity from the medium and long optimization for each scenario in 2030.

	80% by 2050		CPP		40% by 2030	
Fuel	Medium	Long	Medium	Long	Medium	Long
Biomass	2.4	2.5	2.4	2.4	2.5	2.5
Coal	5.7	5.5	15.1	5.8	3.8	2.4
Gas	111.9	113.4	104.5	115.0	108.9	111.6
Geothermal	0.5	0.8	0.5	0.6	1.1	1.1
Solar	22.3	21.3	21.3	19.6	27.0	26.2
Storage	0.0	0.0	0.0	0.0	0.0	0.0
Uranium	7.7	7.7	7.7	7.7	7.7	7.7
Water	66.7	66.7	66.7	66.7	66.7	66.7
Wind	39.2	37.6	37.4	33.7	47.4	42.0

coal power plants in the medium optimization —a carbon lock-in. On the other hand, the medium optimization invests less in gas power plants compared to the long optimization. The more carbon intensive mix in 2030 in the medium optimization requires an abrupt technological change (2030 – 2050, i.e. 20 years instead of 40) to comply with 2050 stringent carbon caps. The scenario that shows the greatest difference in installed coal and gas power plants between the medium and long optimization in 2030 is "CPP". There is an excess of 9.3 GW of coal power plants and a lack of 11 GW of gas.

Comparison of optimal energy generation by 2030 between the medium and long optimization

As expected, the difference between the energy generated in the 2030 period in the medium and long optimization follows the same pattern as the capacity installed. Fig. 4.4 shows the difference in electricity generation by 2030 per fuel between the medium and long optimization.

In all scenarios in the period 2030, the medium optimization generates more electricity from coal plants than in the long optimization. The energy produced by coal plants in the medium optimization exceeds the long optimization from 13 TWh ("80 by 2050") up to 690 TWh ("CPP"). In general, the excess in generation from coal power plants substitutes generation from gas power plants. "CPP" shows the greatest difference in generation across

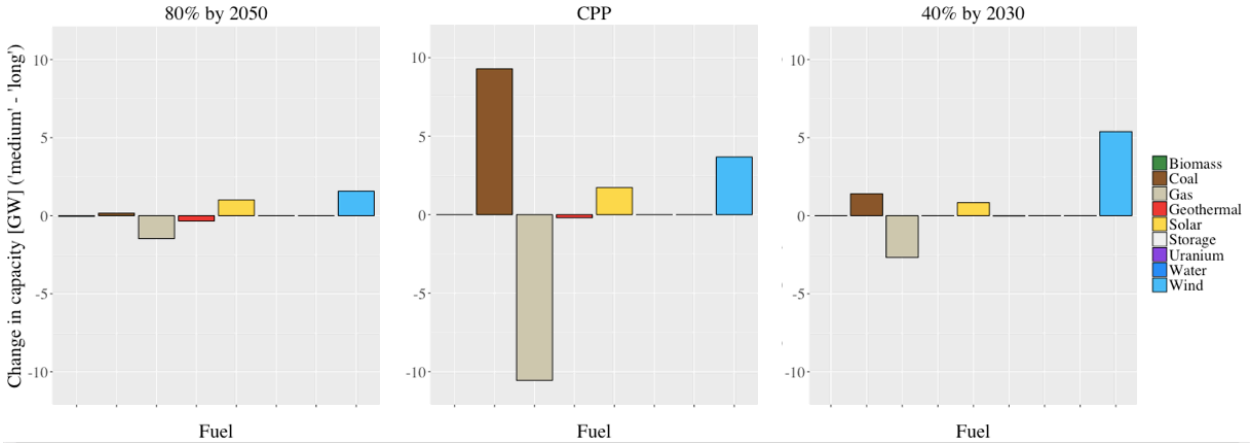

Figure 4.3: Change in capacity installed in gigawatts per fuel by 2030 for the scenarios studied. The difference corresponds to capacity per fuel installed by 2030 in the medium optimization minus the capacity installed in 2030 in the long optimization. On the left is the "80% by 2050" scenario, in the middle the "CPP" scenario (where more coal and less gas are installed in the medium optimization), and on the right side the "40% by 2030" scenario.

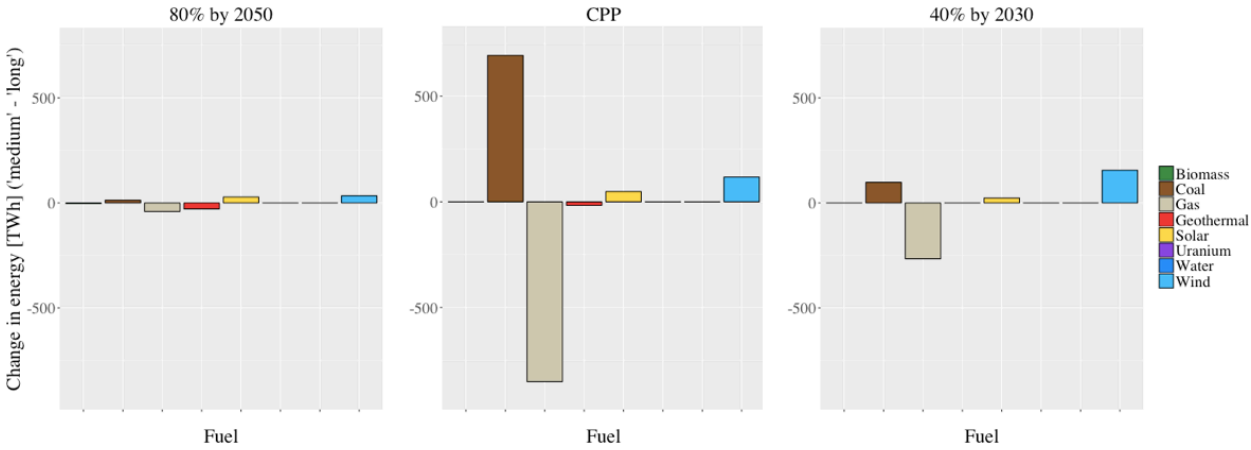

Figure 4.4: Change in energy generated in terawatt hour per fuel during the period 2030 for the scenarios studied. The difference corresponds to the generation per fuel by 2030 in the medium optimization minus the generation in 2030 in the long optimization. On the left is the "80% by 2050" scenario, in the middle the "CPP" scenario (where more coal and less gas are deployed in the medium optimization), and on the right side the "40% by 2030" scenario.

all scenarios. In the medium optimization, it produces 690 TWh more of energy from coal plants compared to the long optimization. To put this in perspective, 690 TWh is roughly 7.4% of the total load in the 2030 period. The change in energy for the rest of the scenarios is less than 2% of the total load by 2030. This substitution of gas in favor of coal for the "CPP" scenario can be explained by the fact that "CPP" does not have a stringent carbon cap by 2030. Therefore the medium optimization does not transition from more carbon intensive technologies to cleaner ones as early as 2030. However, decisions made for 2030 in the long optimization take into account the stringent carbon cap by 2050. This results in a considerable decommission of coal by 2030 to cost effectively reach the 2050 emissions target.

Comparison of optimal emissions by 2030 between the medium and long optimization

The explanation behind the carbon lock-in in the medium-term optimizations for "CPP" lies in the optimal CO_2 emissions by 2030. Fig. 4.5 shows emissions in the year 2030 for all the scenarios for the medium (in yellow) and long (in blue) optimizations. The red dashed lines correspond to the carbon cap for each scenario in 2030.

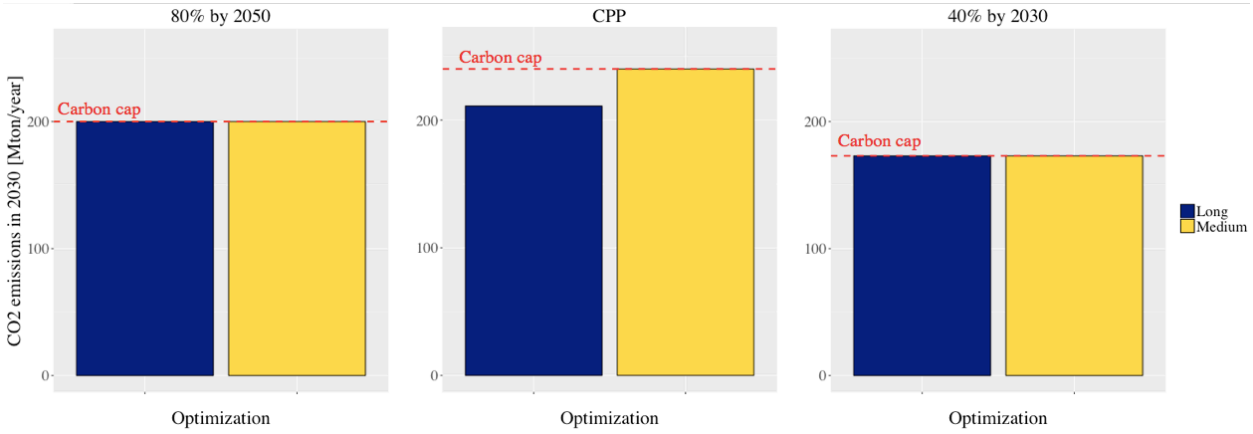

Figure 4.5: CO_2 emissions in the year 2030 for the medium (yellow) and long optimization (blue). The red dashed line represents the carbon cap for the year 2030 for each scenario. On the left side is the "80% by 2050" scenario, in the middle the "CPP" scenario, and on the right side the "40% by 2030" scenario.

The medium optimization does not have an early foresight of the more stringent carbon caps it will have to face after 2030 during its second optimization stage. Therefore, it is optimal to emit as much carbon as its 2030 cap allows. This can be observed where yellow bars are at the same height as the carbon cap. For the "CPP" case, the long optimization emits less carbon (blue bar) in 2030 than the carbon cap. This occurs because the long optimization has perfect foresight in 2030 of the more stringent carbon cap target in 2050. Therefore, the long optimization realizes that it is cost effective to start deploying cleaner energy as early as 2030 in order to optimally reach the stricter emissions goal of 2050. This shows the importance of optimizing the power system in the long-term when medium term policies are weak. In the case of the medium optimization for "CPP", due to its lack of foresight, it emits CO_2 at the maximum allowed in 2030. Therefore, the second step of the medium optimization has to transition more abruptly to cleaner technologies to achieve the 2050 target. This capacity expansion is suboptimal (Refer to Cost analysis section). On the other hand, for the scenarios "80% by 2050" and "40% by 2030" optimal carbon emissions in the year 2030 in the case of the long-term optimizations are equal to their respective carbon caps. This suggests that the carbon caps in 2030 for "80% by 2050" and "40% by 2030" are well aligned with the carbon cap in 2050. Therefore, through these two scenarios we show that stronger medium-term policies yield to an expansion of the power grid closer to the optimal expansion resulting from optimizing in the long-term. In practice, one way to cope with the lack of foresight of optimizing in the medium term would be to enforce more stringent policies for 2030. These policies would be designed to mimic the optimal results of the long optimization. For example, for the "CPP" scenario, we would need to force a 26% carbon emissions reductions from 1990 levels by 2030 (which corresponds to the optimal reductions achieved in the long optimization by 2030).

Clean Power Plan carbon lock-in maps in 2030

Fig. 4.6 shows the difference in installed capacity by 2030 between the medium and long optimization for coal (bottom) and gas (top) for the "CPP" scenario for each zone. Darker blue represents more installed capacity in the medium optimization, while darker red means less.

In general, there is a substitution between installed coal and (lack of installed) gas power plants in the medium optimization among the geographical zones.

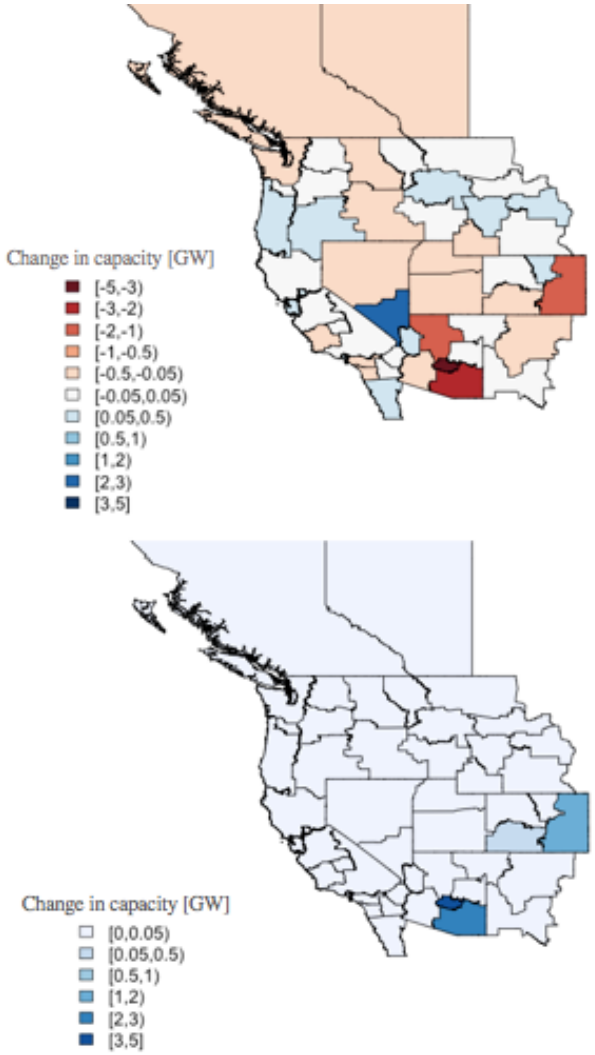

Figure 4.6: Change in gas (top) and coal (bottom) power plants' capacity in gigawatts by 2030 for "CPP" scenario. The difference corresponds to capacity installed by 2030 in the medium optimization minus the capacity installed by 2030 in the long optimization.

Cost analysis

Fig. 4.7 shows the increase in cost per period from using the medium optimization instead of the long optimization.

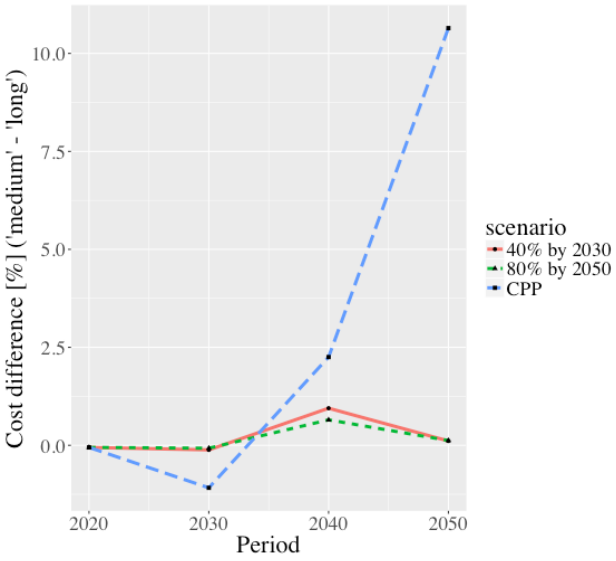

Figure 4.7: Increase in cost per period from using the medium optimization instead of the long optimization. The red solid line represents cost increases from "40% by 2030" scenario, the short dashed green line corresponds to "80% by 2050," and the long dashed blue line represents "CPP" scenario.

There are minor to no savings in 2020 and 2030 from using the medium optimization. Thus, there is no economic benefit of having weaker policies by 2030. However, the expansion and operation of the power system from the medium optimization in 2040 and 2050 is more expensive than the cost incurred by the long optimization in those periods. The most extreme case is for the "CP" scenario, where the total cost of expanding and operating the grid in 2050 is 11% more expensive than for the long optimization. In other words, the cost of electricity in 2050 obtained from using the medium optimization is of \$179.70/MWh, instead of \$162.41/MWh achieved by the long optimization. Thus, we have shown the sub optimality of the solution provided by the medium optimization. This is due to the more abrupt transition to clean energy that has to take place in the last two decades. This contrasts the expansion and operation of the long optimization for "CPP" because it transitions progressively over the decades to meet its 2050 carbon cap cost effectively. In

the other two scenarios, the increase in cost is small. Nonetheless, this minor increase in cost in 2040 and 2050 reflects the fact that more coal is deployed in 2030 instead of gas compared to the long optimization. Therefore, these two scenarios also have to adjust their grid in the last two decades, but to a lesser extent compared to "CPP". Thus, their medium-term carbon policies are strong enough to allow a closer-to-optimal transition to meet the strongest carbon cap policy by 2050.

4.6 Conclusions and Policy Implications

Throughout this work we study the question of planning the power system in the medium (2030) or long-term (2050). Results are conclusive by depicting a higher deployment of coal power instead of gas by 2030 in the medium-term optimizations compared to results from the long-term optimizations for the same year. Conversely, the long-term optimizations show a progressive transition towards a cleaner electric grid from early stages (2030). The medium-term optimizations do not foresee the more stringent carbon cap by 2050. Thus, they have to transition quicker to a cleaner grid in the last two decades (second step of the optimization) instead of progressively transitioning during the four periods. This is clearly observed in the "CPP" case, where its carbon cap by 2030 is inactive in the long optimization. This means that it is optimal to emit less CO_2 than it is required in 2030 to achieve the 2050 goals cost effectively. To address the impact of medium term planning, we recommend to either place more stringent targets in the medium term (2030) or plan until 2050 with its more restrictive carbon cap by the end of the simulation. Given that it is impractical to suggest regulators to optimize the grid until 2050, we recommend to design stronger near-term policies (e.g. 2030) that would result in mimicking decisions made by optimizing in the long-term. For the"CPP" scenario, instead of enforcing a reduction on emissions to 11% below 1990 levels by 2030, a reduction in emissions by 26% in 2030 in the WECC would mimic the optimal and cost-effective energy transition of planning in the long-term.

Chapter 5

Power System Planning in Western North America: Deterministic and Stochastic Scenarios under Climate Change

5.1 Preface

The work in this chapter is part of the work presented to the California Energy Commission through the technical report titled "Building a Healthier and More Robust Future: 2050 Low Carbon Energy Scenarios for California" by Max Wei, Shuba Raghavan and Patricia Hidalgo-Gonzalez (primary authors) [101].

5.2 Introduction

It is expected that future electricity systems will have high levels of renewable sources such as solar and wind. This variability and volatility may pose several challenges in power systems, in particular when high penetration levels of these sources are present. Earlier studies indicate that greater storage and transmission expansion are necessary to promote the efficient integration of variable renewables while maintaining a reliable and secure system. To decide these optimal investments, complex temporal and spatial resolution must be considered in expansion planning models. Traditionally, expansion planning models in electricity systems consider a simplified version of the grid to decide what types of infrastructure to

install, as well as where and when to install them in the system, such as generators or transmission lines. These models usually do not capture the chronological sequence of time and the spatial location of the resources, and so the complex temporal and spatial distribution of variable renewable resources is not considered. Investment portfolios are then evaluated in detailed models to simulate the operational performance of the system in particular years. This study used the SWITCH 2.0 model [56] (i.e. Python version) to decide the optimal investment decisions and explore the cost of generation, transmission, and storage options for a future electricity system.

SWITCH 2.0[1] is a Python package that can be used to create and solve power system expansion planning models. Taking advantage of the Python framework, SWITCH uses a modular architecture that allows users to include specific components through a list of modules depending on the complexity of study; these components are depicted in Fig. 5.1. It uses the open-source Python Optimization Modeling Objects (Pyomo) package as a framework to define optimization models, load data, and solve the optimization models using commercial or open-source solvers.

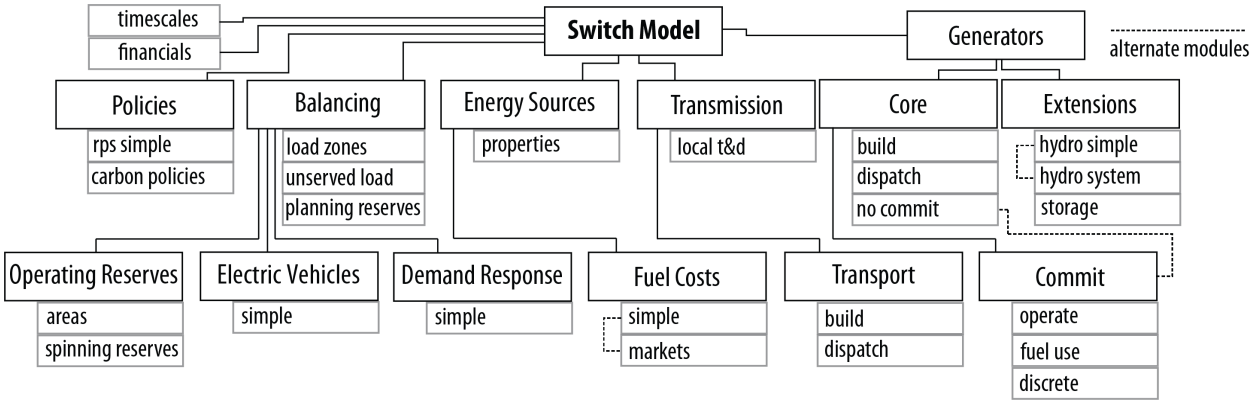

Figure 5.1: List of Modules in SWITCH 2.0.

SWITCH operates using many different spatial and temporal scales to minimize the cost of transitioning from the current state to a future decarbonized power system. The

[1]The SWITCH electric power system planning model was initially created at the University of California, Berkeley by Dr. Matthias Fripp, then developed by Dr. James Nelson, Dr. Ana Mileva, Dr. Josiah Johnston and Patricia Hidalgo-Gonzalez. SWITCH WECC Python was adapted and further developed by Patricia Hidalgo-Gonzalez, Dr. Josiah Johnston and Rodrigo Henriquez-Auba. The model is maintained and developed in Professor Daniel Kammen's Renewable and Appropriate Energy Laboratory (RAEL) at the University of California, Berkeley.

model uses a set of chronological time series with hourly demand and renewable generation profiles in a planning expansion model. Using this framework allows consideration of the hourly behavior of renewable variable sources, such as wind and solar power, and storage in representative time series over several periods. The model also considers an electric network with several load zones connected through a transmission system with limitations to realistic capacity levels by using a derating technique over the lines. Also, policies as Renewable Portfolio Standard and carbon cap constraints are simultaneously considered with the investment decisions to evaluate the changes on the power system infrastructure. SWITCH concurrently optimizes investment decisions and dispatch of the power system infrastructure.

In this study, SWITCH is used to examine the future of the electric power system in California and western North America (WECC) under different scenarios of climate change and policies through the present day to 2050. These scenarios, with their particular characteristics, are detailed in Section 5.3, Subsection Description of Scenarios.

5.3 Long-term Power System Planning in Western North America: Deterministic Scenarios

Model Description

We evaluate different policy relevant scenarios using the Python SWITCH WECC model. SWITCH is a long-term power system capacity expansion model with high temporal and geographical resolution. As an optimization problem, it is classified as a deterministic linear or mixed integer program. The objective function minimizes the total power system cost: investment and operation costs of generation and transmission. In addition to operational (reserves, ramping, etc.), technological and resource potential constraints, different policy constraints can be modeled (e.g. carbon cap, carbon tax, Renewable Portfolio Standard (RPS), etc.). For its detailed mathematical description refer to Appendix A. To the best of our knowledge, SWITCH's high time and geographical resolution makes it a power system capacity expansion model without precedent. This allows a more realistic study of the expansion and operation of the electrical grid with the presence of renewable intermittent resources, such as wind and solar power. The optimization horizon is divided in four investment periods of 10 years: 2016-2025 ("2020"), 2026-2035 ("2030"), 2036-2045 ("2040"), and 2046-2055 ("2050"). Each period simulates 144 hours of dispatch. For one year per period, we sample every month, two days per month (median and peak load days) and every four hours per day (12 months $\times$ 2 days/month $\times$ 6 hour/day = 144 hours). The peak days have

the weight of one and the median days of $n-1$ where n is the number of days of that month, and this represents a full month. Geographically, the SWITCH WECC model divides the WECC in 50 zones or load areas (Fig. 5.2).

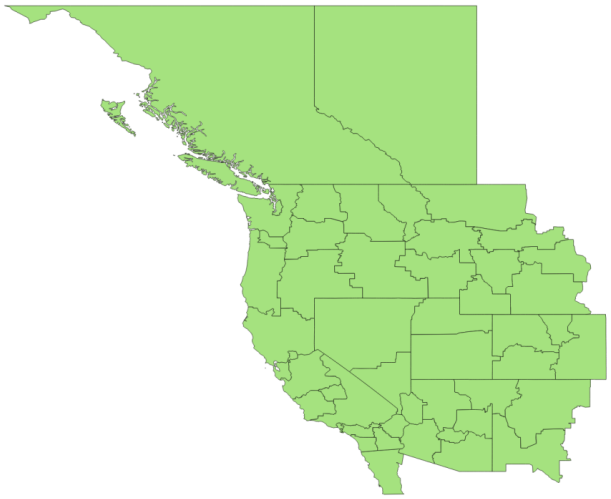

Figure 5.2: WECC Divided in 50 SWITCH Load Zones

The transmission system was obtained from Ventyx geolocated transmission line data [26] also using data on the thermal limits from the Federal Energy Regulatory Commission (FERC) [21]. In total, there are 105 existing transmission lines connecting load zone in SWITCH. SWITCH can decide to build more transmission lines if it is optimal. De-rating of lines and transmission losses are taken into account.

Electricity demand profiles come from historical hourly loads from 2006 [20], [25] (and ITRON). These profiles were updated to current projections described in Section 5.3, Subsection Description of Scenarios. Hourly existing wind farm power output is derived from the 3TIER Western Wind and Solar Integration Study wind speed dataset [60], [63] using idealized turbine power output curves on interpolated wind speed values. Afterwards, a proportion of possible wind sites were removed from California according to Category 3 from [106]. Category 3 encompasses areas that are legally excluded for energy deployment, protected ecological and areas of social value, and conservation areas. For solar energy, hourly capacity factors of each project over the course of the year 2006 were simulated using the System Advisor Model from the National Renewable Energy Laboratory.

All current (2017) Renewable Portfolio Standards were modeled for each load zone in the WECC as unbundled. A WECC-wide carbon cap was modeled to achieve the 80% emissions

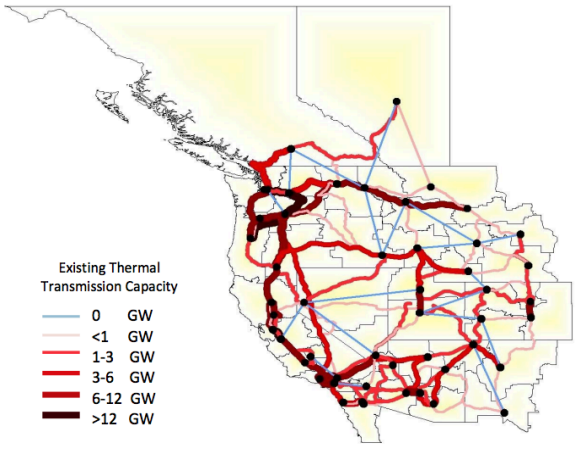

Figure 5.3: In light blue are non-existing lines, but that can be installed in the optimization. Each black dot represents the largest substation in the load zone.

reductions from 1990 levels by 2050. Additionally, a California carbon cap was modeled to attain 40% emissions reductions by 2030, and a linear decrease to achieve 80% reductions by 2050.

Fuel prices projections were obtained from the United States Environmental Information Agency (EIA) (2017) [3]. Capital costs and operation and maintenance costs were obtained from Black and Veatch [98] and Energy and Environmental Economics [33]. The current pool of existing power plants in the WECC was also obtained from EIA (EIA-860, EIA-923, 2016 data). Hydropower historical generation was also obtained from EIA-923 data.

Description of Scenarios

Electricity Demand Scenarios and Climate Change Scenarios

Eight different demand scenarios are modeled for this study. Table 5.1 shows the Frozen, Intermediate energy efficiency with and without electrification (SB350), and Aggressive energy efficiency with and without electricity cases.

Fig. 5.4 and 5.5 show total annual demands for the WECC and California in the periods simulated with the Python SWITCH WECC model. In addition to these five load scenarios, we also model three load projections from climate change models. The climate models are CanESM2, HadGEM2ES and MIROC5. Industrial Economics and the U.S. Environmental Protection Agency (EPA) provided heating degree days (HDD) and cooling degree days

Table 5.1: Electricity demand scenarios modeled.

Scenario	Description
Frozen	This case essentially assumes the baseline case from the California Energy Commission demand projections without SB350 savings, and a low rate of electrification for 2030 and 2050.
Intermediate no electrification	This case achieves the SB350 target of doubling the rate of energy efficiency by 2030. A low rate of electrification for buildings is assumed.
Intermediate + electrification	This scenario is the same as the Intermediate no electrification scenario but adds aggressive building electrification starting in 2020.
Aggressive EE no electrification	This scenario assumes a higher rate of energy efficiency (EE) retrofits starting in 2020 than the SB350 case but with a low rate of building electrification.
Aggressive EE + electrification	This case is similar to the preceding case but with aggressive building electrification starting in 2020 and more aggressive adoption of electrical vehicles in transportation.

(CDD) projections with a spatial resolution of 5,163 ½ degree grids for the U.S. for all years until 2100 . Using this data, HDD/CDD projections for the SWITCH load zones until 2100 are calculated (but we model the electricity system until 2050). The National Renewable Energy Laboratory provided 135 linear regression models [91] to predict hourly changes in load using as input HDD/CDD, hour of the day, and season of the year. The linear regression models predict hourly load changes for the ReEDS balancing areas [62]. We translate their prediction models into equivalent models for the SWITCH WECC load zones. Finally, the hourly load predictions are post-processed so they are aligned with the predictions for California from the University of California, Irvine.

For the climate change scenarios, in addition to new hourly load projections, we also include monthly hydropower availability projections until 2050 from Industrial Economics. The spatial resolution of these hydropower projections match the 135 ReEDS balancing areas. We map these projections to each hydropower plant in the WECC.

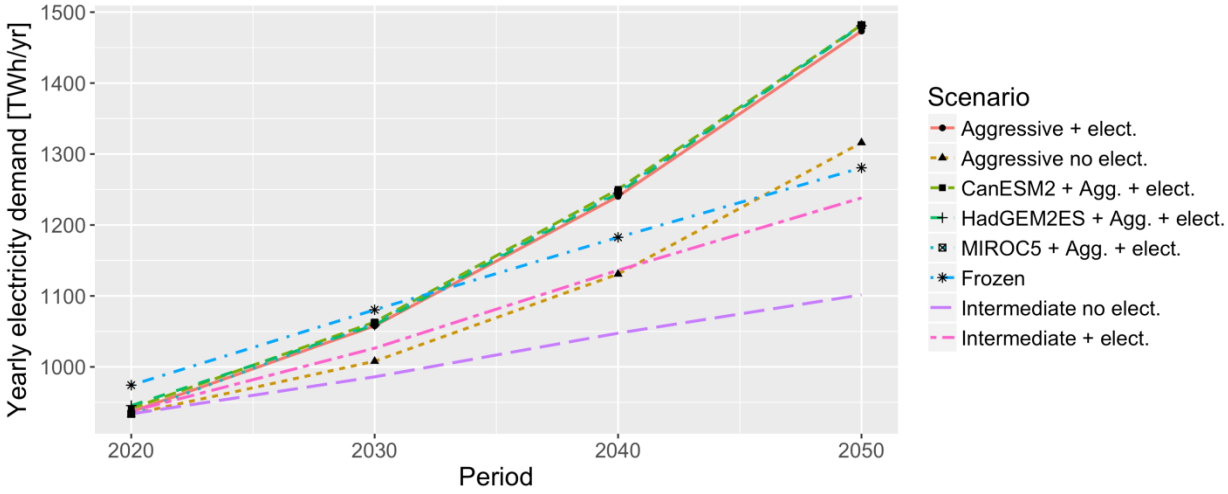

Figure 5.4: Electricity Demand Scenarios for the WECC.

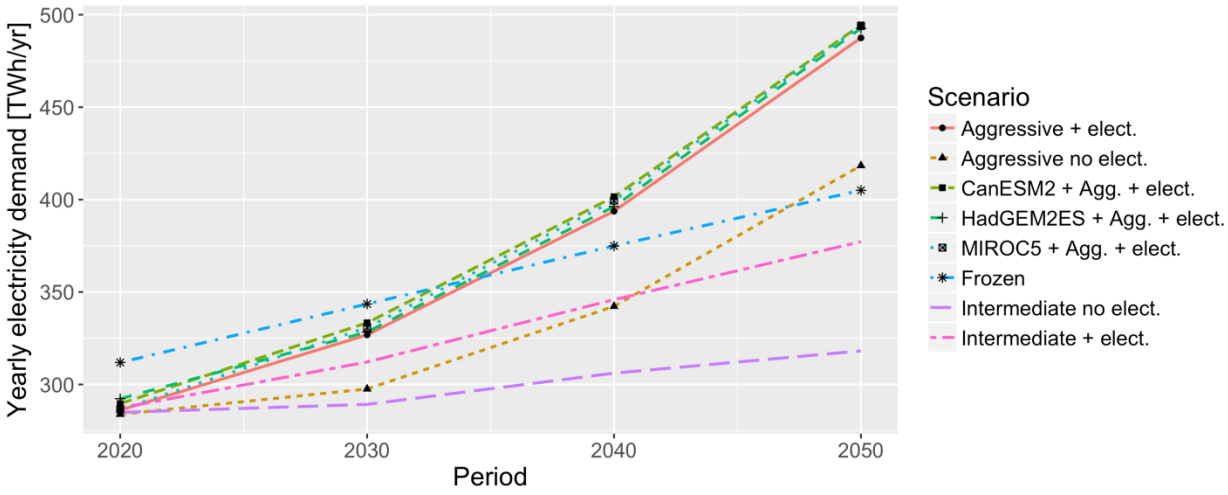

Figure 5.5: Electricity Demand Scenarios for California.

Table 5.2: Expected Device Stocks in Millions and Energy Required for Charging per Zone and Year.

	LDVs stock [million]				Energy required [GWh]			
Zone	2020	2030	2040	2050	2020	2030	2040	2050
CA	0.85	6.59	19.98	31.67	2637	16363	46857	91493
RM-AZNM	0.007	0.41	3.09	9.77	200.00	1600	8292	24107
WECC-CAN	0.044	0.72	3.28	7.21	600	4223	12738	26123
NWPP	0.09	1.40	6.25	13.48	1200	8192	24215	48808

Electrical Vehicles and Demand Response: Aggressive Efficiency with Electrification

In this study, the impacts of smart charging of light duty electric vehicles (LDVs) are analyzed in SWITCH. In particular, we study the differences in investment portfolios and dispatch decisions when the availability of flexible charging of LDVs is controllable by system operators or system resource aggregators at no cost.

For this purpose, the trajectory of charging must be between two bounds, determined by the BEAM model, detailed in [40], that will depend on users' characteristics and charging profiles. The BEAM model simulates the mobility and charging behavior for a representative day in a week, for three types of chargers: public, residential and work. Each of these vehicles will have particular charging constraints that depend on users' availability to charge. For example, for four random plug-in electric vehicles (PEV) on BEAM, Fig. 5.6 depicts an example of maximum and minimum charging profiles on a typical day for these PEVs.

Based on those charging sessions, aggregated profiles (calculated as the addition of the vehicles) are created for defining energy bounds for the cumulative charge of vehicles. Fig.5.7 presents the aggregated profiles, and then normalized per kWh. This generates the region of feasible trajectories for the charging of PEVs used in the SWITCH model.

Table 5.2 provides the estimation of energy use for EVs, based on growth projection on expected sales of EVs and average expected use, in particular miles traveled per year and efficiency of the batteries in kWh/miles.

These energy requirements will be enforced in SWITCH through scaling the normalized charging profile, depending on each zone and year. In addition, load shifting service of demand response (DR) at no cost is available with this scenario. In this case study, we are interested in assessing the value of DR for residential and commercial buildings. When DR is being considered, the amount of load that can be shifted per hour is limited to a specified amount of energy. This amount of energy will depend on the specific flexibility at each load

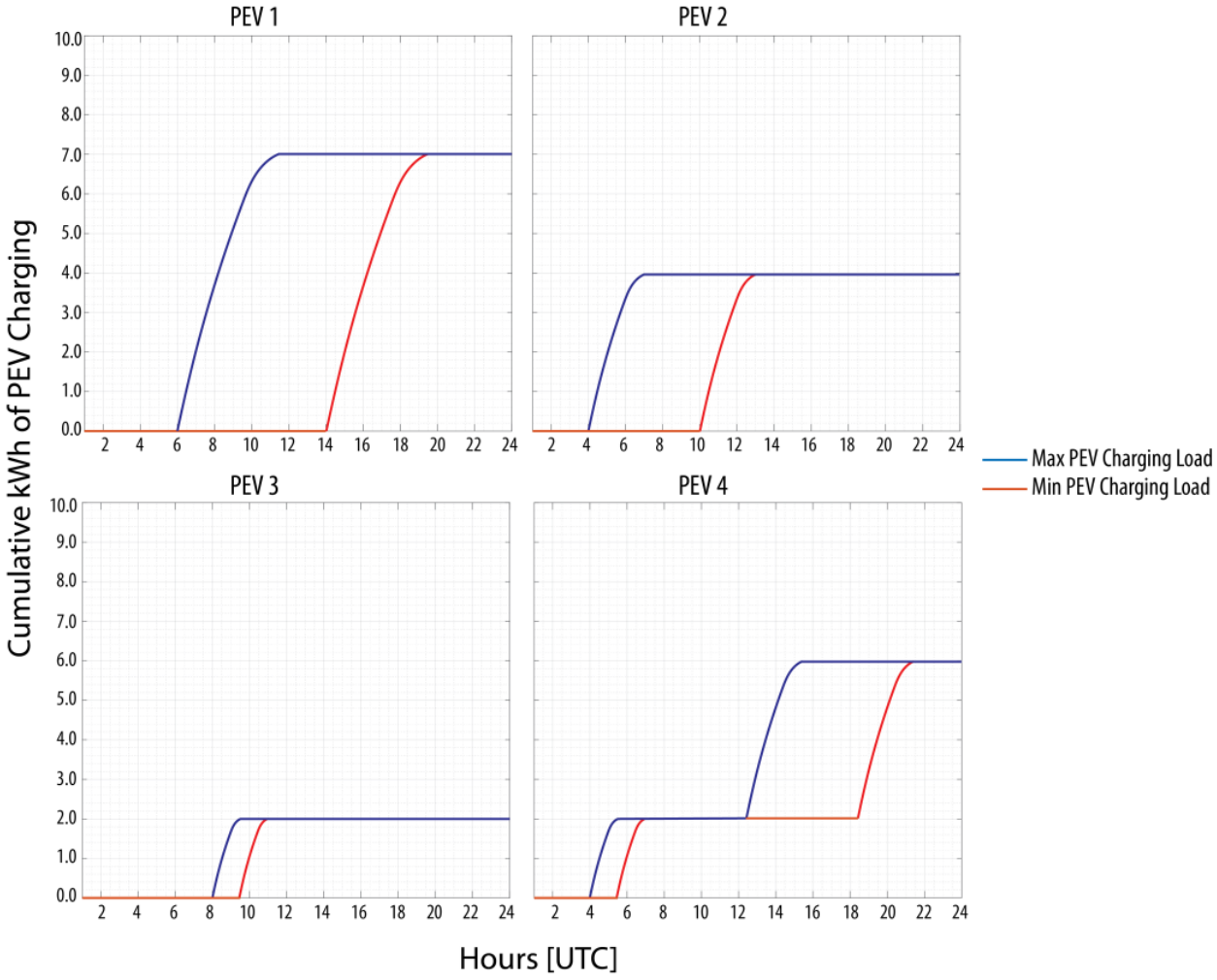

Figure 5.6: Example Constraints on Charging Profiles on Different PEVs.

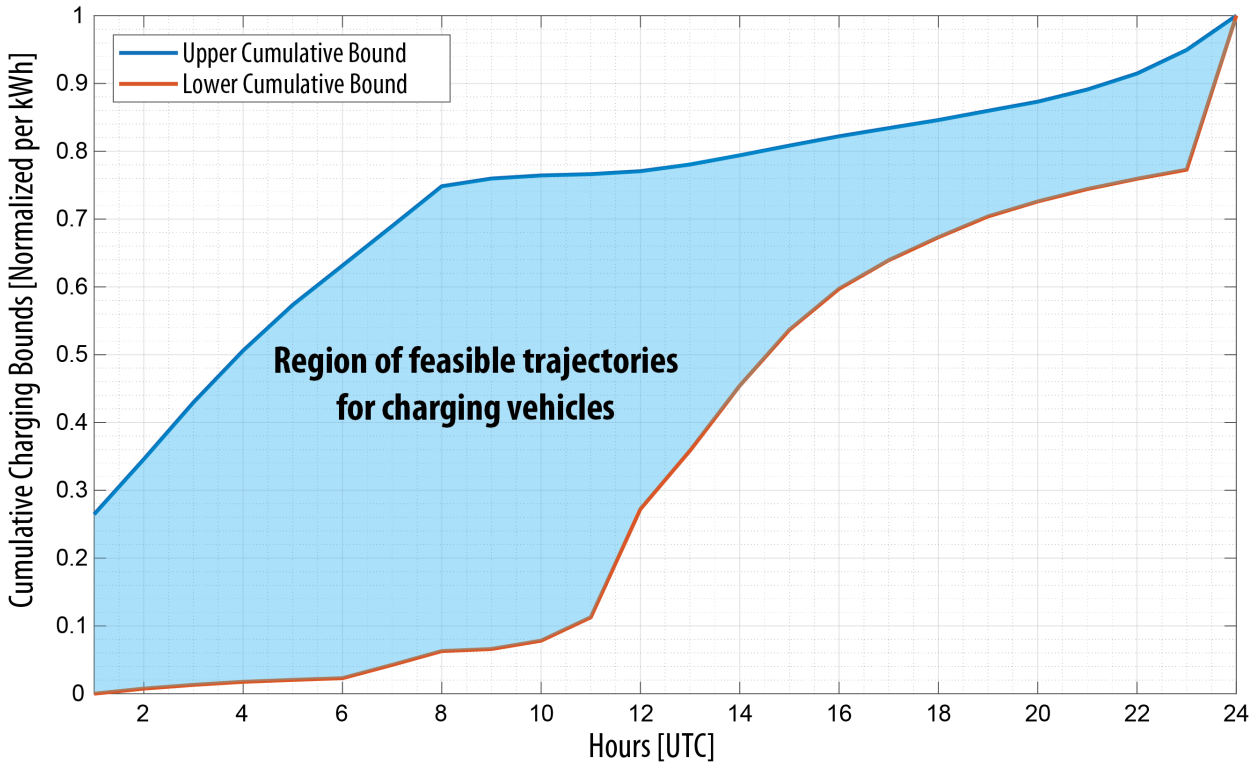

Figure 5.7: Average Bounds on Cumulative Charging Trajectories.

Table 5.3: Fraction of Shifted Demand by Period and Zone.

	Period			
Average Moveable Percentage of Hourly Total Demand	2020	2030	2040	2050
Total % CA [w.r.t. total load]	0.30%	2.00%	7.00%	10.00%
Total % non-CA [w.r.t. total load]	0.00%	0.30%	2.00%	7.00%

zone and period. The percentages of available load shifting are shown in Table 5.3.

Through the day, the total load shifted between hours must add up to zero. This condition is crucial to guarantee that the total demand is the same despite DR being available or not.

Results and Analysis

Installed Capacity by 2050 in the WECC and California

Fig. 5.8 and 5.9 show installed capacity by fuel in the WECC and California, respectively. As expected, the capacity required in the WECC by 2050 increases as the electricity demand increases for each scenario.

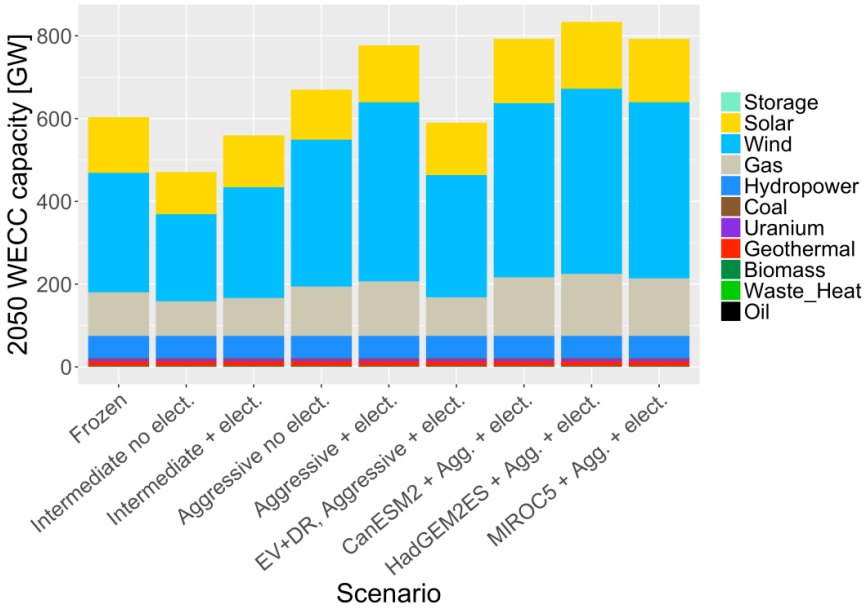

Figure 5.8: Installed Capacity in the WECC by 2050 for All Scenarios.

In all scenarios, wind power is the dominant technology. The greatest wind share is 56% in the Aggressive Efficiency with Electrification case, and the smallest wind share is 45% in the Intermediate Efficiency (SB 350) scenario. The second most used technology in the WECC by 2050 is solar power with its share ranging between 22% (frozen and intermediate efficiency scenarios) and 18% (aggressive efficiency without climate change scenarios). Gas power comes in third place with capacity installed by 2050 ranging between 16% and 18%. Hydropower's capacity ranges from 6% and 11%. There is less than 3% of installed capacity for geothermal, nuclear energy and biomass.

In the climate change scenarios, the total capacity installed in the WECC is 2% to 7% higher than in their non-climate change counterpart (aggressive efficiency and electrification).

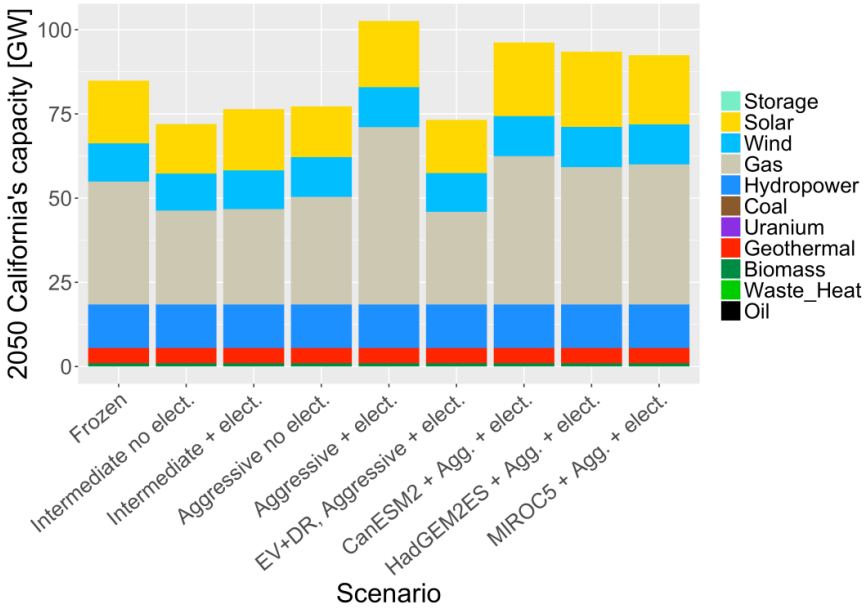

Figure 5.9: Installed Capacity in California by 2050 for All Scenarios.

Load and hydropower availability projections from HadGEM2ES present the highest stress for the power grid (total capacity 7% higher).

California observes a similar trend as the WECC for total installed capacity by 2050. As expected, the total capacity increases along with total load in the different scenarios. Gas power is the predominant technology for California in 2050 with its share ranging from 51% to 38%, in the aggressive efficiency and electrification scenario and in the EV and DR scenario, respectively. The next technology that follows gas power is solar energy. Solar power ranges between 24% and 19%. The climate change scenario from HadGEM2ES and the intermediate efficiency and electrification scenario show a 24% share of solar power. The next technology used the most in California is hydropower. Hydropower's installed capacity ranges between 13% and 18% depending on the scenario, then wind power, with one or two percent lower fraction compared to hydropower. The smaller participation of wind power in California compared to the WECC can be explained by the land exclusion applied to wind farm deployment in California (refer to [106]).

The climate change scenarios show interesting results in California. The total capacity installed by 2050 for the three scenarios using climate change is lower than their non-climate change counterpart (aggressive efficiency and electrification). The total capacity in the cli-

mate change scenarios is 6% to 10% lower than the capacity installed in the aggressive efficiency and electrification scenario. This result is counterintuitive due to the higher annual load that California faces under climate change. Transmission lines expansion between California and the rest of the WECC explains this result. Thus, the strategy to face climate change impacts that will minimize costs will rely on investing more in transmission capacity between California and the rest of the WECC.

Installed Transmission by Periods in the WECC and California

In Fig. 5.10, we observe how two of the climate change scenarios expand the transmission system between California and the rest of the WECC more than in the non-climate change scenario (aggressive efficiency and electrification). For HadGEM2ES, there is 6% more transmission capacity used in 2050 between California and the WECC compared to the non-climate change scenario. In the MIROC5 scenario, there is 4% more transmission capacity installed.

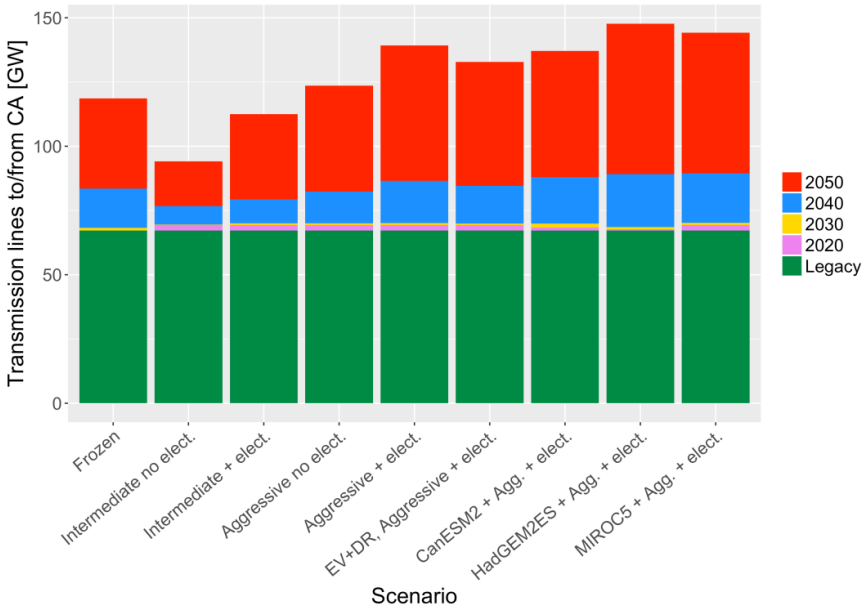

Figure 5.10: Existing and New Transmission Lines Capacity for All Periods and All Scenarios Between California and the Rest of the WECC.

This increase in transmission capacity between California and the rest of the WECC is optimal compared to instead increasing the capacity of the generation in California.

Another interesting finding is that to meet the strict carbon cap goals and higher load by 2050, transmission lines must expand more aggressively in 2050 compared to the other periods simulated. Between 18% and 40% of the total transmission lines capacity is built in the 2050 time frame depending on the scenario.

Fig. 5.11 shows the expansion in transmission capacity in the WECC by period for each scenario. There is a positive correlation between the scenarios with more annual load and more transmission capacity expanded. Between 18% and 44% of the total transmission capacity is installed in the last period (2050) depending on the scenario.

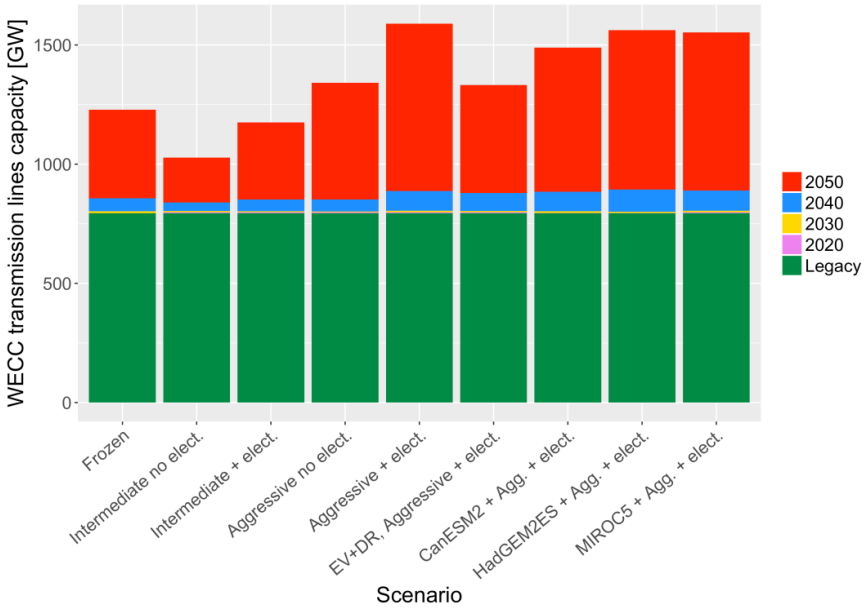

Figure 5.11: Existing and New Transmission Lines Capacity for All Periods in the WECC for All Scenarios.

Fig. 5.12 shows transmission capacity expansion within California by period for all scenarios. Most of the transmission capacity is already in place in the system. In 2050, the Californian transmission system gets expanded by 5% to 12% of the cumulative installed capacity.

Yearly Generation by 2050 in the WECC and California

Fig. 5.13 and 5.14 show yearly electricity generation in 2050 for the WECC and California, respectively. The majority of the energy generated in 2050 in the WECC comes from

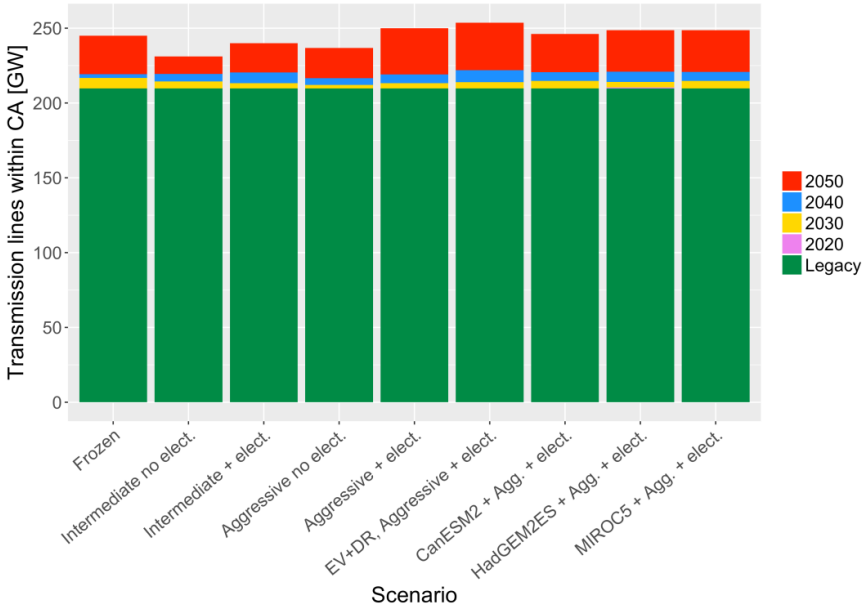

Figure 5.12: Existing and New Transmission Lines Capacity for All Periods and All Scenarios Between Load Zones in California.

wind power. Wind generation constitutes between 47% and 59% of the energy mix by 2050 depending on the scenario. The scenarios that show the highest participation of wind generation are the aggressive efficiency and electrification scenario (59%) and also the climate change scenarios (56% - 58%). Solar generation is the next most prevalent supply source, generating between 15% and 21%. Because the EV flexibility provides more efficient use of the solar PV peak output, the electrical vehicles and demand response scenario deploys solar energy the most (21%) compared to the other scenarios. Generation from hydropower ranges between 10% and 15%. Gas power generation varies between 7% and 9%. The scenarios that show the lowest gas share (7%) are the Aggressive efficiency and electrification, electrical vehicles and demand response, and the climate change scenarios.

In the case of California, geothermal, hydropower, and solar power generate the majority of the energy for all scenarios in 2050 (between 59% and 73%). Wind power comes next, with a generation share ranging between 14% and 17%. Generation from gas power plants is restricted to 9% - 14%, except for the aggressive efficiency and electrification where its share is 22%. As expected, the electrical vehicles and demand response scenario shows the smallest gas share (9%) and the greatest share from solar generation (34%) among all the scenarios.

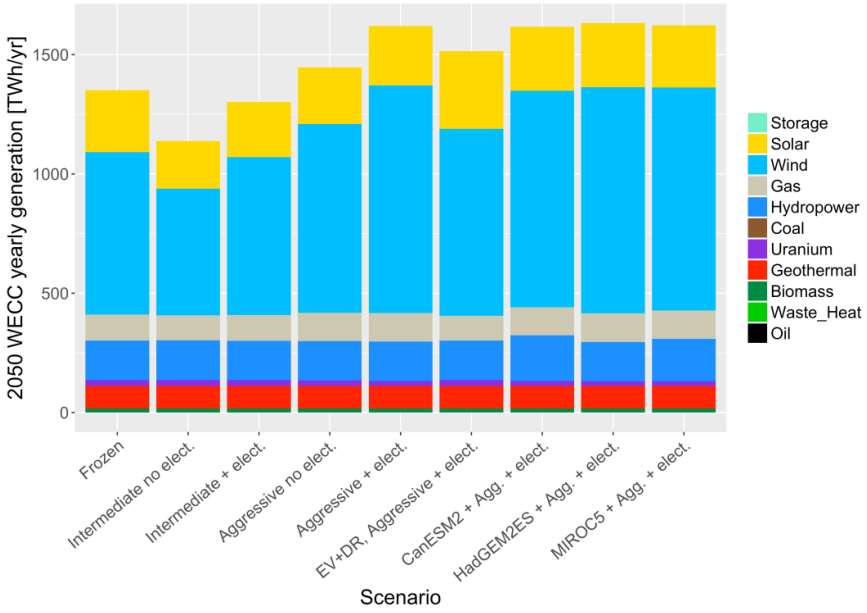

Figure 5.13: Yearly Generation in the WECC by 2050 For All Scenarios.

This is because the flexibility provided by EV and DR can replace the flexibility that gas peaker plants provide. In the climate change scenarios, we observe less total energy generated in-state compared to its analogous scenario without climate change. This corroborates the importance of the transmission system between California and the rest of the WECC to minimize total costs to operate the grid under climate change.

Electrical Vehicles and Demand Response: Aggressive Efficiency With Electrification

Runs using SWITCH show significant differences in installed capacity when the flexibility from EV and DR is considered in the model. Fig. 5.15 depicts the installed capacity in the WECC by technology through periods 2020 to 2050.

It can be observed that total installed capacity in 2050 is reduced by more than 100 GW, while the proportion of installed solar energy increases. This occurs because the flexibility from EVs and DR is used to reduce the load peak of the system, which reduces the necessity of capacity during peak hours, while also shifting load and charging vehicles during sunny hours. This leads to an efficient deployment and use of solar power. This effect is also observed in the generated energy in the region as observed in Fig. 5.16.

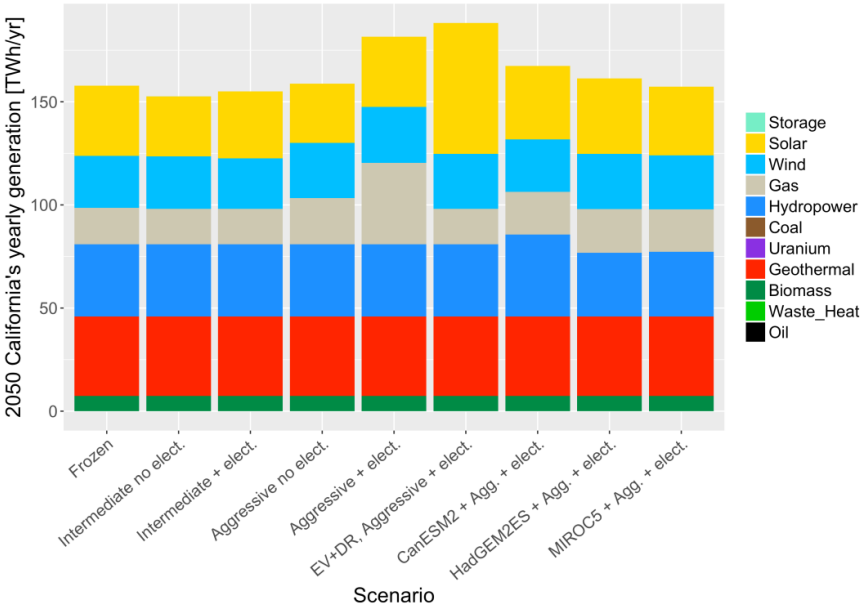

Figure 5.14: Yearly Generation in California by 2050 for All Scenarios.

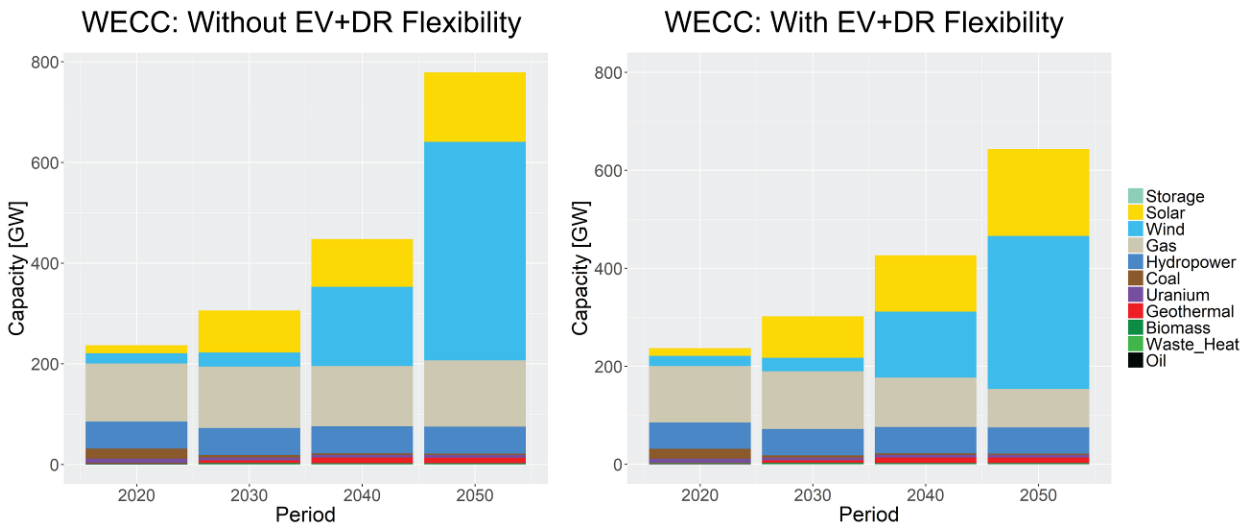

Figure 5.15: Installed Capacity in the WECC Without and With Flexibility from EV and DR.

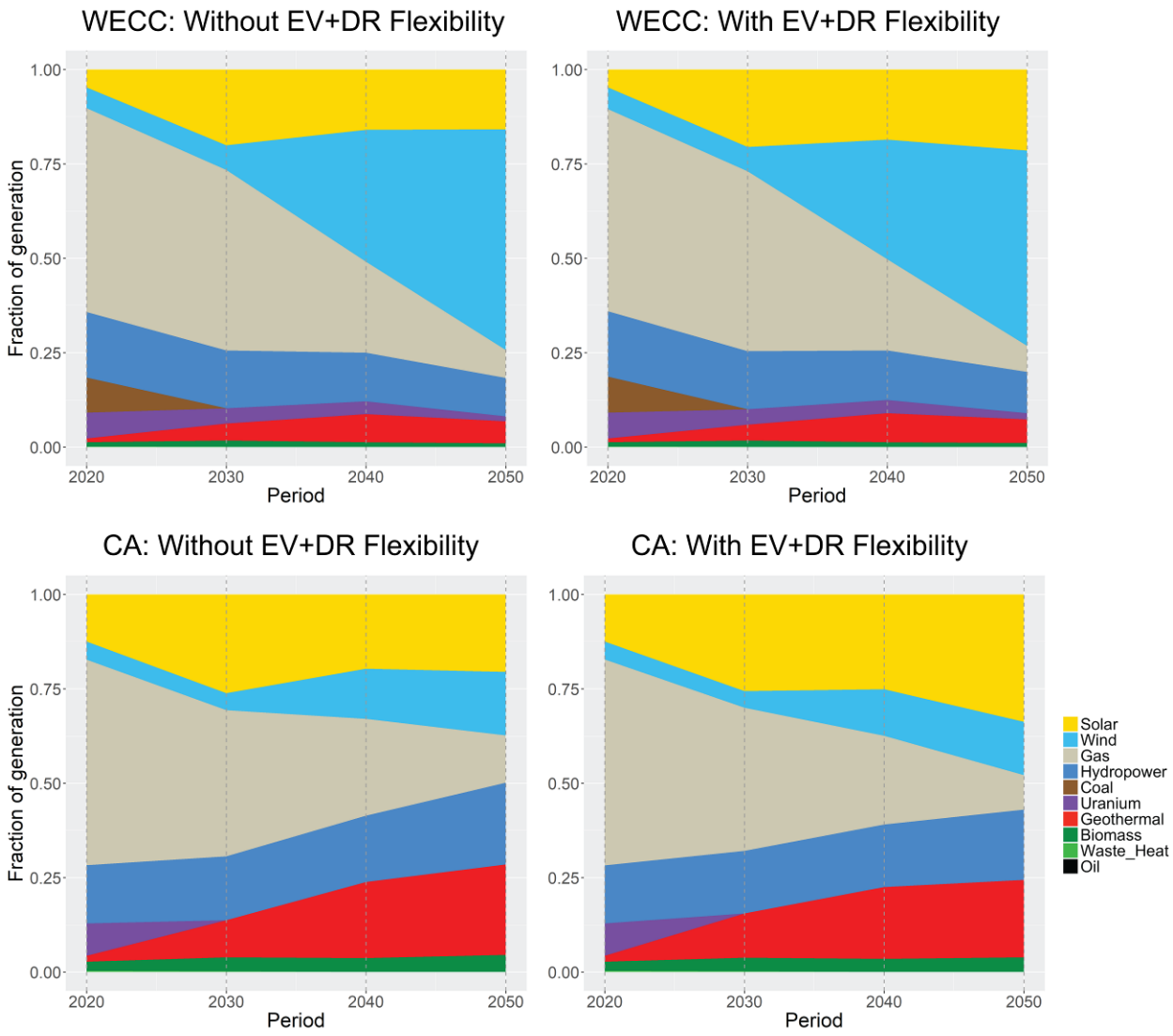

Figure 5.16: Fraction of Generation in the WECC and California Systems Without/With Flexibility of EV and DR.

Thanks to this flexibility, solar energy can be used more efficiently, particularly in California, where the flexibility from EV and DR is higher than in other states. This allows the percentage of solar energy use to increase by 12% in California by 2050. Results show that this flexibility yields savings around 5.2% of the total investment and operational costs through 2020 to 2050. However, these results implicitly assume that smart charging and DR is free to dispatch and procure, and demand shifting is controlled by the system planner, operator, or third-party service provider.

Conclusions

In all the scenarios modeled, wind power shows the greatest share in capacity installed in the WECC by 2050 (∼51%), followed by solar power (∼20%). The total capacity in the climate change scenarios in the WECC by 2050 increases by 2% to 7% compared to the non-climate change scenario. In terms of generation in the WECC by 2050, wind generates 57%, followed by solar with 18% on average. The generation in California by 2050 is dominated by geothermal, solar, and hydropower (67% on average). Wind generation has the fourth highest renewable contribution due to the land environmental restrictions in California to develop wind farms. Transmission line expansion between California and the rest of the WECC is the optimal strategy to minimize costs when facing climate change. In the case of HadGEM2ES, there is 6% more transmission capacity deployed in 2050 between California and the WECC compared to the non-climate change scenario. In the MIROC5 scenario, there is 4% more transmission capacity installed. Another interesting finding is that to meet the strict carbon cap goals and higher load by 2050 for all scenarios, transmission lines between California and the rest of the WECC need to expand more aggressively in 2050 compared to the other periods simulated. Between 18% and 40% of the total transmission lines capacity gets built in 2050 depending on the scenario.

5.4 Stochastic Optimization Under Climate Change Uncertainty

Introduction

Expanding the capacity of a power system and operating it in a cost-effective manner is a complex task. On one hand, power plants have lifetimes that range from 20 years to more than 50 years. On the other hand, transmission lines can be used for more than 100 years. Deciding the mix of power plant technologies and transmission lines to build, their

capacity, location, and year to start building can be a convoluted problem. In addition, this complexity increases due to the long lifetimes of the components of the system, and their high capital costs. This challenge becomes a high financial burden if decisions are not made optimally. Moreover, adding the operational layer to the capacity expansion problem increases the complexity because the size of the optimization increases from making yearly decisions (expansion of capacity) to hourly decisions (operation of the power system).

Besides this complexity, there is the uncertainty in the parameters used as inputs during the entire time horizon modeled. This uncertainty makes it even more challenging to find an optimal solution. Sources of this uncertainty include: how capital costs will vary over the years for each technology, how fuel costs will fluctuate, what will be the hourly electricity demand, the variability of hourly capacity factors for wind and solar power plants, hydropower seasonal and annual variability, etc. In most power system capacity expansion studies, the method used to address this uncertainty is to analyze different possible scenarios. To generate data for different types of analyses, there is research that focuses on forecasting demand, solar and wind capacity factors, fuel prices, etc.

Lastly, climate change adds another dimension of complexity in the prediction of climate driven parameters. Electricity demand and hydrology are the main parameters in power systems modeling that could be affected by climate change. There has been an ongoing effort to predict demand and hydrology under different climate models and RCPs (Representative Concentration Pathways). There exist several climate change models. However, the scientific community has not been able to determine which climate model will predict more accurately the changes in temperature, precipitation and snowfall. The impacts on these variables vary widely depending on the climate model.

Consequently, to study the optimal expansion of a power system considering the uncertainty on impacts from climate change, a scenario-based approach will only shed light on independent possible routes of capacity expansion. Each set of inputs projected from a climate change model would produce an independent possible capacity expansion. Although this type of approach can provide useful information in discovering how the system should expand and operate for each of the different load and hydrological projections, it falls short in providing a robust answer for policy makers, regulators, and investors. A robust approach would provide an optimal and unique capacity expansion given the lack of knowledge about which climate model will better predict loads and hydrology. Therefore, a robust approach to this problem would use as input different load and hydrological projections from different climate models. These possible scenarios (each with an associated probability) would need to be feasible from an operational perspective and would minimize the expected value of the total cost (investment and operation). The optimal solution would provide a unique optimal build out of power plants and transmission lines for all the years of the simulation and it

would be robust and resilient since it would be optimized considering different possible scenarios. This approach removes the need to find a perfect model to predict climate change, and uses a range of possible climate change predictions.

One stochastic optimization approach that models well the robust approach to power system capacity expansion under uncertainty is the multi-stage optimization [23]. More details on how we pose the optimization problem are described in the Subsection Model Description: Stochastic SWITCH WECC Python.

Recently, there have been two power systems models of the WECC that, to some extent, incorporate uncertainty in the framework of stochastic programming. The Pacific Northwest National Laboratory developed a model in 2015 [71] that simulates operation (not investment) in a probabilistic manner for 38 load zones in the WECC. This model considers load, wind, and solar forecast errors (not from climate change), and generation outages. Johns Hopkins University developed the JHSMINE model for the WECC in 2016 [51]. JHSMINE makes investment decisions for transmission and power plants in addition to operational decisions (similarly to SWITCH). However, their planning horizon is until 2024 (opposed to 2050 for SWITCH). JHSMINE takes into account different scenarios for fuel prices, load growth, technology and policies but does not consider uncertainty from climate change.

The novelty and contribution of this work is that it is the first stochastic long-term (2050) capacity expansion and operations model of the WECC with a high temporal (hourly) and spatial resolution (50 load zones and ∼8000 possible power plants to decide to install), which also takes into account uncertainty in hourly loads and hydropower availability due to climate change. The stochastic SWITCH WECC model can take into account uncertainty in any of its inputs (loads, capacity factors, fuel costs, capital costs, hydropower availability, transmission costs, and policies). For this study, we focus on modeling uncertainty from climate change, thus we incorporate uncertainty from hourly loads and hydropower availability for each month and year of the simulation period.

Model Description: Stochastic SWITCH WECC Python

The mathematical formulation we use is a two-stage optimization. We model three climate change scenarios: CanESM2ES, HadGEM2ES and MIROC5. Each scenario is assumed to have the same probability 1/3. The SWITCH model has two types of decision variables: investment and operation. In the two-stage formulation, the investment decisions are the first stage variables, and the operational decisions are the second stage variables. In other words, investment decisions for all periods will be the same for the three scenarios (i.e., resilient investment decisions), and operational decisions will be specific to each climate change scenario. The objective function is the expected value of the total net present value of the

three climate change scenarios. Fig. 5.17 depicts a schematic of decision variables and how they relate to each scenario.

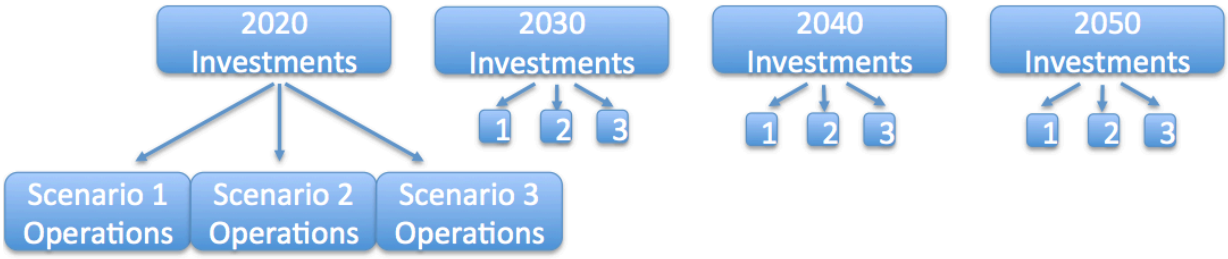

Figure 5.17: Decision Variables for Stochastic SWITCH WECC Python.

The equivalent robust formulation by extension is the following:

$$\min \quad \mathbb{E}\{f_1(x), f_2(x), f_3(x)\}$$

s.t.

$(A.2)$ power balance constraints $\forall$ scenario $i \in \{1,2,3\}$

$(A.15) - (A.18)$ dispatch constraints $\forall$ scenario $i \in \{1,2,3\}$

$(A.10) - (A.14)$ investment constraints $\forall$ scenario $i \in \{1,2,3\}$

$(A.26) - (A.30)$ fuel usage constraints $\forall$ scenario $i \in \{1,2,3\}$

$(A.31) - (A.33)$ transmission investment and flow $\forall$ scenario $i \in \{1,2,3\}$

$(A.34) - (A.35)$ demand response constraints $\forall$ scenario $i \in \{1,2,3\}$

$(A.36) - (A.37)$ hydropower generation constraints $\forall$ scenario $i \in \{1,2,3\}$

$(A.38) - (A.43)$ storage investment and operation constraints $\forall$ scenario $i \in \{1,2,3\}$

$(A.44)$ RPS constraints $\forall$ scenario $i \in \{1,2,3\}$

$(A.45) - (A.46)$ carbon cap constraints $\forall$ scenario $i \in \{1,2,3\}$

$K^{\mathrm{G}}_{g,p,1} = K^{\mathrm{G}}_{g,p,2} = K^{\mathrm{G}}_{g,p,3}$ equal generator capacity $\forall g \in \mathcal{G}, \forall p \in \mathcal{P}$

$K^{\mathrm{L}}_{\ell,p,1} = K^{\mathrm{L}}_{\ell,p,2} = K^{\mathrm{L}}_{\ell,p,3}$ equal transmission capacity $\forall \ell \in \mathcal{L}, \forall p \in \mathcal{P}$

where $f_i(x)$ corresponds to the objective function A.1 as defined in the Appendix A for the climate change scenario $i \in \{1,2,3\}$, $\mathbb{E}\{f_1(x), f_2(x), f_3(x)\}$ is the expected value of the cost function (i.e. $\frac{1}{3}\sum_{i=1}^{3} f_i(x)$), (A.X) is the set of investment and operational constraints defined in Appendix A for each climate scenario i, $K^{\mathrm{G}}_{i,g,p}$ is the installed capacity for generation

project g during period p in climate scenario i, $K^{\mathrm{L}}_{i,\ell,p}$ is the installed transmission line capacity of line ℓ until period p for climate scenario i, $\mathcal{G}$ is the set of possible generators, $\mathcal{L}$ is the set of possible transmission lines, and $\mathcal{P}$ is the set of periods in the optimization.

For this study, we developed Stochastic SWITCH-WECC and made this software open source[2]. The value for policy makers of this modeling approach is that a unique optimal capacity expansion portfolio is obtained as an output with an input of three possible climate change scenarios. Thus, a climate change resilient capacity expansion is found with this two-stage stochastic optimization approach.

Results and Analysis

Installed Capacity by 2050 in the WECC and California

Fig. 5.18 and 5.19 show the optimal capacity expansion for 2050 in the WECC and California, respectively. The first notable finding is the optimal capacity installed in the WECC by 2050 in the "Stochastic" or climate change resilient simulation is higher than in the rest of the deterministic climate scenarios. By 2050, 840 GW are installed in the "Stochastic" simulation, and in the deterministic climate change scenarios the total capacity ranged between 790 GW and 830 GW. This result is expected because the "Stochastic" simulation has to invest in enough capacity by 2050 to provide feasible and optimal dispatch decisions for each of the climate change scenarios.

Another interesting finding is that the share in capacity of gas power plants increases to 19% in the "Stochastic" formulation compared to 18% in the deterministic cases. This can be explained because the "Stochastic" formulation has to face three different dispatch scenarios instead of a single one (deterministic case). Facing three times the number of constraints (dispatch equal to load for all hours) compared to the deterministic cases will result in a greater need for flexibility, which can be provided by gas power plants. Total installed capacity by 2050 of wind and solar power decreases by 1% in the "Stochastic" formulation.

Similar findings can be observed in the total capacity installed by 2050 in California for the "Stochastic" climate change formulation compared to the deterministic climate change scenarios. By 2050, 97 GW are installed in the "Stochastic" case, whereas the total capacity installed in the deterministic scenarios varies between 92 and 96 GW. The gas capacity installed in the "Stochastic" formulation corresponds to 46% of the total capacity. Gas capacity in the deterministic climate change scenarios varies between 46% and 44%.

[2]https://github.com/RAEL-Berkeley/switch/tree/wecc

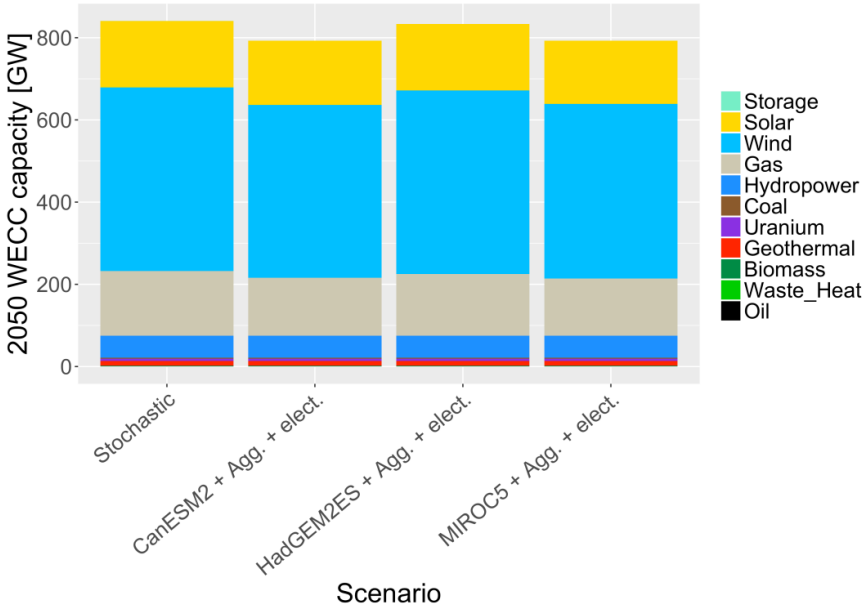

Figure 5.18: Installed Capacity in the WECC by 2050 for Deterministic and Stochastic Climate Change Scenarios.

Installed Transmission by Periods in the WECC and California

The total transmission capacity by 2050 in the WECC is slightly lower for the "Stochastic" climate change simulation compared to the deterministic scenarios (Fig. 5.20). The "Stochastic" simulation optimally installs 1,550 GW of transmission, while the deterministic cases install between 1,560 and 1,450 GW. This difference can be explained by the greater total installed capacity the "Stochastic" simulation shows. Less transmission is necessary because more capacity is available for generation in the WECC.

Despite the overall slight reduction in total transmission installed by 2050 in the WECC for the "Stochastic" simulation, the transmission between California and the WECC increases compared to the deterministic climate change scenarios (Fig. 5.21). Transmission installed in the "Stochastic" case is 145 GW, while the deterministic cases range between 137 and 144 GW.

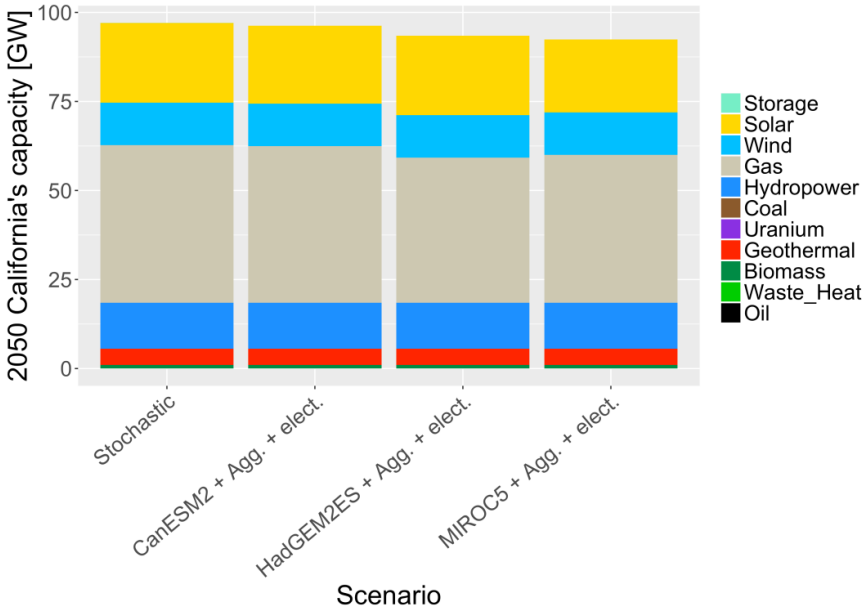

Figure 5.19: Installed Capacity in California by 2050 for Deterministic and Stochastic Climate Change Scenarios.

Conclusions

Typical electricity-grid capacity expansion models make investment decisions with fixed inputs (for example fixed electricity demands and hydro-power availability). The resultant electricity supply system may not be robust to future climate change-driven uncertainties in energy demand and supply. This work presents, to the authors' knowledge, the first climate change stochastic long-term (2050) capacity expansion and operation electricity grid model (Stochastic SWITCH WECC) for the Western North America electricity region, with high temporal and spatial resolution. The Stochastic SWITCH WECC model generates an optimal (least cost) portfolio of power plants capacity that is robust to varying future climate conditions using a multi-stage optimization approach with varying electricity-demand and hydropower-availability inputs under three climate change scenarios (CanESM2ES, HadGEM2ES and MIROC5, RCP 8.5). We find that an optimal robust electricity supply portfolio in the WECC for 2050 has about 4% higher overall installed capacity than the average mix of the three scenarios modeled separately, and about 5.6% higher installed gas capacity, because of the greater need of operational flexibility under the wider range of possible conditions.

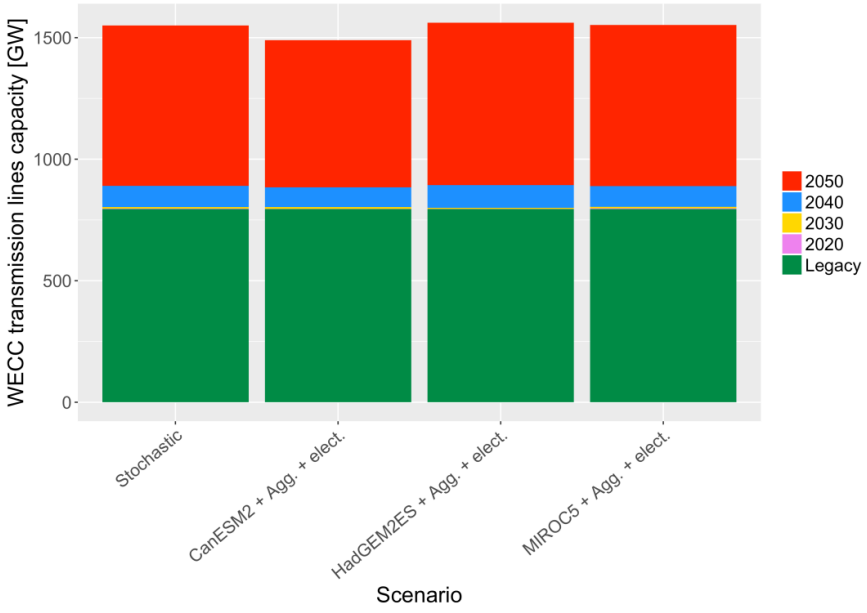

Figure 5.20: Existing and New Transmission Lines Capacity for All Periods in the WECC for Deterministic and Stochastic Climate Change Scenarios.

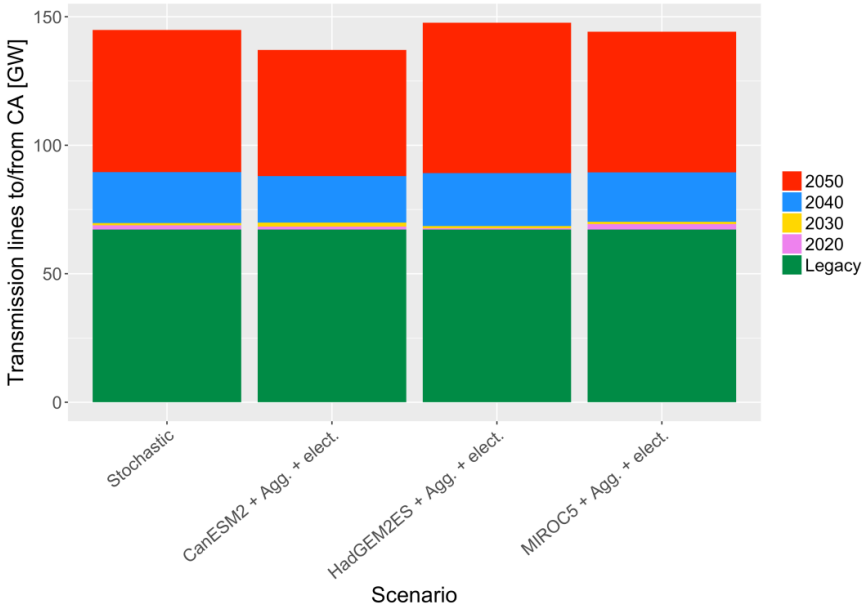

Figure 5.21: Existing and New Transmission Lines Capacity Between California and the WECC for All Periods, for the Deterministic and Stochastic Climate Change Scenario.

Chapter 6

Conclusions and Future Directions

6.1 Summary of Findings

The body of work in this dissertation addresses two time scales of challenges associated to the integration of RES: real-time and long-term, Part I and Part II, respectively. The long-term capacity expansion work in Western North America shows that by 2050, the power system needs to be mostly dominated by RES to achieve the goal of 80% emissions reductions from 1990 levels. This result inspires the portion of work that addresses real-time operations. In a grid with a generation mix that varies depending on the time of the day, and predominantly inverter connected, i.e. low and variable inertia, how can frequency be controlled in order to maintain it at its nominal value. In this section we summarize the main findings from both pieces of work.

As more non-synchronous RES participate in power systems, the system's inertia decreases and becomes time dependent, challenging the ability of existing control schemes to maintain frequency stability. System operators, research laboratories, and academic institutes have expressed the importance to adapt to this new power system paradigm. However, power dynamics have been modeled as time-invariant, by not modeling the variability in the system's inertia. To address this the work in Chapter 2 proposes a new modeling framework for power system dynamics to simulate a time-varying evolution of rotational inertia coefficients in a network. Power dynamics are modeled as a hybrid system with discrete modes representing different rotational inertia regimes of the network. With this new framework, we test two standard frequency control designs and propose a third design: Linear MPC, Inertia Placement, and Dynamic Inertia Placement. As expected, the Linear MPC formulation is better in terms of cost and energy injection/absorption to control frequency. This finding encourages researchers to continue designing controllers in order to attain such opti-

mality without having to optimize in real time (closed-loop MPC). Another relevant finding is the fact that the Dynamic Inertia Placement proves to be more efficient in terms of cost and energy usage of the controller compared to the classical Inertia Placement case. This finding sheds light on the importance of modeling dynamics over time assuming temporal variability in the system's inertia. Additionally, it highlights the importance of designing a more flexible controller that would adapt over time.

Using this new modeling framework for power dynamics, Chapter 3 studies how to control frequency in a network by learning a controller (Section 3.2) and then reducing communication between the control agents (Section 3.3). The work in Section 3.2 proposes a new framework for obtaining a constant data-driven controller for uncertain and time-varying power system dynamics. This is relevant because it can be intractable to solve frequency dynamics in real time (time-varying LQR) in large power networks. In addition, time-varying controllers, as the one from LQR, rely in the ability to predict or identify the current mode of the hybrid system. Finally, given the existing infrastructure and droop control, it would be simpler to implement a proportional controller with fixed gains compared to a time-varying control. Using the mathematical formulation for power dynamics introduced in Chapter 2, we find optimal controllers using an LQR formulation. We use the solution (x, u) from the LQR as a dataset to train a fixed controller. We test our learned controller in different modes against optimal controllers. Results show that our learned controller can be used to obtain a similar performance as the optimal LQR controllers in the different modes. Finally, we show that adding a virtual inertia controller can stabilize the system for low inertia modes. This highlights the importance of using more flexible controllers when considering temporal variability in the system dynamics.

In Section 3.3 we study how restricting communication between nodes affects the performance and stability of a time-invariant controller designed for time-varying power system dynamics due to RES. To do this, we generate a training set by solving an MPC formulation for different scenarios of frequency control. We design controllers with different numbers of features (states) via Lasso regressions. We add virtual inertia to these controllers to guarantee stability. For the 11-bus test system we study, we are able to show that it is possible to reduce the number of features in the controller (to 5 in our case study) without negatively impacting performance and stability for any fixed inertia of the system. We also show how increasing information availability beyond a threshold (10 features) does not enhance performance or stability metrics. We are able to show global asymptotic stability for the hybrid system using controllers with 10 features or more. Finally, by analyzing optimal feature selection for sparse controllers, we find a positive correlation between feature selection and connectivity of the nodes.

The work in Chapter 4 studies the question of planning the power system in the medium

(2030) or long-term (2050). Results are conclusive by depicting a higher deployment of coal power instead of gas by 2030 in the medium optimizations compared to results from the long optimizations for the same year. Conversely, the long optimizations show a progressive transition towards a cleaner electric grid from early stages (2030). The medium optimizations do not foresee the more stringent carbon cap by 2050. Thus, they have to transition quicker to a cleaner grid in the last two decades (second step of the optimization) instead of progressively transitioning during the four periods. To address the impact of medium term planning, we recommend to either place more stringent targets in the medium term (2030) or plan until 2050 with its more restrictive carbon cap by the end of the simulation. Given that it is impractical to suggest regulators to optimize the grid until 2050, we recommend to design stronger near-term policies (e.g. 2030) that would result in mimicking decisions made by optimizing in the long-term. For the"CPP" scenario, instead of enforcing a reduction on emissions to 11% below 1990 levels by 2030, a reduction in emissions by 26% in 2030 in the WECC would mimic the optimal and cost-effective energy transition of planning in the long-term.

In Chapter 5 we show results from different scenarios implemented in SWITCH WECC Python (deterministic and stochastic). In all the deterministic scenarios modeled (Section 5.3), wind power shows the greatest share in capacity installed in the WECC by 2050 (51%), followed by solar power (20%). The total capacity in the climate change scenarios in the WECC by 2050 increases by 2% to 7% compared to the non-climate change scenario. In terms of generation in the WECC by 2050, wind generates 57%, followed by solar with 18% on average. Transmission line expansion between California and the rest of the WECC is found to be the optimal strategy to minimize costs when facing climate change. Another interesting finding is that to meet the strict carbon cap goals and higher load by 2050 for all scenarios, transmission lines between California and the rest of the WECC need to be expanded more aggressively in 2050 compared to the other periods simulated. Between 18% and 40% of the total transmission lines capacity gets built in 2050 depending on the scenario.

The work in Section 5.4 presents, to the authors' knowledge, the first climate change stochastic long-term (2050) capacity expansion and operation electricity grid model (Stochastic SWITCH WECC) for the Western North America electricity region, with high temporal and spatial resolution. Typical electricity-grid capacity expansion models make investment decisions with fixed inputs (for example fixed electricity demands and hydro-power availability). The resultant electricity supply system may not be robust to future climate change-driven uncertainties in energy demand and supply. The Stochastic SWITCH WECC model generates an optimal (least cost) portfolio of power plants capacity that is robust to varying future climate conditions using a multi-stage optimization approach with varying electricity-demand and hydropower-availability inputs under three climate change scenar-

ios (CanESM2ES, HadGEM2ES and MIROC5, RCP 8.5). We find that an optimal robust electricity supply portfolio in the WECC for 2050 has about 4% higher overall installed capacity than the average mix of the three scenarios modeled separately, and about 5.6% higher installed gas capacity, because of the greater demand for operational flexibility under the wider range of possible conditions.

6.2 Future Directions

Wildfire Mitigation: Microgrids + Distribution Networks

A subfield that requires work is how to operate and design market schemes for islanded distribution networks supplied by RES. This work is motivated by the wildfires that have occurred in California and other regions. A risk mitigation strategy that is being considered is to disconnect portions of the grid at the distribution level with self generation available. To do this effectively, we need to ensure a reliable operation of the resulting microgrid and a tariff scheme that will support its efficient operation. Some of the aspects of interest to study are the stochasticity of the residential solar resource and of the electricity demand, the challenge of a microgrid with zero inertia, and the coupling/decoupling of the microgrid to the transmission network. These factors can inform how dispatch could be optimized and how frequency and voltage could be controlled.

Frequency Dynamics and Power Flow to Design Ancillary Services

It is of importance to continue to shed light on how to effectively control power dynamics (frequency and voltage) in power systems dominated by RES. The work in this dissertation focuses on designing frequency regulation control schemes at the transmission level. This line of work can be expanded by also studying voltage regulation under high penetration of distributed solar panels.

Additionally, in collaboration with my colleague Dr. Line Roald, we plan to redesign the market for ancillary services in the grid with high penetration of RES. Power dynamics and optimal power flow have been traditionally modeled separately due to their different time resolutions. However, the market can be optimized by considering both time scales jointly in order to economically efficiently encourage the necessary ancillary services that a future grid with only RES would require. I would establish a collaboration with the California Independent System Operator in order to implement this new market scheme.

Frequency Regulation with Low and Variable Inertia

This work can be extended by studying optimal placement and communications needs of the control agents in these transmission networks. The importance of this question, under normal operations, lies on the cost effectiveness that would transpire from optimally placing, for example, batteries to provide frequency regulation in certain nodes of the grid. In addition to the cost effectiveness argument, this work would enhance reliability in the power system by taking into account potential faults and identifying strategic placement for frequency regulation. To approach this question we can use graph theory by exploring controllability guarantees in any given power systems network. It is also imperative to propose electricity market redesigns that promote the adoption of these new control schemes. To address this question, I have started a collaboration with my colleague Dr. Bala Poolla using the framework in [83].

ML and Safety for Power Systems

Traditionally, this field has relied on optimality and safety guarantees that optimization and control theory provide. In this new era of big data, new tools have become available to solve these prevailing challenges. Machine learning and artificial intelligence have gained popularity in the power systems community to tackle some open questions.

The recent usage of machine learning algorithms to operate the grid require these techniques to be adequately connected to the system operator's planning cycles to guarantee learned behaviors remain adequate in shifting environments. Understanding and mitigating these vulnerabilities requires additional analysis and design thinking that is often overlooked in traditional power systems literature. For this reason, it is relevant to study these vulnerabilities, propose guidelines to avoid safety risks, as we did in [30], and propose mathematical frameworks to use machine learning algorithms while at the same time embedding stability guarantees at the learning stage. More generally, the new subfield of dynamical systems' safety and learning poses many research questions that invite the scientific community to advance knowledge.

Appendix A

SWITCH

This Appendix contains the objective function, variables, parameters, and constraints for the modules that were implemented for the SWITCH WECC model, and for Stochastic SWITCH WECC Python. For a full description of the SWITCH model refer to [56]. This Appendix was adapted and synthesized from the Supplemental material in [56].

A.1 Objective Function

The objective function minimizes the total cost of investments and operations (as net present value):

$$\min \sum_{p \in \mathcal{P}} d_p \left\{ \sum_{c^{\mathrm{f}} \in \mathcal{C}^{\mathrm{fixed}}} c_p^{\mathrm{f}} + \sum_{t \in \mathcal{T}_p} w_t^{\mathrm{year}} \sum_{c^{\mathrm{v}} \in \mathcal{C}^{\mathrm{var}}} c_t^{\mathrm{v}} \right\} \tag{A.1}$$

Where $\mathcal{P}$ is the set of periods in the optimization, $\mathcal{C}^{\mathrm{fixed}}$ is the set of fixed costs, $\mathcal{C}^{\mathrm{var}}$ is the set of variable costs, $\mathcal{T}_p$ is the set of timepoints in the optimization, and p, c^{f}, t and c^{v} are respective elements in those sets. The term c_p^{f} is the fixed cost that occurs during period p, c_t^{v} is the variable cost per timepoint t, w_t^{year} scales costs from a sampled timepoint to an annualized value, and d_p is the discount factor that converts the costs to net present value.

A.2 Operational Constraints

Power balance

Power injection and withdrawal must be equal in each load zone for all timepoints.

$$\sum_{p^{\mathrm{i}} \in \mathcal{P}^{\mathrm{inject}}} p_{z,t}^{\mathrm{i}} = \sum_{p^{\mathrm{w}} \in \mathcal{P}^{\mathrm{withdraw}}} p_{z,t}^{\mathrm{w}}, \qquad \forall z \in \mathcal{Z}, \forall t \in \mathcal{T} \tag{A.2}$$

Depending on the SWITCH modules used, power injection $\mathcal{P}^{\mathrm{inject}}$ includes power output $P_{g,t}$ for every generation project g located in load zone z and incoming transmission flows to the load zone z, $F_{\ell_z^{\mathrm{in}},t}$. Power withdrawal $\mathcal{P}^{\mathrm{withdraw}}$ typically includes electricity loads $l_{z,t}$ and outgoing transmission flows $F_{\ell_z^{\mathrm{out}},t}$.

Dispatch

When unit commitment is not being modeled, the power generation constraint per generator g is the following:

$$0 \leq P_{g,t} \leq \eta_{g,t} K^{\mathrm{G}}_{g,p}, \qquad \forall \ell \in \mathcal{L}, p \in \mathcal{P}, \forall t \in \mathcal{T}_p \tag{A.3}$$

For firm generators, $\eta_{g,t}$ is constant and represents average outage rates. For intermittent generators, $\eta_{g,t}$ also represents the renewable source's capacity factor at a timepoint t.

If the unit commitment module is included in the optimization, the set of constraints are the following:

$$0 \leq W_{g,t} \leq \eta_g K^{\mathrm{G}}_{g,p}, \qquad \forall g \in \mathcal{G}, \forall p \in \mathcal{P}, \forall t \in \mathcal{T}_p \tag{A.4}$$

$$d^{\min}_g W_{g,t} \leq P_{g,t} \leq W_{g,t}, \qquad \forall g \in \mathcal{G}, \forall t \in \mathcal{T} \tag{A.5}$$

$$W_{g,t} - W_{g,t-1} = U_{g,t} - V_{g,t}, \qquad \forall g \in \mathcal{G}, \forall t \in \mathcal{T} \tag{A.6}$$

Eq. (A.4) limits committed capacity $W_{g,t}$ to available capacity. Eq. (A.5) limits dispatch $P_{g,t}$ based on the generator's minimum dispatch fraction $d^{\min}_g$ and committed capacity. Eq. (A.6) defines startup and shutdown state-tracking variables ($U_{g,t}$ and $V_{g,t}$) as the change in committed capacity over time. Startup costs (fuel and O&M) are accounted for in the objective function.

The constraint on transmission limits flows $F_{\ell,t}$ through a line ℓ based on capacity $K^{\mathrm{L}}_{\ell,p}$ and derated by the factor η^{L}_{ℓ}:

$$0 \leq F_{\ell,t} \leq \eta^{\mathrm{L}}_{\ell} K^{\mathrm{L}}_{\ell,p}, \qquad \forall \ell \in \mathcal{L}, p \in \mathcal{P}, \forall t \in \mathcal{T}_p \tag{A.7}$$

Minimum up and down times

When the unit commitment module is included, constraints on minimum up and down times are modeled:

$$W_{g,t} \geq \sum_{t'=t-\hat{\tau}^{\mathrm{u}}_g}^{t} U_{g,t'}, \qquad \forall g \in \mathcal{G}, \forall t \in \mathcal{T} \tag{A.8}$$

$$W_{g,t} \leq \eta_g K^{\mathrm{G}}_{g,p(t)} - \sum_{t'=t-\hat{\tau}^{\mathrm{d}}_g}^{t} V_{g,t'}, \qquad \forall g \in \mathcal{G}, \forall t \in \mathcal{T} \tag{A.9}$$

where $\hat{\tau}_g$ is the number of prior timepoints to t to consider. SWITCH uses circular indexing for time series, so that $t = -1$ refers to the last timepoint in the same time series (end state equal to start).

A.3 Investment Constraints

Generation projects that have a cap, $\overline{k^{\mathrm{G}}}_g$, on their maximum capacity installed are constrained by A.10. Eqs. (A.11) and (A.13) represent cumulative installed capacity for generation projects $K^{\mathrm{G}}_{g,p}$ and transmission lines $K^{\mathrm{L}}_{\ell,p}$ until period p. As such, they are defined as the sum of previous capacity additions $B^{\mathrm{G}}_{g,p'}$ and $B^{\mathrm{L}}_{\ell,p'}$, including existing infrastructure. The set $\mathcal{P}^{\mathrm{on}}_{g,p}$ corresponds to the set of all periods when capacity of type g could be built and still be in service in period p. Eqs. (A.12) and (A.14) fix the investment decisions of some generation projects and transmission lines over some periods $\mathcal{P}^{\mathrm{G}}_g$ and $\mathcal{P}^{\mathrm{L}}_\ell$ with predetermined values specified in input files (which is the case of existing, or pre-planned capacity).

$$0 \leq K^{\mathrm{G}}_{g,p} \leq \overline{k^{\mathrm{G}}}_g, \qquad \forall g \in \mathcal{G}^{\mathrm{rc}}, p \in \mathcal{P} \tag{A.10}$$

$$K^{\mathrm{G}}_{g,p} = \sum_{p' \in \mathcal{P}^{\mathrm{on}}_{g,p}} B^{\mathrm{G}}_{g,p'}, \qquad \forall g \in \mathcal{G}, \forall p \in \mathcal{P} \cup \{p_0\} \tag{A.11}$$

$$B^{\mathrm{G}}_{g,p} = b^{\mathrm{G}}_{g,p}, \qquad \forall g \in \mathcal{G}, \forall p \in \mathcal{P}^{\mathrm{G}}_g \tag{A.12}$$

$$K^{\mathrm{L}}_{\ell,p} = \sum_{p' \in \mathcal{P} \cup \{p_0\} : p' \leq p} B^{\mathrm{L}}_{p',k}, \qquad \forall \ell \in \mathcal{L}, \forall p \in \mathcal{P} \tag{A.13}$$

$$B^{\mathrm{L}}_{\ell,p} = b^{\mathrm{L}}_{\ell,p}, \qquad \forall \ell \in \mathcal{L}, \forall p \in \mathcal{P}^{\mathrm{L}}_\ell \tag{A.14}$$

A.4 SWITCH Modules

Treatment of time

SWITCH uses three levels of time scales: timepoints, timeseries and period. Timepoints represent the highest time granularity in the optimization. Depending on the user of SWITCH, a timepoint can represent one hour or a set of hours. Timeseries are a set of consecutive timepoints. Examples of timeseries would be a day, a few days, a week, a month, or a year. A period is a set of consecutive years where investments can be made. Table A.1 summarizes the time components in SWITCH.

Type	Symbol	Component Name	Description
Set	$\mathcal{P}$	PERIODS	Set of all investment periods, indexed by p.
Parameter	st_p	period_start[p]	Year in which period p begins.
Parameter	y_p	period_length_years[p]	Length in years of period p.
Set	$\mathcal{S}$	TIMESERIES	Set of all time series. Indexed by s.
Subset	$\mathcal{S}_p$	TS_IN_PERIOD[p]	Subset of time series that fall in period p.
Parameter	num_s	ts_num_tps[s]	Number of time points in time series s.
Parameter	Δ_s^{S}	ts_duration_of_tp[s]	Duration in hours of each time point in time series s. Used for short-term thermodynamics such as energy storage calculations.
Parameter	Δ_t^{T}	tp_duration_hrs[t]	Duration in hours of time point t (equal to Δ_s^{S} for the corresponding timeseries).
Parameter	w_t^{period}	tp_weight[t]	Weight of timepoint t within simulation (hours).
Parameter	w_t^{year}	tp_weight_in_year[t]	Weight of timepoint t within its year (hours/year).
Parameter	θ_s	ts_scale_to_period[s]	Number of times a time series s (or equivalent conditions) occurs in its period. Used statistically for sample weighting for economics, pollution and long-term energy demand.
Set	$\mathcal{T}$	TIMEPOINTS	Set of all time points, indexed by t.
Subset	$\mathcal{T}_s$	TPS_IN_TS[s]	Subset of time points that fall in time series s.
Subset	$\mathcal{T}_p$	TPS_IN_PERIOD[p]	Subset of time points that fall in period p.

Table A.1: Model components defined in the `timescales` module.

The weight of a timepoint's within a period is given by

$$w_t^{\text{period}} = \Delta_t^{\text{T}} \cdot \theta_s, \qquad \forall p \in \mathcal{P}, \forall s \in \mathcal{S}_p, \forall t \in \mathcal{T}_s.$$

This reflects the fact that each timepoint represents Δ_t^{T} hours within its timeseries, and each timeseries is treated as recurring θ_s times in its period.

Financial components

Type	Symbol	Component Name	Description
Parameter	r	discount_rate	Annual real discount rate used to convert future dollars to present.
Parameter	i	interest_rate	Annual real interest rate used to finance investments.
Parameter	baseyear	base_financial_year	Base financial year in which future costs will be converted to net present value via discount rate r.
Set	$\mathcal{C}^{\text{fixed}}$	Cost_Components_Per_Period	Fixed cost components that contribute to the total cost in the cost-minimizing objective function.
Set	$\mathcal{C}^{\text{var}}$	Cost_Components_Per_TP	Variable cost components that contribute to the total cost in the cost-minimizing objective function.

Table A.2: Model components defined in the `financials` module.

Load zones and power injection/withdrawal

Type	Symbol	Component Name	Description
Set	$\mathcal{Z}$	LOAD_ZONES	Set of all load zones, indexed by z.
Parameter	$l_{z,t}$	zone_demand_mw[z, t]	Demand in MW at zone z at time point t.
Subset	$\mathcal{Z}^{\text{peak}}$	EXTERNAL_COINCIDENT_PEAK_DEMAND_ZONE_PERIODS	Subset of load zones, period pairs for which and expected peak load has bbeen provided.
Parameter	$l_{z,p}^{\text{peak}}$	zone_expected_coincident_peak_demand[z,p]	Expected peak load demand in zone z in period p, $(z, p) \in \mathcal{Z}^{\text{peak}}$ (optional).
Set	$\mathcal{P}^{\text{inject}}$	Zone_Power_Injections	Model components that inject power to the central bus of each load zone.
Set	$\mathcal{P}^{\text{withdraw}}$	Zone_Power_Withdrawals	Model components that withdraw power from the central bus of each load zone.

Table A.3: Model components defined in the `balancing.load_zones` module.

Energy sources

Type	Symbol	Component Name	Description
Set	$\mathcal{E}$	ENERGY_SOURCES	Set of all energy sources, indexed by f.
Subset	$\mathcal{E}^{\text{F}}$	FUELS	Subset of all fuel-based energy sources.
Subset	$\mathcal{E}^{\text{R}}$	NON_FUEL_ENERGY_SOURCES	Subset of all non-fuel energy sources.
Parameter	$\xi_f, f \in \mathcal{E}^{\text{F}}$	f_co2_intensity[f]	Direct emissions of CO2 of a fuel in tCO2/MMBtu.
Parameter	$\mu_f, f \in \mathcal{E}$	f_upstream_co2_intensity[f]	Emissions attributable to an energy-source before it is consumed in tCO2/MMBtu.

Table A.4: Model components defined in the `energy_sources.properties` module.

Investment components

Type	Symbol	Component Name	Description
Set	$\mathcal{G}$	GENERATION_PROJECTS	Set of all generation projects, indexed by g.
Subset	$\mathcal{G}^{\mathrm{B}}$	BASELOAD_GENS	Subset of all generation projects that are baseload.
Subset	$\mathcal{G}^{\mathrm{F}}$	FUEL_BASED_GENS	Subset of all generation projects that use fuels.
Subset	$\mathcal{G}^{\mathrm{R}}$	VARIABLE_GENS	Subset of all generation projects that are variable renewable.
Subset	$\mathcal{G}^{\mathrm{rc}}$	CAPACITY_LIMITED_GENS	Subset of all generation projects that are resource constrained.
Subset	$\mathcal{G}_z^{\mathrm{Z}}$	GENS_IN_ZONE[z]	Subset of all generation projects that are located in load zone z.
Parameter	b_g^{unit}	gen_unit_size[g]	Size of individual generating units within project g (optional).
Subset	$\mathcal{G}^{\mathrm{unit}}$	DISCRETELY_SIZED_GENS	Subset of generation projects for which a discrete unit size $\mathrm{b}_g^{\mathrm{unit}}$ has been specified.
Subset	$\mathcal{E}_g^{\mathrm{F}}$	FUELS_FOR_GEN[g]	Subset of fuels that can be used by generator g.
Parameter	$\mathrm{ly}_g^{\mathrm{G}}$	gen_max_age[g]	Operational lifetime of capacity added to generation project g (years). Capital costs are also amortized over this period.
Parameter	$b_{g,p}^{\mathrm{G}}$	gen_predetermined_cap[g,p]	Predetermined addition of capacity in project g during period p (MW).
Set	$\mathcal{GP}^{\mathrm{B}}$	GEN_BLD_YRS	Set of tuples of generation projects g and periods p in which capacity may be added.
Subset	$\mathcal{GP}^{\mathrm{D}}$	PREDETERMINED_GEN_BLD_YRS	Subset of generation projects g and periods p for which the capacity additions are predetermined (may include years before the main study).
Subset	$\mathcal{P}_{g,p}^{\mathrm{on}}$	BLD_YRS_FOR_GEN_PERIOD[g,p]	Set of periods (including p) when capacity of type g could have been built and still be in service in period p. This excludes capacity that would be retired before period p.
Subset	$\mathcal{P}_g^{\mathrm{on}}$	PERIODS_FOR_GEN[g]	Subset of periods when generation project g may have capacity online. This excludes periods before g can be built or after it must be retired.
Parameter	$\overline{k^{\mathrm{G}}}_g$	gen_capacity_limit_mw[g]	Maximum allowed capacity for project g (MW).
Variable	$B_{g,p}^{\mathrm{G}}$	BuildGen[g,p]	Amount of capacity built (added) in project g in period p; $(g,p) \in \mathcal{GP}^{\mathrm{B}}$.
Variable	$K_{g,p}^{\mathrm{G}}$	GenCapacity[g,p]	Cumulative capacity of project g as of period p.
Parameter	$\hat{c}_g^{\mathrm{G,inv}}$	gen_overnight_cost[g,p]	Overnight capital cost per MW to add capacity to project g in period p; $(g,p) \in \mathcal{GP}^{\mathrm{B}}$.
Parameter	$\hat{c}_g^{\mathrm{G,upg}}$	gen_connect_cost_per_mw[g]	Overnight cost of grid upgrades to support the project g, per MW installed.
Parameter	$c_g^{\mathrm{G,fix}}$	gen_fixed_om[g,p]	Fixed operation and maintenance costs per MW of capacity per year, for capacity added to project g in period p; $(g,p) \in \mathcal{GP}^{\mathrm{B}}$. This cost recurs every year until the capacity retires ($\mathrm{ly}_g^{\mathrm{G}}$ years).
Parameter	$c_g^{\mathrm{G,var}}$	gen_variable_om[g]	Variable operation and maintenance costs per MWh of power produced by project g.
Parameter	h_g	gen_full_load_heat_rate[g]	Full load heat rate (inverse of thermal efficiency), in MMBtu per MWh. May be supplemented by part-load heat rates in generators.core.commit.fuel_use.

Table A.5: Model components defined in the `generators.core.build` module.

Dispatch components

Type	Symbol	Name	Description
Subset	$\mathcal{T}_g^{\text{on}}$	TPS_FOR_GEN[g]	Subset of timepoints when generation project g may have capacity online. Corresponds to $\mathcal{P}_g^{\text{on}}$ defined in generators.core.build.
Subset	$\mathcal{GT}^{\text{on}}$	GEN_TPS	Set of tuples of generator g and timepoint t when capacity can be online. $\mathcal{GT}^{\text{on}} = \{(g,t) : g \in \mathcal{G} \text{ and } t \in \mathcal{T}_g^{\text{on}}\}$.
Subset	$\mathcal{T}_{g,p}^{\text{on}}$	TPS_FOR_GEN_IN_PERIOD[g,p]	Subset of timepoints when generation project $g \in \mathcal{G}$ has capacity available during period $p \in \mathcal{P}$. Includes all timepoints in p if $(g,p) \in \mathcal{GT}^{\text{on}}$, otherwise the empty set.
Variable	$P_{g,t}$	DispatchGen[g,t]	Average power in MW produced by project g during timepoint t.
Variable	$R_{g,t,f}$	GenFuelUseRate[g,t,f]	Rate of use of fuel $f \in \mathcal{E}_g^{\text{F}}$ by project $g \in \mathcal{G}^{\text{F}}$ during timepoint t (in MMBtu/h). Each generator may use multiple fuels.
Parameter	η_g	gen_forced_outage_rate[g]	Fraction of time a project $g \in \mathcal{G}$ is expected to be available (used to de-rate for forced outages).
Parameter	$\eta_{g,t}$	gen_max_capacity_factor[g,t]	Maximum possible output from renewable project $g \in \mathcal{G}^{\text{R}}$ in timepoint t (per-unit).

Table A.6: Model components defined in the `generators.core.dispatch` module.

Type	Symbol	Component Name	Description
Variable	$P_{g,p}^{\text{B}}$	DispatchBaseloadByPeriod[g,p]	Amount of power to produce from baseload generator $g \in \mathcal{G}^{\text{B}}$ during all timepoints in period $p \in \mathcal{P}_g^{\text{on}}$ (MW)

Table A.7: Model components defined in the `generators.core.no_commit` module.

The constraints for no unit commitment are the following:

$$P_{g,t} = P_{g,p(t)}^{\text{B}}, \qquad \forall g \in \mathcal{G}^{\text{B}}, \forall t \in \mathcal{T}_g^{\text{on}} \tag{A.15}$$

$$0 \leq P_{g,t} \leq \eta_g K_{g,p(t)}^{\text{G}}, \qquad \forall g \in \mathcal{G} - \mathcal{G}^{\text{R}}, \forall t \in \mathcal{T}_g^{\text{on}} \tag{A.16}$$

$$0 \leq P_{g,t} \leq \eta_g \eta_{g,t} K_{g,p(t)}^{\text{G}}, \qquad \forall g \in \mathcal{G}^{\text{R}}, \forall t \in \mathcal{T}_g^{\text{on}} \tag{A.17}$$

$$\sum_{f \in \mathcal{E}_g^{\text{F}}} R_{g,t,f} = h_g P_{g,t}, \qquad \forall g \in \mathcal{G}^{\text{F}}, \forall t \in \mathcal{T}_g^{\text{on}} \tag{A.18}$$

Table A.8 and constraints A.19 - A.23 apply when unit commitment is modeled.

Type	Symbol	Component Name	Description
Variable	$W_{g,t}$	CommitGen[g,t]	How much capacity to commit (have online) in project g in timepoint $t \in \mathcal{T}_g^{\text{on}}$.
Variable	$U_{g,t}$	StartupGenCapacity[g,t]	How much additional capacity to commit (startup) in project g in timepoint $t \in \mathcal{T}_g^{\text{on}}$.
Variable	$V_{g,t}$	ShutdownGenCapacity[g,t]	How much committed capacity to decommit (shutdown) in project g in timepoint $t \in \mathcal{T}_g^{\text{on}}$.
Parameter	$d_g^{\min}$	gen_min_load_fraction[g]	Minimum dispatch fraction (minimum load) of the committed capacity (defaults to 1 for baseload projects, 0 for others).
Parameter	$c_g^{\text{up,OM}}$	gen_startup_om[g]	O&M costs per MW for starting up capacity.
Parameter	$\delta_g^{\text{up,fuel}}$	gen_startup_fuel[g]	Fuel requirements for starting up additional generation capacity, in units of MMBtu/MW.
Parameter	τ_g^{u}	gen_min_uptime[g]	Minimum time that generator g can be committed (up, online) in hours.
Parameter	τ_g^{d}	gen_min_downtime[g]	Minimum time that generator g can be uncommitted (down, offline) in hours.

Table A.8: Model components defined in the `generators.core.commit.operate` module.

$$0 \leq W_{g,t} \leq \eta_g K_{g,p(t)}^{\text{G}}, \qquad \forall g \in \mathcal{G}, \forall t \in \mathcal{T}_g^{\text{on}} \tag{A.19}$$

$$d_g^{\min} W_{g,t} \leq P_{g,t}, \qquad \forall g \in \mathcal{G}, \forall t \in \mathcal{T}_g^{\text{on}} \tag{A.20}$$

$$P_{g,t} \leq W_{g,t}, \qquad \forall g \in \mathcal{G} - \mathcal{G}^{\text{R}}, \forall t \in \mathcal{T}_g^{\text{on}} \tag{A.21}$$

$$P_{g,t} \leq \eta_{g,t} W_{g,t}, \qquad \forall g \in \mathcal{G}^{\text{R}}, \forall t \in \mathcal{T}_g^{\text{on}} \tag{A.22}$$

$$W_{g,t} - W_{g,t-1} = U_{g,t} - V_{g,t}, \qquad \forall g \in \mathcal{G}, \forall t \in \mathcal{T}_g^{\text{on}} \tag{A.23}$$

$$W_{g,t} \geq \sum_{t'=t-\hat{\tau}_g^{\text{u}}}^{t} U_{g,t'}, \qquad \forall g \in \mathcal{G}, \forall t \in \mathcal{T} \tag{A.24}$$

$$\eta_g K_{g,p(t)}^{\text{G}} - W_{g,t} \geq \sum_{t'=t-\hat{\tau}_g^{\text{d}}}^{t} V_{g,t'}, \qquad \forall g \in \mathcal{G}, \forall t \in \mathcal{T} \tag{A.25}$$

where $\hat{\tau}_g = \text{round}\{\tau_g / \Delta_t^{\text{T}}\}$.

The startup operation and maintenance costs for each generator at each timepoint are converted to an hourly rate as $c_g^{\text{up,OM}} \cdot U_{g,t} / \Delta_t^{\text{T}}$ and then added to the set $\mathcal{C}^{\text{var}}$ in the objective function (A.1).

Fuel costs

Fuels costs can be modeled as a yearly cost per fuel for each load zone, and as a supply curve for a regional market (set of load zones).

Type	Symbol	Component Name	Description
Parameter	$c^{\text{fuel}}_{z,f,p}$	fuel_cost[z,f,p]	Cost per MMBtu for fuel f in load zone z during period p.
Set	$\mathcal{F}^{\text{unav}}$	GEN_TP_FUELS_UNAVAILABLE	Set of tuples of (project g, timepoint t, fuel f) where fuel f is not available (i.e., user has not specified a cost).

Table A.9: Model components defined in the `energy_sources.fuel_costs.simple` module.

Total fuel costs for each zone and timepoint are calculated as

$$\sum_{g \in \mathcal{G}^{\text{Z}}_z : t \in \mathcal{T}^{\text{on}}_g} \sum_{f \in \mathcal{E}^{\text{F}}_g} c^{\text{fuel}}_{z,f,p(t)} \times R_{g,t,f}, \qquad \forall z \in \mathcal{Z}, t \in \mathcal{T}. \tag{A.26}$$

Type	Symbol	Component Name	Description
Set	$\mathcal{M}$	REGIONAL_FUEL_MARKETS	Set of all regional fuel markets (rfm), indexed by m.
Parameter	f^{M}_m	rfm_fuel[m]	Type of fuel that is sold in the regional fuel market m.
Subset	$\mathcal{Z}^{\text{M}}_m$	ZONES_IN_RFM[m]	Set of all load zones served by the regional fuel market m.
Set	$\Sigma_{m,p}$	SUPPLY_TIERS_FOR_RFM_PERIOD	Set of supply tiers (i.e., complete supply curve) for a given regional fuel market m and period p, indexed by σ.
Set	$\mathcal{MP\Sigma}$	RFM_SUPPLY_TIERS	Set of valid tuples of regional fuel market m, period p and supply curve tier σ; $\mathcal{MP\Sigma} = \{(m,p,\sigma) : m \in \mathcal{M}, p \in \mathcal{P}, \sigma \in \Sigma_{m,p}\}$
Set	$\mathcal{F}^{\text{unav}}$	GEN_TP_FUELS_UNAVAILABLE	Set of tuples of (project g, timepoint t, fuel f) where fuel f is not available.
Parameter	$c^{\text{fuel}}_{m,p,\sigma}$	rfm_supply_tier_cost[m,p,σ]	Cost of a fuel in a particular tier of a supply curve $(m,p,\sigma) \in \mathcal{MP\Sigma}$.
Parameter	$\text{limit}_{m,p,\sigma}$	rfm_supply_tier_limit[m,p,σ]	Annual limit of fuel available for a particular tier in the supply curve $(m,p,\sigma) \in \mathcal{MP\Sigma}$.
Variable	$R^{\text{tier}}_{m,p,\sigma}$	ConsumeFuelTier[m,p,σ,]	The annual rate of fuel consumption in each tier of a supply curve, $(m,p,\sigma) \in \mathcal{MP\Sigma}$, in MMBtu/year.

Table A.10: Model components defined in the `energy_sources.fuel_costs.markets` module.

Constraints regarding the tier limits and linkage with power production are defined in

this module:

$$0 \leq R^{\text{tier}}_{m,p,\sigma} \leq \text{limit}_{m,p,\sigma}, \qquad \forall (m,p,\sigma) \in \mathcal{MP\Sigma} \tag{A.27}$$

$$\sum_{\sigma \in \Sigma_{m,p}} R^{\text{tier}}_{m,p,\sigma} = \sum_{z \in \mathcal{Z}^{\text{M}}_m} \sum_{g \in \mathcal{G}^{\text{Z}}_z : f^{\text{M}}_m \in \mathcal{E}^{\text{F}}_g} \sum_{t \in \mathcal{T}_p \cap \mathcal{T}^{\text{on}}_g} w^{\text{year}}_t R_{g,t,f}, \qquad \forall m \in \mathcal{M}, \forall p \in \mathcal{P} \tag{A.28}$$

$$R_{g,t,f} = 0, \qquad \forall (g,t,f) \in \mathcal{F}^{\text{unav}} \tag{A.29}$$

Total fuel costs of all tiers of a supply curve from all regional fuel markets during period p are calculated as:

$$\text{AnnualFuelCosts}_p = \sum_{m \in \mathcal{M}} \sum_{\sigma \in \Sigma_{m,p}} c^{\text{fuel}}_{m,p,\sigma} \cdot R^{\text{tier}}_{m,p,\sigma}, \qquad \forall p \in \mathcal{P}$$

These are added to the set $\mathcal{C}^{\text{fixed}}$ in order to be considered in the objective function (A.1).

When unit commitment is modeled, fuel costs are handled with the module `fuel_use`. Table A.11 shows its components.

Type	Symbol	Component Name	Description
Set	$\mathcal{U}_g$	FUEL_USE_SEGMENTS_FOR_GEN[g]	Ordered set of segments used to define the heat rate curve of project g, indexed by u.
Parameter	$p^{\min}_{g,u}$	power_start_mw*	Minimum power in MW of segment line u of project g.
Parameter	$p^{\max}_{g,u}$	power_end_mw*	Maximum power in MW of segment line u of project g. It is required that $P^{\max}_u = P^{\min}_{u+1}$.
Parameter	γ_g	fuel_use_rate*	Fuel use rate in MMBtu/h at minimum power of project g.
Parameter	$\delta_{g,u}$	ihr*	Incremental heat rate in MMBtu/MWh for segment line u of project g.
Expression	$n_{g,u}$	intercept*	Normalized y-intercept in MMBtu/(h · MW-capacity) of the segment u of project g. Derived from $p^{\min}_{g,u}, p^{\max}_{g,u}, \gamma_g$ and $\delta_{g,u}$.
Set	$\mathcal{GTNL\Delta}$	GEN_TPS_FUEL_PIECEWISE_CONS_SET	Set of tuples of generator g, timepoint t, y-intercept $n_{g,u}$ and incremental heat rate $\delta_{g,u}$ needed for generator fuel usage calculations. This includes one tuple for each combination of fuel-based generators $g \in \mathcal{G}^{\text{F}}$, segments of the piecewise-linear heat-rate curve $u \in \mathcal{U}_g$ for those generators, and active timepoints for those generators $t \in \mathcal{T}^{\text{on}}_g$.

Table A.11: Model components defined in the `generators.core.commit.fuel_use` module. Components marked with * are local to the module (some read from input tables), and are not added to the main model.

Total fuel use (MMBtu/h) for each generation project is constrained as:

$$\sum_{\forall f \in \mathcal{E}_g^{\mathrm{F}}} R_{g,t,f} \geq \frac{1}{\Delta_t^{\mathrm{T}}}(\delta_g^{\mathrm{up,fuel}} \cdot U_{g,t}) + n_{g,u} \cdot W_{g,t} + \delta_{g,u} \cdot P_{g,t}, \quad \forall (g,t,n_{g,u},\delta_{g,u}) \in \mathcal{GTN\Delta} \tag{A.30}$$

Transmission components

Type	Symbol	Component Name	Description
Set	$\mathcal{L}$	TRANSMISSION_LINES	Set of all transmission corridors, indexed by ℓ.
Parameter	ζ_ℓ^1	trans_lz1[l]	Load zone at the start of corridor ℓ.
Parameter	ζ_ℓ^2	trans_lz2[l]	Load zone at the end of corridor ℓ.
Parameter	km_ℓ	trans_length_km[l]	Length in km of transmission corridor $\ell \in \mathcal{L}$.
Parameter	η_ℓ^L	trans_derating_factor[l]	Overall derating factor for transmission corridor ℓ that can reflect forced outage rates, stability or contingency limitations.
Parameter	$\eta_\ell^{\mathrm{L,ef}}$	trans_efficiency[l]	Efficiency; proportion of power sent through corridor ℓ that reaches the other end.
Subset	$\mathcal{LB}$	TRANS_BLD_YRS	Set of transmission corridors ℓ and periods p where capacity can be added
Parameter	b_ℓ^{L}	existing_trans_cap[l]	Transfer capability existing in corridor ℓ prior to the start of the study.
Variable	$B_{\ell,p}^{\mathrm{L}}$	BuildTx[l,p]	Transfer capability added in corridor ℓ during period p (MW); $(\ell,p) \in \mathcal{LB}$.
Expression	$K_{\ell,p}^{\mathrm{L}}$	TxCapacityNameplate[l, p]	Cumulative transfer capability through transmission corridor ℓ as of period p.
Parameter	$\hat{c}^{\mathrm{L}}$	trans_capital_cost_per_mw_km	Generic cost of expanding transfer capability in base year dollars per MW per km.
Parameter	α_ℓ	trans_terrain_multiplier	Cost multiplier for expanding capacity on a specific corridor ℓ.
Parameter	β	trans_fixed_om_fraction	Describes the fixed O&M costs per year as a fraction of capital costs.
Parameter	ly^{L}	trans_lifetime_yrs	Lifetime over which capital costs are amortized (years). Note that capacity is assumed to continue in service after this date, with the same annual payment (equivalent to automatically reconstructing capacity when it retires).
Set	$\mathcal{L}^{\mathrm{D}}$	DIRECTIONAL_TX	Set of directed transmission corridors. It consists of the tuples $(\zeta_\ell^1,\zeta_\ell^2)$ and $(\zeta_\ell^2,\zeta_\ell^1)$, for all $\ell \in \mathcal{L}$. Elements of this set refer to flows from the first zone of the tuple to the second zone.
Set	$\mathcal{L}_z^{\mathrm{D}}$	TX_CONNECTIONS_TO_ZONE[z]	Set of directed transmission corridors that flow into zone z (i.e., the second element is equal to z).

Table A.12: Model components defined in the `transmission.transport.build` module.

The annualized cost (capital and O&M) per MW of capacity in transmission corridor ℓ is:

$$c_{\ell}^{\mathrm{L,inv}} = \left(\frac{i}{1-(1-i)^{-\mathrm{ly}^{\mathrm{L}}}}\right) \hat{c}^{\mathrm{L}} \cdot \alpha_{\ell} \cdot \mathrm{km}_{\ell}$$
$$c_{\ell}^{\mathrm{L,fix}} = \beta c_{\ell}^{\mathrm{L,inv}}$$

These costs are multiplied by the installed transmission capacity as of each future period, $K_{\ell,p}^{\mathrm{L}}$, then discounted to the base year, and added to the set $\mathcal{C}^{\mathrm{fixed}}$ for inclusion in the objective function (A.1).

The installed capability until period p is calculated as:

$$K_{\ell,p}^{\mathrm{L}} = b_{\ell}^{\mathrm{L}} + \sum_{p':(\ell,p')\in\mathcal{LB} \text{ and } p'\leq p} B_{\ell,p'}^{\mathrm{L}}, \qquad \forall \ell \in \mathcal{L}, \forall p \in \mathcal{P}. \tag{A.31}$$

Type	Symbol	Component Name	Description
Variable	$F_{z,z',t}$	DispatchTx[z,z_,t]	Power flow through a directed corridor $(z, z') \in \mathcal{L}^{\mathrm{D}}$ (i.e., from zone z to zone z') during timepoint t.
Expression	$F_{z,t}^{\mathrm{net}}$	TXPowerNet[z,t]	Net power inflow to zone z from all other zones during timepoint t

Table A.13: Model components defined in the `transmission.transport.dispatch` module.

The constraint of maximum flow through lines is defined as:

$$0 \leq F_{z,z',t} \leq \eta_{\ell(z,z')}^{\mathrm{L}} K_{\ell(z,z'),p}, \qquad \forall (z,z') \in \mathcal{L}^{\mathrm{D}}, \forall p \in \mathcal{P}, \forall t \in \mathcal{T}_p, \tag{A.32}$$

where $\ell(z, z')$ identifies the transmission corridor $\ell \in \mathcal{L}$ corresponding to the directed corridor $(z, z') \in \mathcal{L}^{\mathrm{D}}$. With this approach, net inflows to zone z from all other zones can be calculated as total inflows minus total outflows:

$$F_{z,t}^{\mathrm{net}} = \sum_{z':(z',z)\in\mathcal{L}^{\mathrm{D}}} \eta_{\ell(z',z)}^{\mathrm{L,ef}} F_{z',z,t} - \sum_{z':(z,z')\in\mathcal{L}^{\mathrm{D}}} F_{z,z',t} \qquad \forall z \in \mathcal{Z}. \tag{A.33}$$

$F_{z,t}^{\mathrm{net}}$ is added to the set of power-injecting components $\mathcal{P}^{\mathrm{inject}}$ for inclusion in the power balance equation (A.2).

Demand response components

This is an optional module that was used for the California Energy Commission study.

Type	Symbol	Component Name	Description
Parameter	$l_{z,t}^{\text{max,up}}$	dr_shift_up_limit[z,t]	Maximum increase in demand allowed in load zone z at time point t.
Parameter	$l_{z,t}^{\text{max,down}}$	dr_shift_down_limit[z,t]	Maximum reduction in demand allowed in load zone z at time point t. This value must be less than the local demand.
Variable	$L_{z,t}^{\text{dr}}$	ShiftDemand[z,t]	Describes how much load (in MW) is reduced (if it is negative) or increased (if it is positive) in load zone z at timepoint t.

Table A.14: Model components defined in the `balancing.demand_response.simple` module.

The DR shift is bounded by the specified limits, and another constraint ensures that all the changes in demand balance out over the course of each timeseries:

$$-l_{z,t}^{\text{max,down}} \leq L_{z,t}^{\text{dr}} \leq l_{z,t}^{\text{max,up}}, \qquad \forall z \in \mathcal{Z}, \forall t \in \mathcal{T} \tag{A.34}$$

$$\sum_{t \in \mathcal{T}_s} L_{z,t}^{\text{dr}} = 0, \qquad \forall z \in \mathcal{Z}, \forall s \in \mathcal{S} \tag{A.35}$$

The demand shift $L_{z,t}^{\text{dr}}$ is added to the set $\mathcal{P}^{\text{withdraw}}$ to be included in the balance constraint (A.2).

Hydropower components

Type	Symbol	Component Name	Description
Subset	$\mathcal{G}^{\text{H}}$	HYDRO_GENS	Subset of all hydro-based generation projects.
Parameter	$p_{g,s}^{\text{h,min}}$	hydro_min_flow_mw[g,s]	Minimum flow level, expressed as electrical MW, for all timepoints of timeseries s.
Parameter	$p_{g,s}^{\text{h,avg}}$	hydro_avg_flow_mw[g,s]	Average flow level, in electrical MW, that must be achieved during timeseries s.

Table A.15: Model components defined in the `generators.extensions.hydro_simple` module.

Power dispatch must exceed the minimum level for all timepoints, and the average power production during a time series must be equal to the average flow rate:

$$P_{g,t} \geq p^{\text{h,min}}_{g,s}, \qquad \forall g \in \mathcal{G}^{\text{H}}, \forall s \in \mathcal{S}, \forall t \in \mathcal{T}_s. \tag{A.36}$$

$$\frac{1}{\text{num}_s} \cdot \sum_{t \in \mathcal{T}_s} P_{g,t} = p^{\text{h,avg}}_{g,s}, \qquad \forall g \in \mathcal{G}^{\text{H}}, \forall s \in \mathcal{S}. \tag{A.37}$$

Storage components

Type	Symbol	Component Name	Description
Subset	$\mathcal{G}^{\text{S}}$	STORAGE_GENS	Subset of all generation projects that can store electricity for later discharge.
Subset	$\mathcal{GP}^{\text{S}}$	STORAGE_GEN_BLD_YRS	Subset of all tuples of generation project g and period p when storage projects can be built; $\mathcal{GP}^{\text{S}} = \{(g,p) : (g,p) \in \mathcal{GP}^{\text{G}} \text{ and } g \in \mathcal{G}^{\text{S}}\}$.
Parameter	η^{S}_g	gen_storage_efficiency[g]	Round trip efficiency of a storage technology. Self-discharge over time is assumed to be negligible.
Parameter	$\hat{c}^{\text{S,inv}}_{g,p}$	gen_storage_energy_overnight_cost[g]	Overnight capital cost per MWh adding energy storage capacity (not power output) to storage project g in period p.
Parameter	r^{max}_g	gen_store_to_release_ratio[g]	The maximum charging rate for storage project g, expressed as a ratio relative to the maximum power output rate.
Parameter	$r^{\text{S,ep}}_g$	gen_storage_energy_to_power_ratio[g]	Fixed ratio of storage capacity to power rating (hours) for storage project g. Optional; if not specified, Switch optimizes the amount of energy storage capacity.
Parameter	$n^{\text{S,max}}_g$	gen_storage_max_cycles_per_year[g]	Maximum amount of discharging allowed per year, for storage project g, expressed as a multiple of the installed storage capacity (optional).
Variable	$B^{\text{S}}_{g,p}$	BuildStorageEnergy[g,p]	Amount of energy storage capacity to add to project g in period p, in MWh; $(g,p) \in \mathcal{GP}^{\text{S}}$.
Variable	$K^{\text{S}}_{g,p}$	StorageEnergyCapacity[g,p]	Cumulative capacity in MWh of storage project g at period p.
Variable	$C^{\text{S}}_{g,t}$	ChargeStorage[g,t]	Decision of how much to charge a storage project g at time point t.
Variable	$P_{g,t}$	DispatchGen[g,t]	Decision of how much to discharge a storage project g at time point t, i.e., how much power to deliver to the grid (defined in `generators.core.build`).
Variable	$\overline{P_{g,t}}$	DispatchUpperLimit[g,t]	Maximum possible power production by project g at timepoint t, (defined by equation (A.16) or (A.21)).
Variable	$Z^{\text{S}}_{g,t}$	StateOfCharge[g,t]	State of charge in MWh of storage project g at timepoint t.

Table A.16: Model components defined in the `generators.extensions.storage` module.

Overnight costs $\hat{c}^{\text{S,inv}}_{g,p}$ are annualized and added to the set $\mathcal{C}^{\text{fixed}}$ to be part of the objective function (A.1).

Power used for charging/discharging is added to the set of withdrawals $\mathcal{P}^{\text{withdraw}}$/ injections $\mathcal{P}^{\text{inject}}$ in the balance equation (A.2).

The constraints introduced to model investment and operation of storage consider cumulative energy storage capacity, charging limits, storage required, and cycle limits per year.

$$K^{\text{S}}_{g,p} = \sum_{p' \in \mathcal{P}:\ p' \leq p} B^{\text{S}}_{g,p'}, \qquad \forall g \in \mathcal{G}^{\text{S}}, p \in \mathcal{P} \tag{A.38}$$

$$0 \leq C^{\text{S}}_{g,t} \leq r^{\max}_{g} \overline{P_{g,t}}, \qquad \forall g \in \mathcal{G}^{\text{S}}, t \in \mathcal{T}^{\text{on}}_{g} \tag{A.39}$$

$$0 \leq Z^{\text{S}}_{g,t} \leq K^{\text{S}}_{g,p}, \qquad \forall g \in \mathcal{G}^{\text{S}}, t \in \mathcal{T}^{\text{on}}_{g} \tag{A.40}$$

$$Z^{\text{S}}_{g,t} = Z^{\text{S}}_{g,t-1} + (\eta^{\text{S}}_{g} C^{\text{S}}_{g,t} - P_{g,t})\Delta^{\text{T}}_{t}, \qquad \forall g \in \mathcal{G}^{\text{S}}, t \in \mathcal{T}^{\text{on}}_{g} \tag{A.41}$$

$$B^{\text{S}}_{g,p} = r^{\text{S,ep}}_{g} B^{\text{G}}_{g,p}, \qquad \forall (g,p) \in \mathcal{GP}^{\text{S}} : r^{\text{S,ep}}_{g} \text{ specified} \tag{A.42}$$

$$\sum_{t \in \mathcal{T}_p} P_{g,t} \Delta^{\text{T}}_{t} \leq n^{\text{S,max}}_{g} K^{\text{S}}_{g,p} y_p, \qquad \forall (g,p) \in \mathcal{GP}^{\text{S}} \tag{A.43}$$

RPS components

Renewable Portfolio Standards were modeled in SWITCH WECC for each State. Table A.17 shows the components used.

Type	Symbol	Component Name	Description
Parameter	i^{RPS}_{f}	f_rps_eligible[f]	Binary indicator of whether fuel $f \in \mathcal{E}^{\text{F}}$ is eligible for the RPS.
Parameter	$\text{rps}_{p,z}$	rps_target[p,z]	Fraction of total demand in period p that must be generated from RPS-elegible sources in load zone z.

Table A.17: Model components defined in the `policies.rps_unbundled` module.

The RPS target in each period is enforced via the following constraint:

$$\sum_{g \in \mathcal{G}^{\text{R}}} \sum_{t \in \mathcal{T}^{\text{on}}_{g,p}} P_{g,t} w^{\text{period}}_{t} + \sum_{g \in \mathcal{G}^{\text{F}}} \sum_{t \in \mathcal{T}^{\text{on}}_{g,p}} \sum_{f \in \mathcal{E}_g : i^{\text{RPS}}_{f} = 1} \frac{R_{g,t,f}}{h_g} w^{\text{period}}_{t} \geq \sum_{z \in \mathcal{Z}} \text{rps}_{p,z} \times \sum_{t \in \mathcal{T}_p} l_{z,t} w^{\text{period}}_{t}, \quad \forall p \in \mathcal{P} \tag{A.44}$$

This requires that generation that qualifies as RPS supply meets the renewable production target. This module assumes all production occurs at the full-load heat-rate (h_g), so the production from fuel f in timepoint t is given by $R_{g,t,f}/h_g$.

Carbon cap components

Type	Symbol	Component Name	Description
Parameter	cap_p	carbon_cap_tco2_per_yr[p]	Carbon cap in tons of CO_2 per year during period p (defaults to ∞).
Parameter	c_p^{carb}	carbon_cost_dollar_per_tco2[p]	Carbon cost per ton of CO_2 in period p (defaults to \$0).

Table A.18: Model components defined in the `policies.carbon_policies` module.

$$\text{AnnualEmissions}_p = \sum_{g \in \mathcal{G}^{\text{F}}} \sum_{f \in \mathcal{E}_g^{\text{F}}} \sum_{t \in \mathcal{T}_g^{on} \cap \mathcal{T}_p} \Delta_t^{\text{T}} R_{g,t,f} \times (\xi_f + \mu_f), \qquad \forall p \in \mathcal{P} \tag{A.45}$$

The constraint that enforces the carbon cap is:

$$\text{AnnualEmissions}_p \leq \text{cap}_p, \qquad \forall p \in \mathcal{P} \tag{A.46}$$

Bibliography

[1] J. T. Abatzoglou and A. P. Williams. "Impact of anthropogenic climate change on wildfire across western US forests". In: *Proceedings of the National Academy of Sciences* 113.42 (2016), pp. 11770–11775. ISSN: 0027-8424. DOI: 10.1073/pnas.1607171113. eprint: https://www.pnas.org/content/113/42/11770.full.pdf. URL: https://www.pnas.org/content/113/42/11770.

[2] J. C. Adam, A. F. Hamlet, and D. P. Lettenmaier. "Implications of global climate change for snowmelt hydrology in the twenty-first century". In: *Hydrological Processes* 23.7 (2009), pp. 962–972. DOI: 10.1002/hyp.7201. eprint: https://onlinelibrary.wiley.com/doi/pdf/10.1002/hyp.7201. URL: https://onlinelibrary.wiley.com/doi/abs/10.1002/hyp.7201.

[3] U.S. Energy Information Administration. *Annual projections to 2050*. 2017. URL: https://www.eia.gov/analysis/projection-data.php.

[4] U.S. Environmental Protection Agency. "Carbon Pollution Emission Guidelines for Existing Stationary Sources: Electric Utility Generating Units". In: (2015), pp. 64661–64964. DOI: EPA-HQ-OAR-2013-0602FRL-9930-65-OAR.

[5] U.S. Environmental Protection Agency. "Inventory of U.S. Greenhouse Gas Emissions and Sinks: 1990-2018". In: *U.S. Environmental Protection Agency* (2020). URL: https://www.epa.gov/ghgemissions/inventory-us-greenhouse-gas-emissions-and-sinks-1990-2018.

[6] U.S. Environmental Protection Agency. *Power Plant Emission Trends*. 2020. URL: https://www.epa.gov/airmarkets/power-plant-emission-trends.

[7] U.S. Environmental Protection Agency. "Repeal of the Clean Power Plan; Emission Guidelines for Greenhouse Gas Emissions From Existing Electric Utility Generating Units; Revisions to Emission Guidelines Implementing Regulations". In: (2019), pp. 32520–32584. DOI: EPA-HQ-OAR-2017-0355:FRL-9995-70-OAR.

[8] R. Alur et al. *Handbook of networked and embedded control systems*. Springer Science & Business Media, 2007.

[9] M. B. Araújo and C. Rahbek. "How Does Climate Change Affect Biodiversity?" In: *Science* 313.5792 (2006), pp. 1396–1397. ISSN: 0036-8075. DOI: 10.1126/science.1131758. eprint: https://science.sciencemag.org/content/313/5792/1396.full.pdf. URL: https://science.sciencemag.org/content/313/5792/1396.

[10] C. Bellard et al. "Impacts of climate change on the future of biodiversity". In: *Ecology Letters* 15.4 (2012), pp. 365–377. DOI: 10.1111/j.1461-0248.2011.01736.x. eprint: https://onlinelibrary.wiley.com/doi/pdf/10.1111/j.1461-0248.2011.01736.x. URL: https://onlinelibrary.wiley.com/doi/abs/10.1111/j.1461-0248.2011.01736.x.

[11] F. Bellizio et al. "Optimized Local Control for Active Distribution Grids using Machine Learning Techniques". In: *2018 IEEE Power Energy Society General Meeting (PESGM)*. Aug. 2018, pp. 1–5. DOI: 10.1109/PESGM.2018.8586079.

[12] C. Bertram et al. "Carbon lock-in through capital stock inertia associated with weak near-term climate policies". In: *Technological Forecasting and Social Change* 90 (2015), pp. 62–72. ISSN: 0040-1625. DOI: https://doi.org/10.1016/j.techfore.2013.10.001. URL: http://www.sciencedirect.com/science/article/pii/S004016251300259X.

[13] H. Bevrani, T. Ise, and Y. Miura. "Virtual synchronous generators: A survey and new perspectives". In: *International Journal of Electrical Power & Energy Systems* 54 (2014), pp. 244–254.

[14] F. Borrelli, A. Bemporad, and M. Morari. "Predictive Control for Linear and Hybrid Systems". In: *Cambridge University Press* (2017).

[15] T. S. Borsche, T. Liu, and D. J. Hill. "Effects of rotational Inertia on power system damping and frequency transients". In: *Decision and Control (CDC), 2015 54th IEEE Conference on*. IEEE. Dec. 2015, pp. 5940–5946. DOI: 10.1109/CDC.2015.7403153.

[16] M. S. Branicky. "Multiple Lyapunov functions and other analysis tools for switched and hybrid systems". In: *IEEE Transactions on automatic control* 43.4 (1998), pp. 475–482.

[17] J. P. Carvallo, P. Hidalgo-Gonzalez, and D. M. Kammen. "Envisioning a sustainable Chile: Five findings about the future of the Chilean electricity and energy system". In: *Natural Resources Defense Council* (2014). URL: https://www.nrdc.org/sites/default/files/envisioning-sustainable-chile-report.pdf.

[18] N. S. Christensen et al. "The Effects of Climate Change on the Hydrology and Water Resources of the Colorado River Basin". In: *Climatic Change* 62 (2004), pp. 337–363. DOI: https://doi.org/10.1023/B:CLIM.0000013684.13621.1f. URL: https://doi.org/10.1023/B:CLIM.0000013684.13621.1f.

[19] Center for Climate and Energy Solutions. *History of UN Climate Talks*. Accessed in 2020. URL: http://www.c2es.org/content/history-of-un-climate-talks/.

[20] Federal Energy Regulatory Commission. *Form 714: Annual Electric Balancing Authority Area and Planning Area Report*. 2006.

[21] Federal Energy Regulatory Commission. *Form 715: Annual Transmission Planning and Evaluation Report, 2009*. 2009.

[22] A. J. Conejo et al. *Decision Making Under Uncertainty in Electricity Markets*. Vol. 153. Springer, Boston, MA, 2010. ISBN: 978-1-4419-7421-1.

[23] A. J. Conejo et al. *Investment in Electricity Generation and Transmission*. Springer International Publishing, 2016. ISBN: 978-3-319-29501-5.

[24] North American Electric Reliability Corporation. *WECC Standard BAL-STD-002-0 - Operating Reserves*. 2007.

[25] Platts Corporation. *POWERmap: Substation Layer*. 2009. URL: http://www.platts.com/Products/powermap.

[26] Ventyx Corporation. *Ventyx EV Energy Map, 2009*. 2009. URL: http://www.ventyx.com/velocity/ev-energy-map.asp.

[27] F. Dantas-Torres. "Climate change, biodiversity, ticks and tick-borne diseases: The butterfly effect". In: *International Journal for Parasitology: Parasites and Wildlife* 4.3 (2015). Including articles from the inaugural conference on "Impact of Environmental changes on Infectious Diseases (IECID)", pp. 452–461. ISSN: 2213-2244. DOI: https://doi.org/10.1016/j.ijppaw.2015.07.001. URL: http://www.sciencedirect.com/science/article/pii/S2213224415300067.

[28] O. Deschênes and M. Greenstone. "The Economic Impacts of Climate Change: Evidence from Agricultural Output and Random Fluctuations in Weather". In: *American Economic Review* 97.1 (Mar. 2007), pp. 354–385. DOI: 10.1257/aer.97.1.354. URL: https://www.aeaweb.org/articles?id=10.1257/aer.97.1.354.

[29] R. Dobbe, D. Fridovich-Keil, and C. J. Tomlin. "Fully Decentralized Policies for Multi-Agent Systems: An Information Theoretic Approach". In: *NIPS*. 2017.

[30] R. Dobbe* et al. "Learning to Control in Power Systems: Design and Analysis Guidelines for Concrete Safety Problems". In: *(submitted)*. 2019.

[31] F. Dörfler and F. Bullo. "Synchronization and transient stability in power networks and non-uniform Kuramoto oscillators". In: *Proceedings of the 2010 American Control Conference*. 2010, pp. 930–937.

[32] M. B. Dyurgerov and M. F. Meier. "Twentieth century climate change: Evidence from small glaciers". In: *Proceedings of the National Academy of Sciences* 97.4 (2000), pp. 1406–1411. ISSN: 0027-8424. DOI: 10.1073/pnas.97.4.1406. eprint: https://www.pnas.org/content/97/4/1406.full.pdf. URL: https://www.pnas.org/content/97/4/1406.

[33] Energy + Environmental Economics. *Decarbonizing Pipeline Gas to Meet California's 2050 Greenhouse Gas*. 2015. URL: https://ethree.com/documents/E3_Decarbonizing_Pipeline_01-27-2015.pdf.

[34] E. Ela, M. Milligan, and B. Kirby. "Operating reserves and variable generation". In: *Nat. Renew. Energy Lab., Golden, CO, USA* (Aug. 2011).

[35] Electricity Reliability Council of Texas (ERCOT). "Future Ancillary Services in ERCOT". In: *ERCOT: Taylor, TX, USA* (2013).

[36] M. Fripp. "Switch: A Planning Tool for Power Systems with Large Shares of Intermittent Renewable Energy". In: *Environmental Science & Technology* 46.11 (2012). PMID: 22506835, pp. 6371–6378. DOI: 10.1021/es204645c. URL: https://doi.org/10.1021/es204645c.

[37] L. Gacitua et al. "A comprehensive review on expansion planning: Models and tools for energy policy analysis". In: *Renewable and Sustainable Energy Reviews* 98 (2018), pp. 346–360. ISSN: 1364-0321. DOI: https://doi.org/10.1016/j.rser.2018.08.043. URL: http://www.sciencedirect.com/science/article/pii/S1364032118306269.

[38] V. Galaz et al. "Polycentric systems and interacting planetary boundaries — Emerging governance of climate change–ocean acidification–marine biodiversity". In: *Ecological Economics* 81 (2012). Special Section: "Planetary Boundaries" and Global Environmental Governance, pp. 21–32. ISSN: 0921-8009. DOI: https://doi.org/10.1016/j.ecolecon.2011.11.012. URL: http://www.sciencedirect.com/science/article/pii/S0921800911004964.

[39] P. H. Gleick. "Climate change, hydrology, and water resources". In: *Reviews of Geophysics* 27.3 (1989), pp. 329–344. DOI: 10.1029/RG027i003p00329. eprint: https://agupubs.onlinelibrary.wiley.com/doi/pdf/10.1029/RG027i003p00329. URL: https://agupubs.onlinelibrary.wiley.com/doi/abs/10.1029/RG027i003p00329.

[40] A. R. Gopal et al. "Modeling plug-in electric vehicle charging demand with BEAM, the framework for behavior energy autonomy mobility". In: *Lawrence Berkeley National Laboratory* (2017).

[41] A. K. Gosain, S. Rao, and D. Basuray. "Climate change impact assessment on hydrology of Indian river basins". In: *Current Science* 90.3 (2006), pp. 346–353. ISSN: 00113891. URL: http://www.jstor.org/stable/24091868.

[42] Office of the Governor Arnold Schwarzenegger. *AB-32 California Global Warming Solutions Act of 2006*. 2006.

[43] Office of the Governor Edmund G. Brown Jr. *AB-398 California Global Warming Solutions Act of 2006*. 2017.

[44] M. Grant and S. Boyd. *CVX: Matlab Software for Disciplined Convex Programming, version 2.1*. http://cvxr.com/cvx. Mar. 2014.

[45] M. Grant and S. Boyd. "Graph implementations for nonsmooth convex programs". In: *Recent Advances in Learning and Control*. Ed. by V. Blondel, S. Boyd, and H. Kimura. Lecture Notes in Control and Information Sciences. Springer-Verlag Limited, 2008, pp. 95–110.

[46] C. D. G. Harley. "Climate Change, Keystone Predation, and Biodiversity Loss". In: *Science* 334.6059 (2011), pp. 1124–1127. ISSN: 0036-8075. DOI: 10.1126/science.1210199. eprint: https://science.sciencemag.org/content/334/6059/1124.full.pdf. URL: https://science.sciencemag.org/content/334/6059/1124.

[47] G. He et al. "SWITCH-China: A Systems Approach to Decarbonizing China's Power System". In: *Environmental Science & Technology* 50.11 (2016). PMID: 27157000, pp. 5467–5473. DOI: 10.1021/acs.est.6b01345. URL: https://doi.org/10.1021/acs.est.6b01345.

[48] P. Hidalgo-Gonzalez et al. "Frequency Regulation in Hybrid Power Dynamics with Variable and Low Inertia due to Renewable Energy". In: *2018 IEEE Conference on Decision and Control (CDC)*. Dec. 2018, pp. 1592–1597.

[49] P. Hidalgo-Gonzalez et al. "Frequency Regulation using Data-Driven Controllers in Power Grids with Variable Inertia due to Renewable Energy". In: *IEEE PES General Meeting*. IEEE. Aug. 2019.

[50] P. Hidalgo-Gonzalez et al. "Frequency Regulation using Sparse Learned Controllers in Power Grids with Variable Inertia due to Renewable Energy". In: *Decision and Control (CDC), 2019 IEEE 58th Annual Conference on*. IEEE. 2019.

[51] J. L. Ho et al. "Planning Transmission for Uncertainty: Applications and Lessons with the Western Interconnection". In: *Western Electricity Coordinating Council* (2016).

[52] O. Hoegh-Guldberg et al. "Coral Reef Ecosystems under Climate Change and Ocean Acidification". In: *Frontiers in Marine Science* 4 (2017), p. 158. ISSN: 2296-7745. DOI: 10.3389/fmars.2017.00158. URL: https://www.frontiersin.org/article/10.3389/fmars.2017.00158.

[53] O. Hoegh-Guldberg et al. "Coral Reefs Under Rapid Climate Change and Ocean Acidification". In: *Science* 318.5857 (2007), pp. 1737–1742. ISSN: 0036-8075. DOI: 10.1126/science.1152509. eprint: https://science.sciencemag.org/content/318/5857/1737.full.pdf. URL: https://science.sciencemag.org/content/318/5857/1737.

[54] C. A. Horowitz. "Paris Agreement". In: *International Legal Materials* 55.4 (2016), pp. 740–755. DOI: 10.1017/S0020782900004253.

[55] World Resources Institute. "World Greenhouse Gas Emissions: 2016". In: *World Resources Institute* (2020). URL: https://www.wri.org/resources/data-visualizations/world-greenhouse-gas-emissions-2016.

[56] J. Johnston et al. "Switch 2.0: A modern platform for planning high-renewable power systems". In: *SoftwareX* 10 (2019), p. 100251. ISSN: 2352-7110. DOI: https://doi.org/10.1016/j.softx.2019.100251. URL: http://www.sciencedirect.com/science/article/pii/S2352711018301547.

[57] M. Koch et al. "Climate change and ocean acidification effects on seagrasses and marine macroalgae". In: *Global Change Biology* 19.1 (2013), pp. 103–132. DOI: 10.1111/j.1365-2486.2012.02791.x. eprint: https://onlinelibrary.wiley.com/doi/pdf/10.1111/j.1365-2486.2012.02791.x. URL: https://onlinelibrary.wiley.com/doi/abs/10.1111/j.1365-2486.2012.02791.x.

[58] E. Kriegler et al. "Making or breaking climate targets: The AMPERE study on staged accession scenarios for climate policy". In: *Technological Forecasting and Social Change* 90 (2015), pp. 24–44. ISSN: 0040-1625. DOI: https://doi.org/10.1016/j.techfore.2013.09.021. URL: http://www.sciencedirect.com/science/article/pii/S0040162513002588.

[59] P. Kundur. "Power System Stability and Control". In: *McGraw-Hill* (1994).

[60] National Renewable Energy Laboratory. *3TIER. Development of regional wind resource and wind plant output datasets*. 2010.

[61] National Renewable Energy Laboratory. *High-Penetration PV Integration Handbook for Distribution Engineers*. 2016.

[62] National Renewable Energy Laboratory. *Regional Energy Deployment System (ReEDS) Model Documentation: Version 2018*. 2018.

[63] National Renewable Energy Laboratory. *Western wind and solar integration study*. 2010. URL: http://www.nrel.gov/wind/systemsintegration/pdfs/2010/wwsis_final_report.pdf.

[64] R. Latifovic and D. Pouliot. "Analysis of climate change impacts on lake ice phenology in Canada using the historical satellite data record". In: *Remote Sensing of Environment* 106.4 (2007), pp. 492–507. ISSN: 0034-4257. DOI: https://doi.org/10.1016/j.rse.2006.09.015. URL: http://www.sciencedirect.com/science/article/pii/S0034425706003439.

[65] T. Laumann and N. Reeh. "Sensitivity to climate change of the mass balance of glaciers in southern Norway". In: *Journal of Glaciology* 39.133 (1993), pp. 656–665. DOI: 10.3189/S0022143000016555.

[66] D. Ponce de Leon Barido et al. "Evidence and future scenarios of a low-carbon energy transition in Central America: a case study in Nicaragua". In: *Environmental Research Letters* 10.10 (Sept. 2015), p. 104002. DOI: 10.1088/1748-9326/10/10/104002. URL: https://doi.org/10.1088%2F1748-9326%2F10%2F10%2F104002.

[67] F. L. Lewis, D. Vrabie, and K. G. Vamvoudakis. "Reinforcement Learning and Feedback Control: Using Natural Decision Methods to Design Optimal Adaptive Controllers". In: *IEEE Control Systems Magazine* 32.6 (Dec. 2012), pp. 76–105. ISSN: 1066-033X. DOI: 10.1109/MCS.2012.2214134.

[68] Y. Liu, J. Stanturf, and S. Goodrick. "Trends in global wildfire potential in a changing climate". In: *Forest Ecology and Management* 259.4 (2010). Adaptation of Forests and Forest Management to Changing Climate, pp. 685–697. ISSN: 0378-1127. DOI: https://doi.org/10.1016/j.foreco.2009.09.002. URL: http://www.sciencedirect.com/science/article/pii/S0378112709006148.

[69] J. Löfberg. "YALMIP : A Toolbox for Modeling and Optimization in MATLAB". In: *In Proceedings of the CACSD Conference*. Taipei, Taiwan, 2004.

[70] G. Luderer et al. "Implications of weak near-term climate policies on long-term mitigation pathways". In: *Climatic Change* (2016), pp. 127–140. DOI: 10.1007/s10584-013-0899-9.

[71] Y. V. Makarov et al. "Stochastic Operations and Planning". In: *Pacific Northwest National Laboratory* (2015).

[72] E. Mallada. "iDroop: A Dynamic Droop controller to decouple power grid's steady-state and dynamic performance". In: *2016 IEEE 55th Conference on Decision and Control (CDC)*. Dec. 2016, pp. 4957–4964. DOI: 10.1109/CDC.2016.7799027.

[73] J. R. Marlon et al. "Wildfire responses to abrupt climate change in North America". In: *Proceedings of the National Academy of Sciences* 106.8 (2009), pp. 2519–2524. ISSN: 0027-8424. DOI: 10.1073/pnas.0808212106. eprint: https://www.pnas.org/content/106/8/2519.full.pdf. URL: https://www.pnas.org/content/106/8/2519.

[74] P. Masson-Delmotte V. et al. "IPCC, 2018: Global Warming of 1.5. An IPCC Special Report on the impacts of global warming of 1.5 above pre-industrial levels and related global greenhouse gas emission pathways, in the context of strengthening the global response to the threat of climate change, sustainable development, and efforts to eradicate poverty". In: *In press* (2020).

[75] R. Mendelsohn and A. Dinar. "Climate Change, Agriculture, and Developing Countries: Does Adaptation Matter?" In: *The World Bank Research Observer* 14.2 (Aug. 1999), pp. 277–293. ISSN: 0257-3032. DOI: 10.1093/wbro/14.2.277. eprint: https://academic.oup.com/wbro/article-pdf/14/2/277/4685665/14-2-277.pdf. URL: https://doi.org/10.1093/wbro/14.2.277.

[76] A. Mileva et al. "Power system balancing for deep decarbonization of the electricity sector". In: *Applied Energy* 162 (2016), pp. 1001–1009. ISSN: 0306-2619. DOI: https://doi.org/10.1016/j.apenergy.2015.10.180. URL: http://www.sciencedirect.com/science/article/pii/S0306261915014300.

[77] A. Mileva et al. "SunShot Solar Power Reduces Costs and Uncertainty in Future Low-Carbon Electricity Systems". In: *Environmental Science & Technology* 47.16 (2013). PMID: 23865424, pp. 9053–9060. DOI: 10.1021/es401898f. URL: https://doi.org/10.1021/es401898f.

[78] K. L. Moore. "Iterative Learning Control: An Expository Overview". In: *Applied and Computational Control, Signals, and Circuits: Volume 1*. Ed. by B. N. Datta. Boston, MA: Birkhäuser Boston, 1999, pp. 151–214.

[79] J. Nelson et al. "High-resolution modeling of the western North American power system demonstrates low-cost and low-carbon futures". In: *Energy Policy* 43 (2012), pp. 436–447. ISSN: 0301-4215. DOI: https://doi.org/10.1016/j.enpol.2012.01.031. URL: http://www.sciencedirect.com/science/article/pii/S0301421512000365.

[80] J. Notenboom et al. *Climate and Energy Roadmaps towards 2050 in north-western Europe: A concise overview of long-term climate and energy policies in Belgium, Denmark, France, Germany, the Netherlands and the United Kingdom*. Tech. rep. Netherlands: PBL Netherlands Environmental Assessment Agency, 2012.

[81] J. M. Pandolfi et al. "Projecting Coral Reef Futures Under Global Warming and Ocean Acidification". In: *Science* 333.6041 (2011), pp. 418–422. ISSN: 0036-8075. DOI: 10.1126/science.1204794. eprint: https://science.sciencemag.org/content/333/6041/418.full.pdf. URL: https://science.sciencemag.org/content/333/6041/418.

[82] B. K. Poolla, S. Bolognani, and F. Dörfler. "Optimal placement of virtual inertia in power grids". In: *IEEE Transactions on Automatic Control* 62.12 (2017), pp. 6209–6220.

[83] B. Poolla et al. "A Market Mechanism for Virtual Inertia". In: *IEEE Transactions on Smart Grid* PP (Nov. 2017). DOI: 10.1109/TSG.2020.2969518.

[84] J. Reilly, N. Hohmann, and S. Kane. "Climate change and agricultural trade: Who benefits, who loses?" In: *Global Environmental Change* 4.1 (1994), pp. 24–36. ISSN: 0959-3780. DOI: https://doi.org/10.1016/0959-3780(94)90019-1. URL: http://www.sciencedirect.com/science/article/pii/0959378094900191.

[85] K. Riahi et al. "Locked into Copenhagen pledges — Implications of short-term emission targets for the cost and feasibility of long-term climate goals". In: *Technological Forecasting and Social Change* 90 (2015), pp. 8–23. ISSN: 0040-1625. DOI: https://doi.org/10.1016/j.techfore.2013.09.016. URL: http://www.sciencedirect.com/science/article/pii/S0040162513002539.

[86] L. Roald et al. "Analytical reformulation of security constrained optimal power flow with probabilistic constraints". In: *2013 IEEE Grenoble Conference*. 2013, pp. 1–6.

[87] F. Santosa and W. W. Symes. "Linear inversion of band-limited reflection seismograms". In: *SIAM Journal on Scientific and Statistical Computing* 4.7 (1986), pp. 1307–1330. ISSN: 00359246.

[88] M. Schaeffer et al. "Mid- and long-term climate projections for fragmented and delayed-action scenarios". In: *Technological Forecasting and Social Change* 90 (2015), pp. 257–268. ISSN: 0040-1625. DOI: https://doi.org/10.1016/j.techfore.2013.09.013. URL: http://www.sciencedirect.com/science/article/pii/S0040162513002424.

[89] O. Sondermeijer et al. "Regression-based inverter control for decentralized optimal power flow and voltage regulation". In: *2016 IEEE Power Energy Society General Meeting (PESGM)*. 2016.

[90] D. V. Spracklen et al. "Impacts of climate change from 2000 to 2050 on wildfire activity and carbonaceous aerosol concentrations in the western United States". In: *Journal of Geophysical Research: Atmospheres* 114.D20 (2009). DOI: 10.1029/2008JD010966. eprint: https://agupubs.onlinelibrary.wiley.com/doi/pdf/10.1029/2008JD010966. URL: https://agupubs.onlinelibrary.wiley.com/doi/abs/10.1029/2008JD010966.

[91] P. Sullivan, J. Colman, and E. Kalendra. "Predicting the Response of Electricity Load to Climate Change". In: *National Renewable Energy Laboratory, Golden, CO* (2015).

[92] U. Tamrakar et al. "Virtual inertia: Current trends and future directions". In: *Applied Sciences* 7.7 (2017), p. 654.

[93] Core Writing Team, R.K Pachauri, and A. (eds.) Reisinger. "IPCC, 2007: Climate Change 2007: Synthesis Report. Contribution of Working Groups I, II and III to the Fourth Assessment Report of the Intergovernmental Panel on Climate Change". In: *IPCC, Geneva, Switzerland* (2007), p. 104.

[94] R. Tibshirani. "Regression Shrinkage and Selection via the Lasso". In: *Journal of the Royal Statistical Society. Series B (Methodological)* 58.1 (1996), pp. 267–288. ISSN: 00359246. URL: http://www.jstor.org/stable/2346178.

[95] A. Ulbig, T. S. Borsche, and G. Andersson. "Impact of low rotational inertia on power system stability and operation". In: *IFAC Proceedings Volumes* 47.3 (2014), pp. 7290–7297.

[96] A. Ulbig et al. "Predictive control for real-time frequency regulation and rotational inertia provision in power systems". In: *Decision and Control (CDC), 2013 IEEE 52nd Annual Conference on*. IEEE. 2013, pp. 2946–2953.

[97] M. K. Van Aalst. "The impacts of climate change on the risk of natural disasters". In: *Disasters* 30.1 (2006), pp. 5–18. DOI: 10.1111/j.1467-9523.2006.00303.x. eprint: https://onlinelibrary.wiley.com/doi/pdf/10.1111/j.1467-9523.2006.00303.x. URL: https://onlinelibrary.wiley.com/doi/abs/10.1111/j.1467-9523.2006.00303.x.

[98] Black & Veatch. *Cost and performance data for power generation technologies*. 2012. URL: http://bv.com/docs/reports-studies/nrel-cost-report.pdf.

[99] C. Vincent et al. "Ice ablation as evidence of climate change in the Alps over the 20th century". In: *Journal of Geophysical Research: Atmospheres* 109.D10 (2004). DOI: 10.1029/2003JD003857. eprint: https://agupubs.onlinelibrary.wiley.com/doi/pdf/10.1029/2003JD003857. URL: https://agupubs.onlinelibrary.wiley.com/doi/abs/10.1029/2003JD003857.

[100] X. Wang and F. Blaabjerg. "Harmonic Stability in Power Electronic-Based Power Systems: Concept, Modeling, and Analysis". In: *IEEE Transactions on Smart Grid* 10.3 (2019), pp. 2858–2870.

[101] M. Wei et al. "Building a Healthier and More Robust Future: 2050 Low-Carbon Energy Scenarios for California". In: *California Energy Commission* Publication Number: CEC-500-2019-033 (2019), pp. 1–167.

[102] M. Wei et al. "California's carbon challenge: Scenarios for achieving 80% emissions reductions in 2050". In: *Lawrence Berkeley National Laboratory, UC Berkeley, UC Davis, and Itron to the California Energy Commission* (2012).

[103] M. Wei et al. "Deep carbon reductions in California require electrification and integration across economic sectors". In: *Environmental Research Letters* 8.1 (Mar. 2013), p. 014038. DOI: 10.1088/1748-9326/8/1/014038. URL: https://doi.org/10.1088%5C%2F1748-9326%5C%2F8%5C%2F1%5C%2F014038.

[104] J. Weyant. "Some Contributions of Integrated Assessment Models of Global Climate Change". In: *Review of Environmental Economics and Policy* 11.1 (Mar. 2017), pp. 115–137. ISSN: 1750-6816. DOI: 10.1093/reep/rew018. eprint: https://academic.oup.com/reep/article-pdf/11/1/115/11117124/rew018.pdf. URL: https://doi.org/10.1093/reep/rew018.

[105] T. Wheeler and J. von Braun. "Climate Change Impacts on Global Food Security". In: *Science* 341.6145 (2013), pp. 508–513. ISSN: 0036-8075. DOI: 10.1126/science.1239402. eprint: https://science.sciencemag.org/content/341/6145/508.full.pdf. URL: https://science.sciencemag.org/content/341/6145/508.

[106] G. C. Wu, M. S. Torn, and J. H. Williams. "Incorporating Land-Use Requirements and Environmental Constraints in Low-Carbon Electricity Planning for California". In: *Environmental Science & Technology* 49.4 (2015). PMID: 25541644, pp. 2013–2021. DOI: 10.1021/es502979v. URL: https://doi.org/10.1021/es502979v.

[107] Q. Zhong and G. Weiss. "Synchronverters: Inverters that mimic synchronous generators". In: *IEEE Transactions on Industrial Electronics* 58.4 (2011), pp. 1259–1267.